Design Improvement and Error Analysis of DARLING, a Device for Assessing the Resistance to Lodging in Grains.

Presented in Partial Fulfillment of the Requirements for the Degree of

Master of Science

With a Major in

Mechanical Engineering

In the

College of Graduate Studies

University of Idaho

By

Joseph DeKold

Major Professor

Daniel J. Robertson, Ph.D.

Committee

Eric Wolbrecht, Ph.D.

Michael Maughan, Ph.D.

Daniel J. Robertson, Ph.D.

Department Administrator

Gabriel Potirniche, Ph.D.

May 2023

Abstract

Up to a quarter of the world's most critical crops are destroyed each year by high winds, hail, and other natural phenomena. This damage is the result of stalk lodging, which refers to the breaking of a plant's stem prior to harvest. In order to reduce these damages and meet future grain demand, reliable methods for measuring lodging resistance are required. Through extensive research, two measurable quantities, stalk bending stiffness and stalk bending strength, have been found to relate strongly to lodging resistance. Derived from engineering beam theory, these parameters allow researchers to measure the abstract trait of lodging resistance with calculable quantities. These quantities are most reliable when measured on stalks in their natural environment. The "DARLING" (Device for Assessing the Resistance to Lodging IN Grains) is an electromechanical device that can reliably measure stalk bending stiffness and stalk bending strength in the field. Distributing the DARLING to all parties involved in lodging reduction efforts will result in larger amounts of data being collected. More data will help these parties identify traits of lodging-resistant stalks and develop lodging-resistant varieties through genetic improvement.

The most effective way to facilitate this distribution is to sell the DARLING commercially. To advance the DARLING toward this goal, three facets were addressed: improvement of the DARLING's current design, development of a "Lite" DARLING, and experimental error analysis of the DARLING's measurements. After making these improvements, the DARLING is better suited for its intended application, more applicable to budget limited research groups, and more accurate in the measurements it obtains. The DARLING is significantly closer to large-scale distribution where it will aid in developing lodging resistance crop varieties critical to meet the growing demand for grain.

Acknowledgements

I would like to thank my major professor, Dr Daniel Robertson. Dan, you have been with this project from its conception, and you have graciously allowed me to be involved in it, thank you. Your mentorship was a guiding light through this process, and you always gave me just enough help to wade through the mire without handing me the solution. I deeply respect the way you approach your work, the way you live your life, and how you care for those who make up your memorized deck of cards.

This material is based upon work supported in part by the National Science Foundation under Grant IOS-1547796.

Dedication

This paper is the consolidation of results produced through hard decisions. Not all decisions in this process were hard to make, however, as the dedication of this paper is undeniably apparent. Mom, you laid down your life for mine and the rest of my siblings' education. You not only sacrificed to teach us the way of the righteous and the elements of the periodic table, but you also surrendered most of your waking hours to be my mother. I would not be submitting this thesis if it wasn't for your continued patience, persistence, hard love, gentle love, and continued encouragement. You have always made me feel loved in my shortcomings, while simultaneously providing me with the support and encouragement necessary to do hard things. Writing this thesis was akin to cleaning the bathroom; I knew I couldn't leave until it was done. Like cleaning bathrooms, this endeavor required many traits that are against my nature, but because of your influence and equipping, I was able to crest the peak. I am deeply thankful for you, I love you, and I hope reading this barely relevant and tedious essay brings you some much deserved pride and gratitud

Table of Contents

Keywords and Terms: *Bending strength, bending stiffness, cereal, corn, stalk lodging.*

List of Tables

List of Figures

Statement of Contribution

All chapters preceding chapter four consist of design, analysis, and documentation work attributed to Joseph DeKold. Chapter four describes research performed by Joseph DeKold with collaborative input from Dr. Daniel Robertson. The specific details of the collaborative work are given in the following description. Both Joseph DeKold and Dr. Daniel Robertson collaborated to devise the experimental design process. The dimensioning and fabrication of the carbon fiber bar was performed by Joseph DeKold. The fixture was designed and fabricated by Joseph DeKold. The data collection methodology was devised by and performed by Joseph DeKold. The raw data processing software was preexisting at the onset of the study and was not developed by Joseph DeKold, but by a team led by Dr. Robertson. The statistical analysis code and figure generation code is all original work by Joseph DeKold. Joseph DeKold was the primary author of the content within the document, with editing collaboratively performed with Dr. Robertson.

Chapter 1: Motivation and Background

1.1 Global Cereal Production

Grain crops feed the world. Cereal grains (wheat (*Triticum)*, rice (*Oryza)*, corn *(Maize)*, barley *(Hordum Vulgare)*, oats *(Avena Sativa)*, and millet *(Panicum Miliaceum)*) comprise 90% of grains grown globally and are the most produced commodities in the world [1]. It is estimated that cereal grains account for over 50% of the average person's calories [1], [2]. Cereal grains are annual grasses which usually have long spindly stalks that support a large grain head. The starchy grains are used for human food, animal feed, and industrial applications such as fuel [1],[3]. Production of cereal grains per capita has outpaced population growth since 1961 (Figure 2), [1]. That trend is expected to become even more dramatic during the next several decades [4].

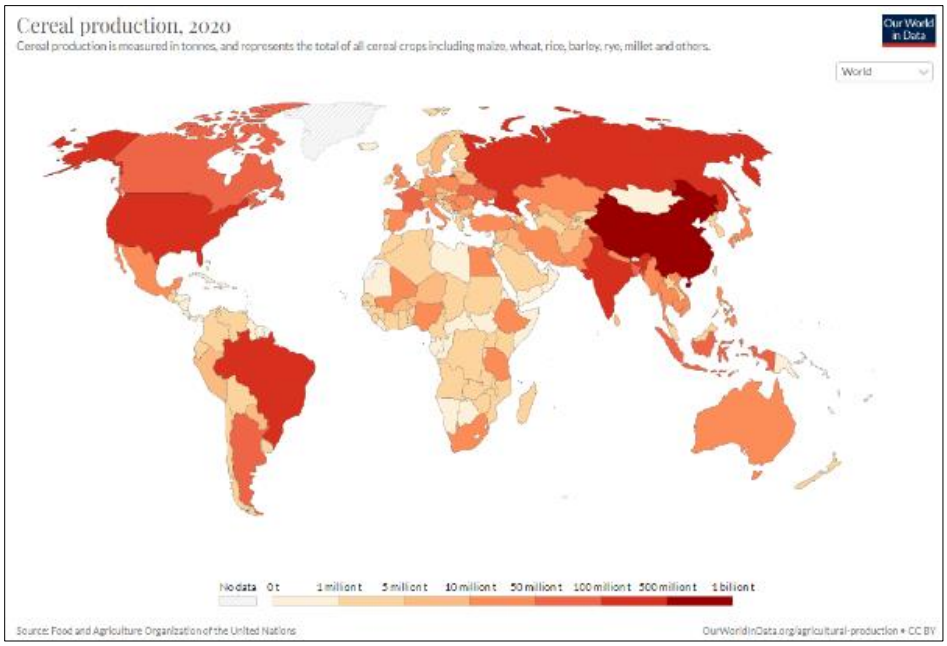

Figure 1: Global cereal production as of 2020. Cereal grains include the three most significant staple crops: corn, wheat, and rice.

The continued growth in cereal consumption raises concerns for the future. Meeting the global demand for grains is becoming increasingly difficult due to numerous factors including climate variability, urbanization, extreme weather events, and droughts, etc. [5]. These ongoing factors inhibit production growth and create a gap between how much grain could theoretically be produced (potential yield), and what is produced (average yield). In coming years, this yield gap may also increase due to a plateau or even decline in average yield [6]. Reducing this crop yield gap is rapidly becoming the primary means to increase crop yields and meet the global grain demand of the future [8],[9].

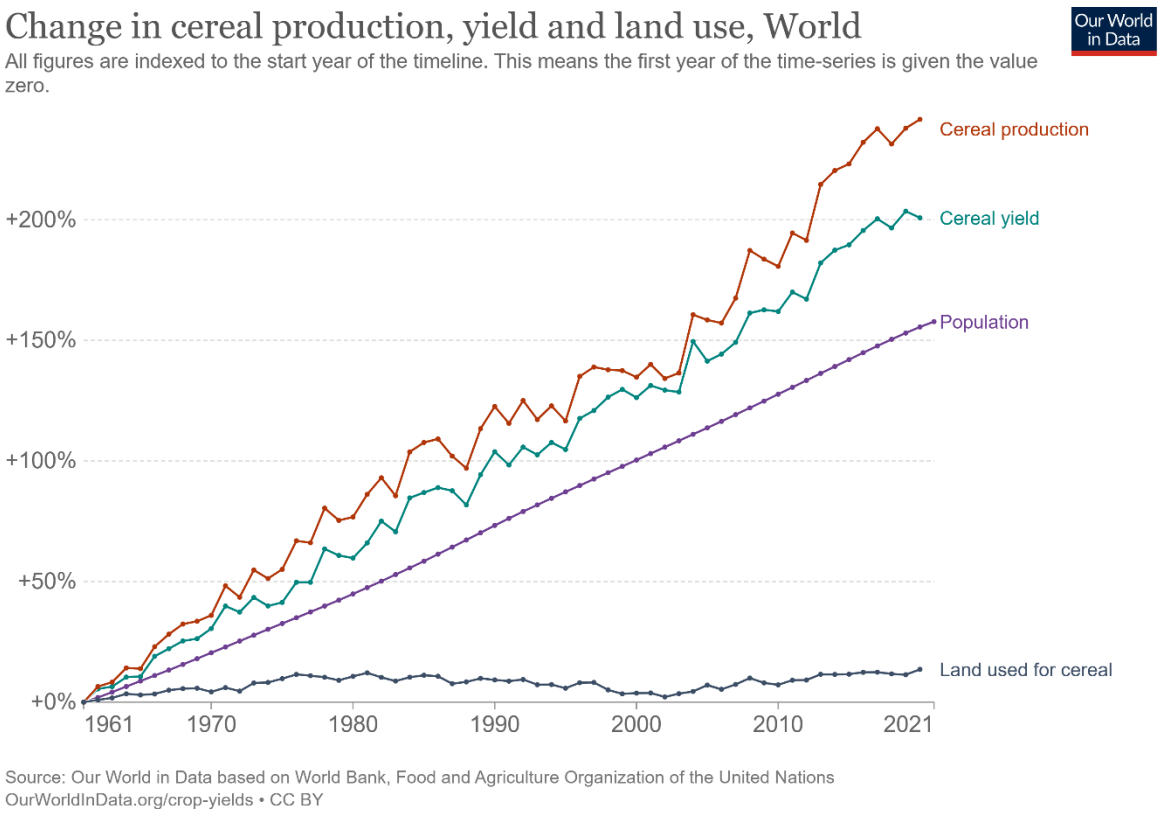

Figure 2: Cereal production, cereal yield, and population growth over time.

1.2 Cereal Stalk Lodging

Stalk lodging is a primary contributor to the cereal yield gap. Lodging occurs when plant stems break during windstorms. Damage from lodging often prevents the grain from being harvested and increases the presence of pests and disease in the field (Figure 3). Cereal grains are particularly vulnerable to stalk lodging due to their natural structure. When acted on by wind forces, the heavy grain heads supported by tall, spindly stalks induce concentrated stresses in the stem which frequently result in fracturing and buckling. Stalk lodging is estimated to destroy 5%-25% of the annual global grain yield, constraining production and resulting in billions of dollars in lost crops annually [8],[9],[11]. Severe in consequence, stalk lodging is extremely difficult to reduce. There is a long history of efforts to mitigate lodging that were initially effective but currently have depleting success rates.

Figure 3: Corn stalk lodging because of high winds. Golden Harvest Seeds, 2022.

1.3 Historical Stalk Lodging Reduction

Over the last century, lodging rates have been significantly reduced through the application of genetic improvement and selective breeding techniques [10]. This reduction in lodging rates has significantly reduced the yield gap for several critical crops. In the early 1940's, the need to increase crop yields was as urgent as it is now with many scholars predicting widespread starvation if yields could not be increased [11]. As farmland became scarcer and operating expenses grew, decreasing the yield gap by improving the efficiencies of crops was the most effective solution. This urgency led to a series of innovations in plant science known as the Green Revolution. The innovations of the Green Revolution were focused on developing new varieties of staple crops with increased yields and improved lodging and pest resistance [11],[12].

One key player of this era was Norman Ernest Borlaug who developed a short-stemmed variety of wheat more suited to support heavy grain head loads and resist windstorm damage. The short stalk allowed for a larger grain head to be supported, and it also had a quicker growing season which meant that two crops per year could be produced [11]. As a result of Borlaug's improved wheat, yields per acre increased by 50% between 1961 and 1971 [11]. Similar innovations were facilitated for other crops as well. A decade later, the IR-8 rice variety was developed. IR-8 rice also featured a dwarfed stem, with an increased amount of grain produced by each plant. The resultant variety, dubbed "miracle rice," significantly increased rice yield per acre in Asia [13]. Over the next several decades, lodging rates were significantly decreased through the introduction of new crop varieties and yield per acre improved. In recent decades, however, genetic improvement methods have dwindled in effectiveness and yield increases appear to have plateaued [14].

The reason behind that plateau can be described by an observation made by agronomists R.J. Garber and P.J. Olson over 100 years ago: "lodging in cereals is dependent on so many factors of

unequal value in the different sorts that no one factor seems to be correlated closely enough with lodging to be of much value as a selection index." Lodging resistance of individual plant stems depends on many morphological (i.e., stem diameter and stem length) and chemical (i.e., lignin and cellulose content) characteristics [15], [16] . In the past, genetic improvement has focused on optimizing a single characteristic such as stem length, in the case of Borlaug's dwarf wheat and IR-8 rice, to increase lodging resistance. As reflected by plateaued trends in growth yields, this method can only go so far until its impact is confounded by the complexity of characteristic interaction. A holistic interplay of plant characteristics into lodging resistance must be considered for effective future variety selection [17].

1.4 Holistic Measurement of Lodging Resistance

Structural quantities are holistic measurements of lodging resistance which consider morphological, chemical, and lodging related factors at play. Stalks are organic structures, and stalk lodging in an engineering sense is a structural failure [18]. Operating on this association, research groups have attempted to use structural quantities such as rind puncture resistance, compression strength, crush resistance, and three-point bending strength to holistically characterize stalk lodging resistance [19]–[24]. However, subsequent research has revealed that many of these structural quantities do not correlate strongly to lodging resistance and are severely limited in their potential [25].

The lodging determinacy of speculative structural quantities can be evaluated with two methods: the statistic and forensic method [16],[23]. The statistical method utilizes extensive data describing the observed lodging rates of different plant breeds. This data is useful because it can gauge if a measurable quantity relates to lodging resistance. To perform the statistical method, speculative structural quantities (crush resistance, rind puncture resistance, bending strength, etc.) of breeds with observed lodging rate data are collected. After speculative quantities from each breed are acquired, the quantities are compared to the lodging rate data of those same breeds to see if there is a discernable relationship between the speculative quantity and the observed lodging rate. The predictability of that relationship helps describe the lodging determinacy of the structural quantity. The forensic evaluation method compares failure modes (creasing, buckling, snapping, etc.) of naturally lodged stalks to those measured with the speculative quantity. Applying boundary and loading conditions to non-prismatic, non-isotropic, and non-homogenous structures (i.e., corn stalks) in such a way that natural failure modes are produced is not trivial [18], [26]. Considering this, if the measurement process of the speculative quantity reproduces natural failure modes, then it is highly likely that the measurement process simulates conditions experienced during natural lodging and that it correlates to lodging resistance. These two methods can offer strong support or opposition for a speculative quantity's lodging

determinacy, but they are not definitive predictors of a parameter's correlation to lodging resistance. Further experimentation is always necessary to enforce the lodging determinacy of a speculative quantity. Through extensive and application of these criteria, two critical quantities have been selected as primary determinants of lodging resistance.

During windstorms, external forces concentrate on the largest amount of surface area of a plant. Grain heads and leaves typically compose the most surface area and are located on the upper portions of the stem. When exerted on the grain heads and leaves, those forces load the stem in bending [27]. This observation led to the selection of bending stiffness and bending strength as speculative correlative quantities. After extensive research and validation, it was determined that both parameters correlate strongly to historical lodging rates and induce failure modes akin to natural lodging, supporting their use for measuring stalk lodging resistance [25], [28]. Since this discovery, both of these quantities have been used extensively in various studies investigating the lodging resistance of many plant species [23], [28]. These quantities use equations similar to structural engineering equations to holistically measure the lodging resistance of individual stems [25], [28], [29]. Bending stiffness and bending strength are calculated with equations *(1)* and *(2)* respectively and utilize several input measurements. Both bending stiffness (EI) and bending strength (S) utilize the measurement of load cell height and applied force, (h and F respectively), but applied force is recorded at different values of deflection for each quantity. Bending stiffness utilizes applied force measured at low deflections within the linear portion of the force vs. displacement curve, while bending strength utilizes max applied force before failure [26]. Bending stiffness requires the additional measurement of horizontal deflection, which is calculated by equation *(3)* using angular deflection (θ) and load cell height. Each of these three measured inputs are defined in Figure 4.

$$EI = f(F, h, \Delta) = \frac{(F \cdot h^3)}{3 \cdot \Delta} \tag{1}$$

And

$$S = f(F_{max}, L) = F_{max} \cdot h \tag{2}$$

$$\Delta = h \cdot sin(\theta) \tag{3}$$

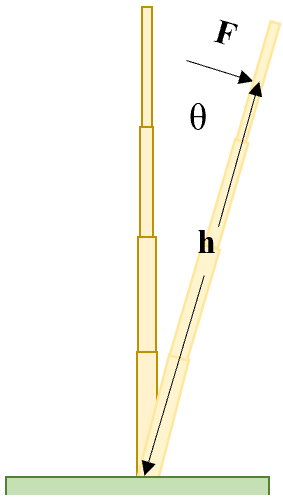

Figure 4: Measured input definitions in relation to a deflected, upright corn stalk.

Stalk bending stiffness and bending strength measurement both require specially designed testing equipment. While lab tests can measure properties in a more controlled environment, in-field measurement is more considerate of lodging related factors such as soil condition and root strength. Not surprisingly, agronomists and scientists have been developing field testing devices to quantify lodging resistance for decades. Field testing devices have taken the form of anything from a force gauge hooked to a plant stalk to a complex mechanical assembly weighing 20 tons. [30],[31],[32]. The various field-testing devices also measure different correlative quantities and different numbers of plants at a time. Some devices measure applied force and angular rotation [33],[15] while other devices consider parameters such as mechanical energy absorption [34]. Devices for densely packed crops such as wheat and rice typically measure the canopy (collective) strength of a group of plants while devices designed for measuring less dense crops such as corn and sorghum measure a single plant at a time [30],[33], [34],[35].

Several examples highlight the diversity of field measurement equipment. One of the earliest, well documented field-testing devices is known as Barry's device. Developed in the UK and introduced to the research community in 2003, this device tested wheat canopy strength [33]. Barry's device consisted of a force gauge and arm on a vertical hinge which would measure the resistance to displacement of several wheat stems at a time [33]. Another device, the Stalker, was introduced in 2019. This device measures the force and displacement of a single maize or sorghum stalk [34]. A third device was developed in China in 2018. Guo's device, as it is known, quantifies the strength of an individual

plant by attaching a data management system and force gauge to the stalk and measuring applied force when the device is pulled in several directions [30].

Each one of the testing devices mentioned contributed to the task of quantifying stalk lodging resistance. Many of the devices measured speculative quantities whose correlation to lodging resistance was hypothetical. Using the statistical and forensic methods, the correlation of many quantities has been dispelled, leaving a remainder of quantities such as bending stiffness and bending strength that are acceptable quantifiers of lodging resistance. Field-testing devices are ideal because they consider more factors than lab methods, and they also reduce the cost of studies by not requiring sample transportation. Field-testing devices which measure acceptable lodging resistance quantifiers are some of the most promising tools for crop improvement.

1.5 DARLING Device introduction and description

The DARLING is one such promising tool. Researchers with various backgrounds developed the electromechanical D.A.R.L.I.N.G. (Device for Assessing Resistance to Lodging in Grains) to reliably measure the bending stiffness and bending strength of corn and sorghum stalks in the field [26]. The DARLING consists of four subsystems: A frame, data management system, applied force measurement system, and angular deflection measurement system (Figure 5: LEFT, 1-4 respectively). The device consists of an upright aluminum tube connected to a horizontal footplate via a pinned hinge at its base. The DARLING measures a single corn or sorghum stalk at a time; Figure 6 describes its operation and the measurements collected. Figure 5: RIGHT, further describes the DARLING's systems and shows an example plot of collected data.

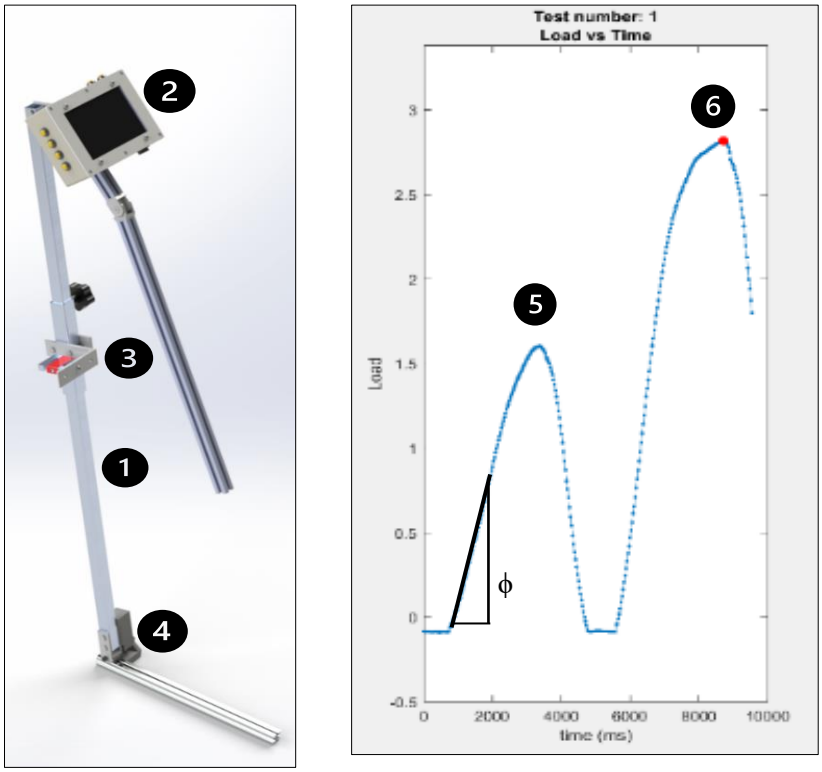

Figure 5: ***LEFT*** *DARLING subsystems and orientation.* ***RIGHT*** *example of a force vs displacement test of a single corn stalk. A field measurement consists of two cycles: stiffness measurement and bending strength measurement. Stiffness measurement is acquired by flexing the stalk to about 10 degrees (5) while measuring the slope of the linear portion of the force vs displacement curve (Φ). After the stalk is flexed, the DARLING returns to vertical before performing the second measurement cycle. The second cycle acquires bending strength by pushing the stalk to failure (6) and measuring the max applied force supported. These inputs combine in equations 1-3 to calculate bending stiffness and bending strength.*

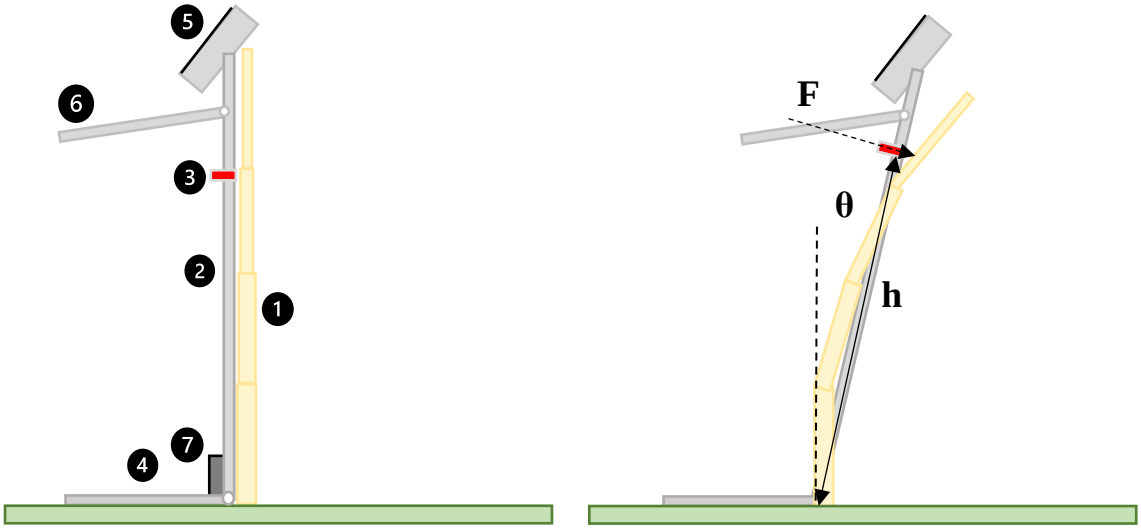

Figure 6: The DARLING's hardware and the definition of its input measurements. At the start of each test, the user places the DARLING adjacent to a vertical stalk (1) with the main tube vertical (2) and the load cell contacting the stalk below the first node (3). Following this, the user secures the device footplate (4) inputs load cell height (h) info into the UI (5) and grabs the handle (6) to begin the test. After the test begins, the DARLING is pushed forward while continuously measuring applied force (F) via a load cell (3) and angular deflection (θ) via an angle sensor (7) for both the stiffness and strength measurement cycles (see figure 5: LEFT). Once both cycles are complete, the DARLING is retrieved back to vertical and moved to the next sample for testing.

Bending stiffness and bending strength require three input measurements: applied force (*F*), angular deflection (*theta*), and load cell height (*h*) used in equations *(1)*,*(2)* and *(3)*. The first two of these parameters are measured using a horizontal load cell and a rotary potentiometer (Figure 7:1-2 respectively). The load cell mounts to an aluminum tube which slides on the main tube which features an engraved ruler (Figure 7-3). The ruler allows for the third parameter, load cell height, to be recorded manually. The load cell and potentiometer are wired to the data management system where an Arduino and a Raspberry Pi calculate and store the measurements. Once a test is complete, the resultant measurements are plotted and displayed to the user for quality confirmation and the addition of meta data.

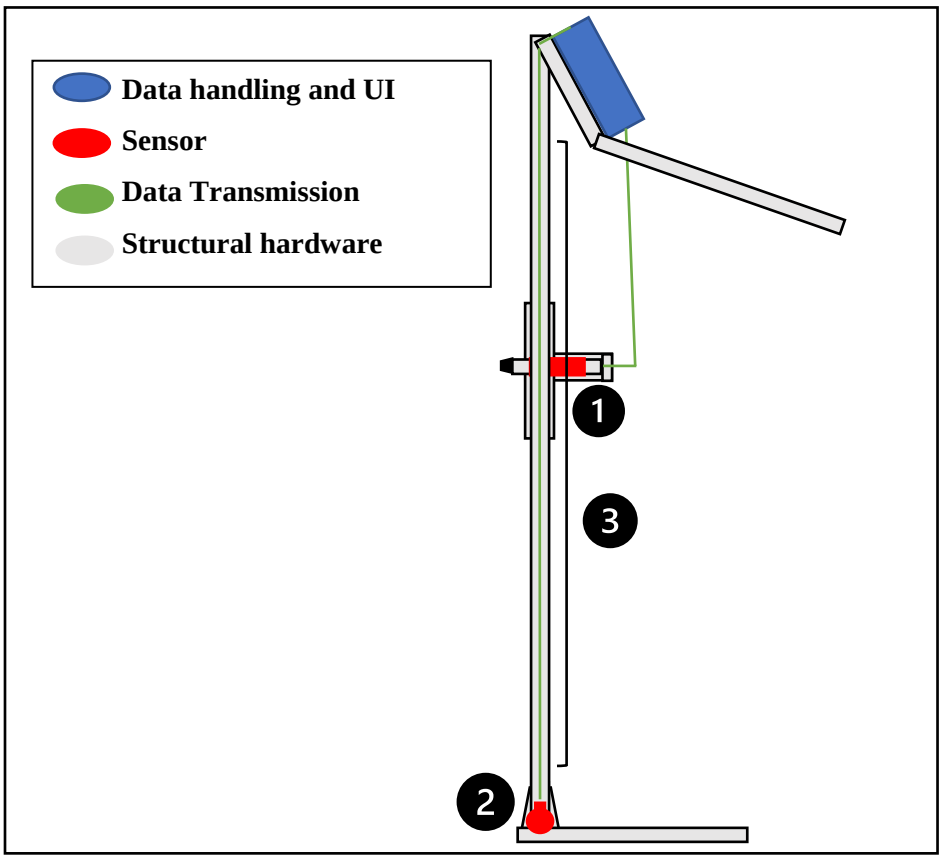

Figure 7: A diagram showing the arrangement of critical sensors and the data transmission path.

The DARLING was designed to measure stalk bending stiffness and bending strength with high accuracy and throughput at low cost. The accuracy of the DARLING was validated by measuring stiffness and strength in the field and comparing these measurements to lab stiffness and strength measurements of the same set of specimens. The results of that comparison showed minimal difference between the DARLING and lab measurements [26]. The throughput of the DARLING averaged 210 stalks/hr which was an acceptable speed for field-measurement. In terms of cost, the device is 80% cheaper than a testing machine utilized for laboratory measurement of the same quantities [36].

1.6 Research Objective: DARLING Three-Faceted Development Approach

The long-term goal of the DARLING project is to widely distribute the device to parties involved in crop improvement (farmers, seed companies, researchers etc.). With access to testing tools like the DARLING, those groups will be able to collect larger amounts of data and collaborate to discover correlations between factors controlled through genetic improvement. This collaboration will

significantly accelerate the genetic improvement process. As these correlations are understood, seed companies and researchers will be able to develop corn varieties with increased lodging resistance.

The most effective way to meet this goal is to sell the DARLING commercially. To be sold commercially, the DARLING must meet basic requirements of reliability, cost, quality, and feature options. In order to advance the DARLING toward this goal, three facets were addressed: improvement of the current design, development of a "Lite" DARLING, and experimental error analysis of the DARLING's measurements. After making these improvements, the DARLING is more prepared for deployment as a commercial product.

Chapter 2: DARLING Mechanical Design Improvement

2.1 Iterative Design Improvement Methodology

The first facet of DARLING development is improving the original design for large-scale distribution. Specific practices from three categories guided design improvement: reliability improvement, design for manufacturing, and design for assembly. Examples of these practices are described in Table 1. Applying these practices to each of the DARLING's subassemblies through iterative design changes significantly improved the design. The DARLING consists of four subassemblies: a supportive frame, data management system, applied force measurement system, and angular rotation measurement system. Additionally, a new subassembly was added which measures load cell height automatically. The design details of this subassembly and the modifications made to the data management system, applied force measurement, and angular rotations measurement subsystems are given in the following sections. The remaining subassembly, the frame, underwent minimal changes and a detailed description of subassembly improvements is not given.

Table 1: Practices for improving the DARLING for large scale distribution. Some practices, such as part count reduction, improve multiple areas of the design (i.e., reliability, manufacturability, and assembly), while other practices are area specific (i.e., reducing manufacturing steps). Implementing these proven practices increases the reliability, manufacturability, and assembly process of the design in addition to improving quality and appearance and reducing cost.

Design for reliability practices	
1	Reduce part count
2	Reduce fastener count
3	Eliminate failure modes
4	Reduce failure mode severity
Design for manufacturing practice	
1	Reduce part count
2	Reduce manufacturing steps
3	Optimize design for manufacturing process
4	Incorporate manufacturing process considerate tolerancing
Design for assembly practices	
1	Reduce part count
2	Reduce fastener count
3	Reduce assembly time
4	Reduce assembly steps
5	Reduce incorrect assembly opportunities

2.2 Load Cell Height Measurement System.

2.2.1 System Introduction

Improving existing features in three of the four subassemblies facilitated significant improvement in the reliability, manufacturability, and assembly process of the DARLING. In most cases, optimizing or eliminating components yields advances. However, the load cell height measurement system required an alternative approach. In the original design, the load cell bolted to an aluminum tube that moved vertically along the main frame tube (Figure 5-3). An incremented ruler engraved into the main vertical tube provided manual measurement of load cell height relative to the ground. Although simple, this system proved susceptible to error which decreased the utility of the DARLING. User errors frequently occur when the load cell height was recorded incorrectly, or when the user neglected to update the load cell height value after changing it. Both situations introduced significant error into the measurements of bending stiffness and bending strength. Even minimal error in the load cell height ($\pm 1cm$) resulted in error as high as 3% in bending strength and 5% in bending stiffness. Chapter 4 goes into further detail evaluating the impacts of this error. Detecting or correcting this error was extremely challenging compared to rectifying other sources, and a design solution which eliminated manual inputs was required. The hardware utilized for angular rotation measurement had proved quite reliable and effective; employing a system with similar hardware would likely provide an equally reliable and effective solution. The requirements of this hypothetical system are outlaid in Table 2.

2.2.2 Height Sensor System Requirements

Height Measurement Sensor Requirements				
Functional	***Mechanical***	***Enviromental***	***Electrical***	***Cost***
Provide absolute position following initial calibration	Withstand 2-3 direct impacts if dropped without requiring repair	Withstand direct sunlight and 100+°C temperatures for up to 6 hours daily	Operate on 5V arduino output	Unit cost must not exceed $400
Measure 90 cm of travel	95% reliability rating for lifecycle of DARLING	Provide moderate dirt and moisture protection		
Measure height with +/-.5cm Accuracy	Cycle for 12 hours without downtime under normal use			
	Outside dimensions of sensor must not prevent DARLING from fitting inside hard case			
	Weight and location of sensor must not confound ergonomics of DARLING operation			

Table 2: Height measurement sensor requirements. The introduction of an additional system removes the need for user height measurement input. Several specific requirements provided the constraints for the design.

2.2.3 Height Sensor System Description

The height sensor removes the need for manual measurement of load cell height using a mechanical system. The new system is enclosed in a 3D printed casing (Figure 8-1) and measures the linear position of the sensor relative to a fixed point. Since the height sensor is attached to the load cell bracket, the distance of the load cell relative to an initial calibration point is indirectly measured. After proper calibration, this calculation accurately measures load cell height relative to an initial calibration point (i.e., the ground) without user intervention. To provide this calculation, the system's internal assembly converts the linear motion of the casing to rotational motion of a potentiometer shaft at the appropriate ratio and resolution. Whenever the casing moves with the load cell, a cable is either extended or retracted. This extending cable is wrapped around a primary spool (Figure 8-2) which rotates a worm gear connected to a rotary potentiometer (Figure 8-3). To retract the extending wire, the primary spool connects via another wrapped wire to a secondary spool (Figure 8-4). This secondary spool is sized to rotate significantly less than the primary spool and is connected to a coil spring (Figure 8-5). This coil spring tensions the primary spool thereby tensioning the extending wire and retracting it when moving back towards where the wire is anchored. The gear ratio between the spool and the potentiometer is scaled so that the required length of cable extension (90 cm) rotates the potentiometer shaft 230 deg, well within its measurable range of 270 deg.

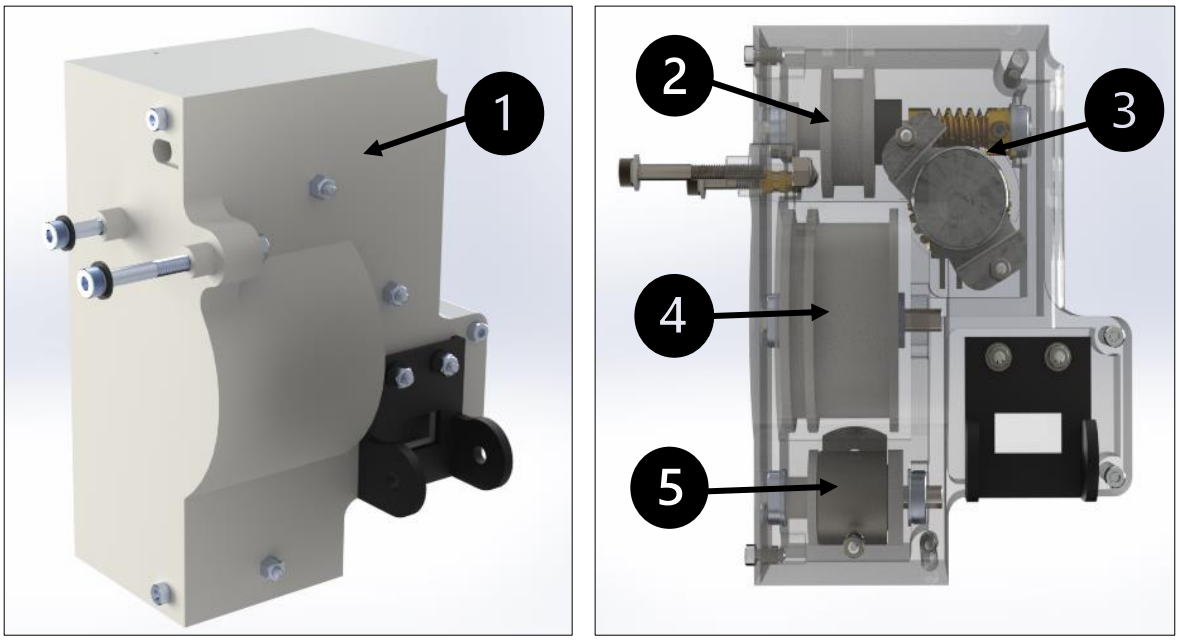

Figure 8: Height sensor external and internal views. The height sensor encloses a rotary potentiometer geared to a set of spring spools (2-5) in an ABS casing (1). By converting the linear motion of the casing to rotational motion of the potentiometer shaft, the height sensor automatically measures the distance of the sensor from an initial calibration point. This function allows for the automatic measurement of load cell height.

2.2.4 Height Sensor Design Evaluation

The design of the height sensor was sufficient to meet the requirements for implementation. After the development process, the design was rigorously tested in a manner representative of its future use in the field using an INSTRON universal testing machine. Both the quality of the recorded data over the course of testing, and the mechanical wear on the parts after testing was inspected. After analysis, there was no significant skew or calibration drift in the data, and the mechanical components showed acceptable wear for the lifecycle requirements. These results were sufficient to justify integrating a beta version of the height sensor system into the DARLING. Further evaluation and design improvement will be required to increase the performance and reliability of the design.

2.3 Data Management System

The data management system serves as the brain of the DARLING and contains the components required for data collection, display, and user interaction. The system consists of an ABS casing, ABS lid, LCD screen, and navigation buttons (Figure 9: 1,2,3 & 4 respectively). Inside the casing is a Raspberry Pi and an Arduino microcontroller to collect, process, and store data. The LCD screen and mechanical buttons allow the user to view and edit the data. Using a double t-nut (Figure 9-5), the casing mounts to a slotted rail with a front facing handle (Figure 9-6). A rigid bracket mounts

the casing and handle to the frame (Figure 9-7). Of all the subassemblies, the original data management system's reliability, manufacturing, and assembly shortcomings comprised most of the DARLING's design challenges. Specifications described by the table in Figure 9 reflect the original design's reliability, manufacturing, and assembly challenges. Specification tables like this one are used to describe the designs of the data management system and the remaining subsystems. The specifications of each nature were calculated the same way for each design. Manufacturing steps were grouped as processes involving a single machine, such as "3D print components" or "Cut tubing" or "Drill and tap holes," etc. Assembly time was estimated by consulting individual and collective experiences of lab workers. Assembly steps are calculated as a process involving a single part such as, "wire in button", or "attach and tighten casing."

In addition to addressing specification challenges, the redesign focused on reducing critical failure modes to improve reliability. Through three successive iterations, the specification challenges and critical failure modes were addressed. Table 3 describes failure modes of the data management system and the progression of how they were eliminated through iterative design modifications. The rows of Table 3 describe the failure modes observed in the design. Four of these failure modes were present in the original design, but one was introduced in a later iteration because of a design modification. The columns of Table 3 represent each iteration, and the fill color of each row in the column indicates whether the failure mode is present in that iterative design. The text within each cell clarifies changes in fill color.

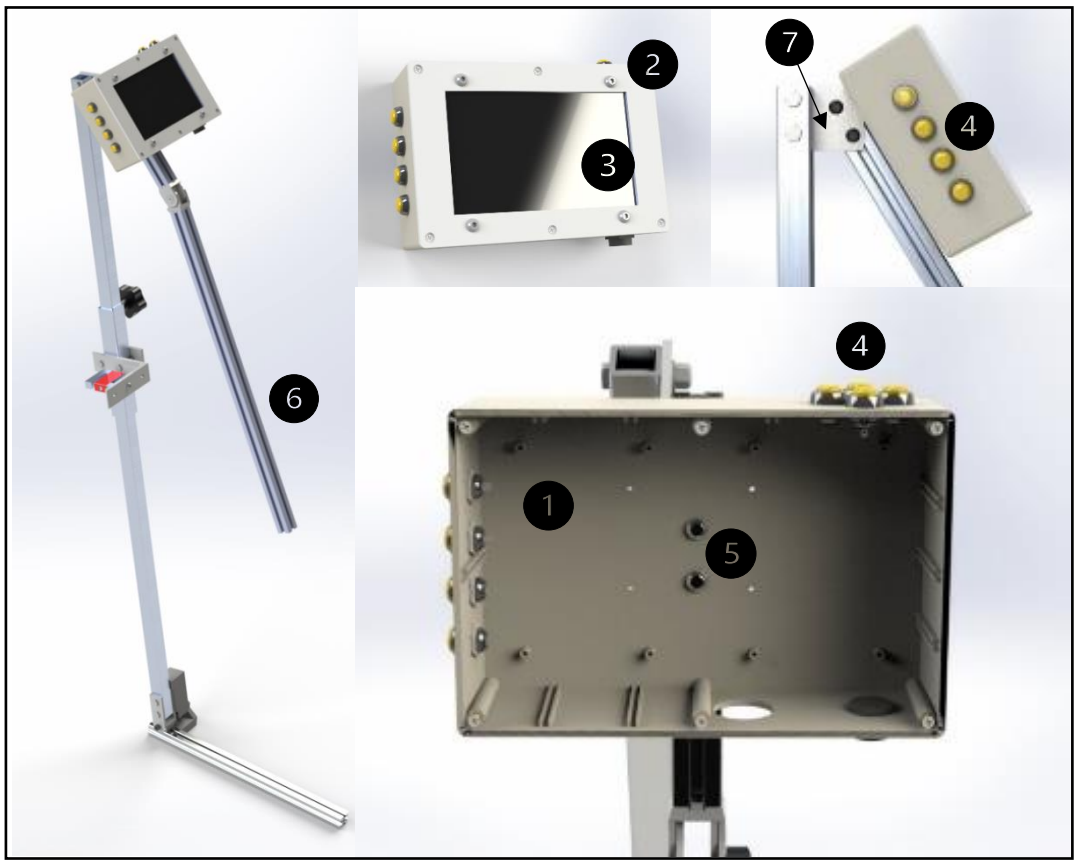

Original Design Specifications	
Reliability Specifications	
Part Count	*19*
Fastener Count	*22*
Critical Failure Modes	*4*
Manufacturing Specifications	
Manufacturing Steps	*6*
Assembly Specifications	
Assembly Time (hrs)	*2.5*
Assembly Steps	*16*

Figure 9: Data management system original design. The specifications for the design were calculated prior to the redesign. Many of the specifications are intuitive, but some require elaboration. Critical failure modes were observed in field testing and described in table 3. Manufacturing steps were grouped as processes involving one machine, such as "3D print components" or, "Cut tubing" or "Drill holes" etc. Assembly time was estimated through consulting individual and collective experience of lab workers. Assembly steps are grouped like manufacturing steps, examples include "Install and wire button", or "fasten mounting t-nut to handle" etc.

Critical Failure Modes Addressed	**Original Design**	**Iteration 1**	**Iteration 2**	**Iteration 3**
Failure During Transportation		Collapsible Mounting bracket replaces rigid bracket		
User Interface Failure			Touch screen replaced mechanical buttons	
Casing Mounting Connection Failure			Notched collapsible bracket replaced t-slot mounting connection	
Casing Impact Failure			Improved material and reinforced casing design	
Collapsible Bracket Impact Failure		Collapsible mounting bracket replaces rigid bracket, the collapsible bracket is vulnerable to impact failure	Notched collapsible bracket introduced but requires reinforcement	Notched collapsible bracket reinforced

Table 3: Failure modes and the iterations at which they were introduced or addressed. Red fill indicates that the failure mode is present in that iteration of the design. Yellow fill indicates that an unsuccessful or a partial attempt was made to address the failure mode and that the failure mode is still present in that iteration. No fill indicates that the failure mode was effectively addressed and is not present for that iterative design.

2.3.1 Data management system 1st Iterative Design

The first iteration implemented a collapsible mounting connection shown in Figure 10. This mounting connection consisted of 3D-printed brackets (Figure 10-1) and a removable hitch pin (Figure 10-2) which allowed the casing to lay flat during travel by pivoting at the frame when the hitch pin is removed. When laid flat, the DARLING's profile was slim enough to fit into a hard case. Using a protective case removed the critical failure mode of transportation damage. However, the replacement of the rigid metal bracket with a 3D-printed bracket introduced an impact failure mode for the bracket as described in Table 3. Table 4 describes the features of different thermoplastics and the reasoning

behind the selection of nylon for the mounting bracket and the remainder of 3D printed parts employed in the DARLING design.

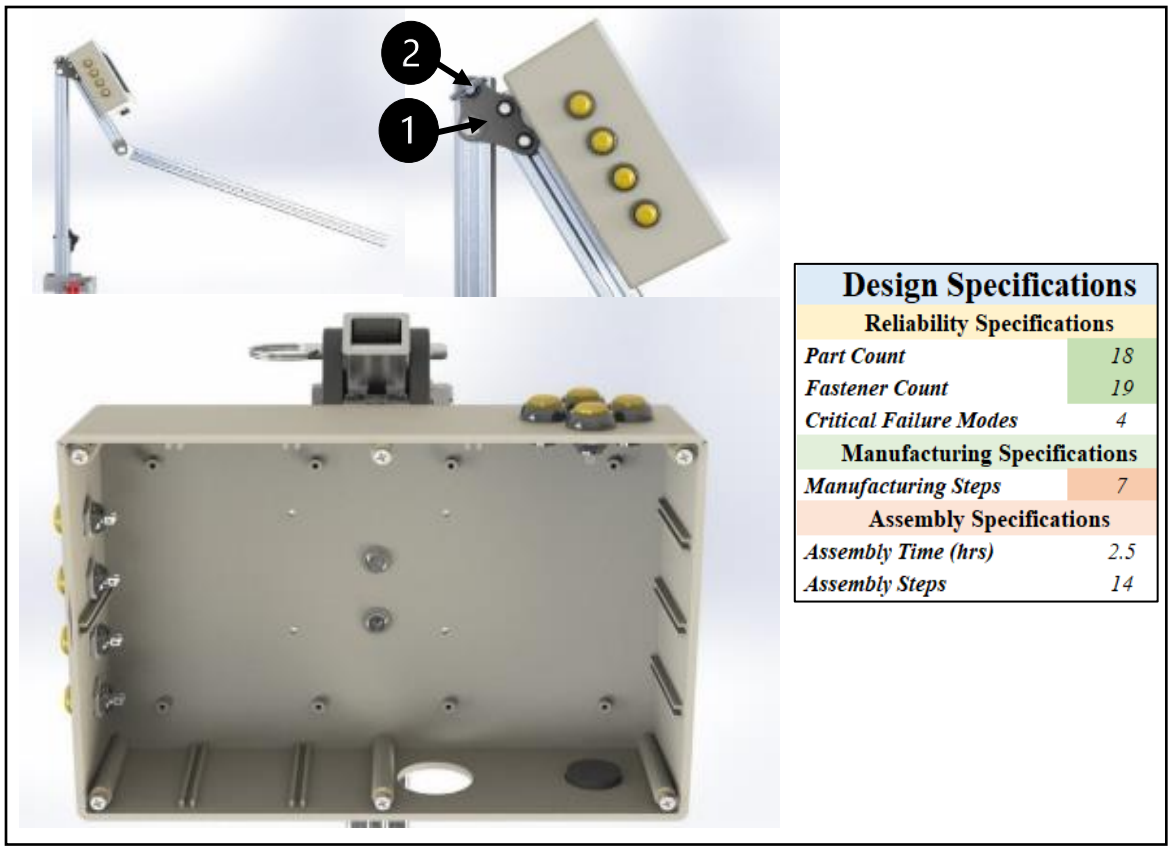

Figure 10: First revision of the casing design and its respective design specifications: green fill in the specification table indicates a positive change, and red fill indicates a negative, or retrogressive change. No fill indicates no change.

Table 4: Properties of AM thermoplastic materials. An in-use field application requires high toughness, durability, and impact resistance. Extensive exposure to the hot sun also demands excellent heat and UV resistance. Tight budgets require minimal material costs. The original ABS casing has moderate, but insufficient durability, toughness, heat resistance and impact resistance. After prototyping and testing several materials using 3D printed samples, Nylon 6 was selected for the casing material. Carbon filled nylon outperformed nylon but was unnecessarily expensive.

Thermoplastic Material Properties					
	Material				
Property	ABS	PLA	PETG	Nylon	Carbon Filled Nylon
Strength					
Stiffness					
Durability					
Toughness					
Heat Resistance					
Impact Resistance					
Material Cost					

2.3.2 Data management system 2nd Iterative Design

The second iteration replaced the ABS casing and lid with a 3D-printed nylon design. This design utilized a notched mechanical connection for the casing mount, replacing the slotted rail t-nuts (Figure 11-1). The notched connection relies on gravitational force and a minimal amount of friction to join the components. A resistive touch screen replaced the mechanical buttons for the user interface. The handle, initially located under the center of the casing, was offset to the dominant side of the user to improve ergonomics, and further reduce the profile of the collapsed device (Figure 11-2). Finally, a cable chain with a clip-fit mount provided wire management and connection reliability without increasing the fastener count (Figure 11-3). Although the notched mounting connection consolidated the mounting bracket and casing mounting connection, the connection itself was unacceptably weak and did not resolve the mounting bracket failure mode. To further improve reliability, the mounting connection and casing required reinforcement.

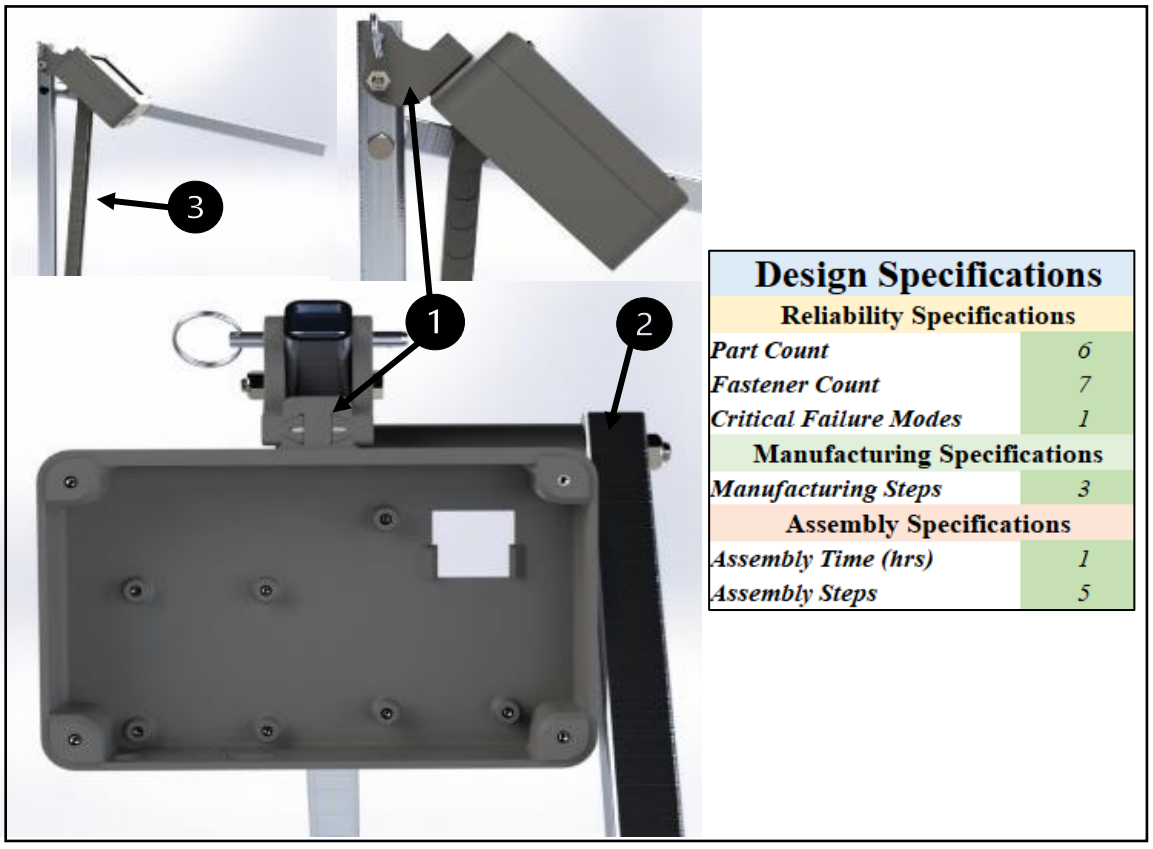

Figure 11: Second iteration of casing design and specifications. This iteration utilized a different material, manufacturing method, and reduced part count to provide UI and supportive hardware features. Green fill in the specification table indicates a positive change, and red fill indicates a negative, or retrogressive change. No fill indicates no change.

2.3.3 Data Management System Final Iterative Design

The final iteration of the casing utilized a reinforced notched joint (Figure 12-Circled). The upper wall of the casing encompasses the joint and the lid bolts into the area around the joint to better distribute impact force. The likelihood of joint failure is severely reduced but if the joint fails, the component which requires replacement is considerably cheap and straightforward to install. Figure 13 shows the final design compared to the original design.

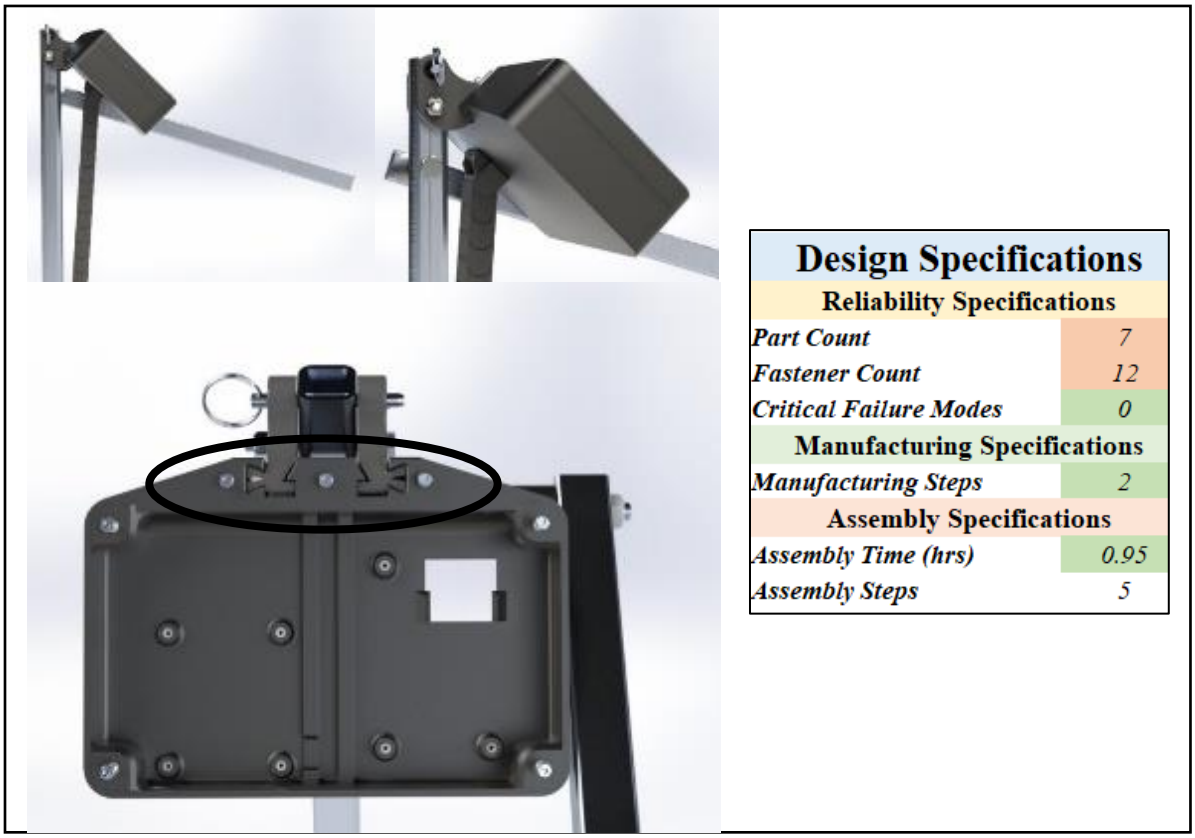

Design Specifications	
Reliability Specifications	
Part Count	*7*
Fastener Count	*12*
Critical Failure Modes	*0*
Manufacturing Specifications	
Manufacturing Steps	*2*
Assembly Specifications	
Assembly Time (hrs)	*0.95*
Assembly Steps	*5*

Figure 12: Final iteration of the casing design and specifications. No additional features are provided by this design, with the significant change being a reinforcement of the notched mounting joint. Green fill in the specification table indicates a positive change, and red fill indicates a

2.3.4 Data management system Original and Revised Design Comparison

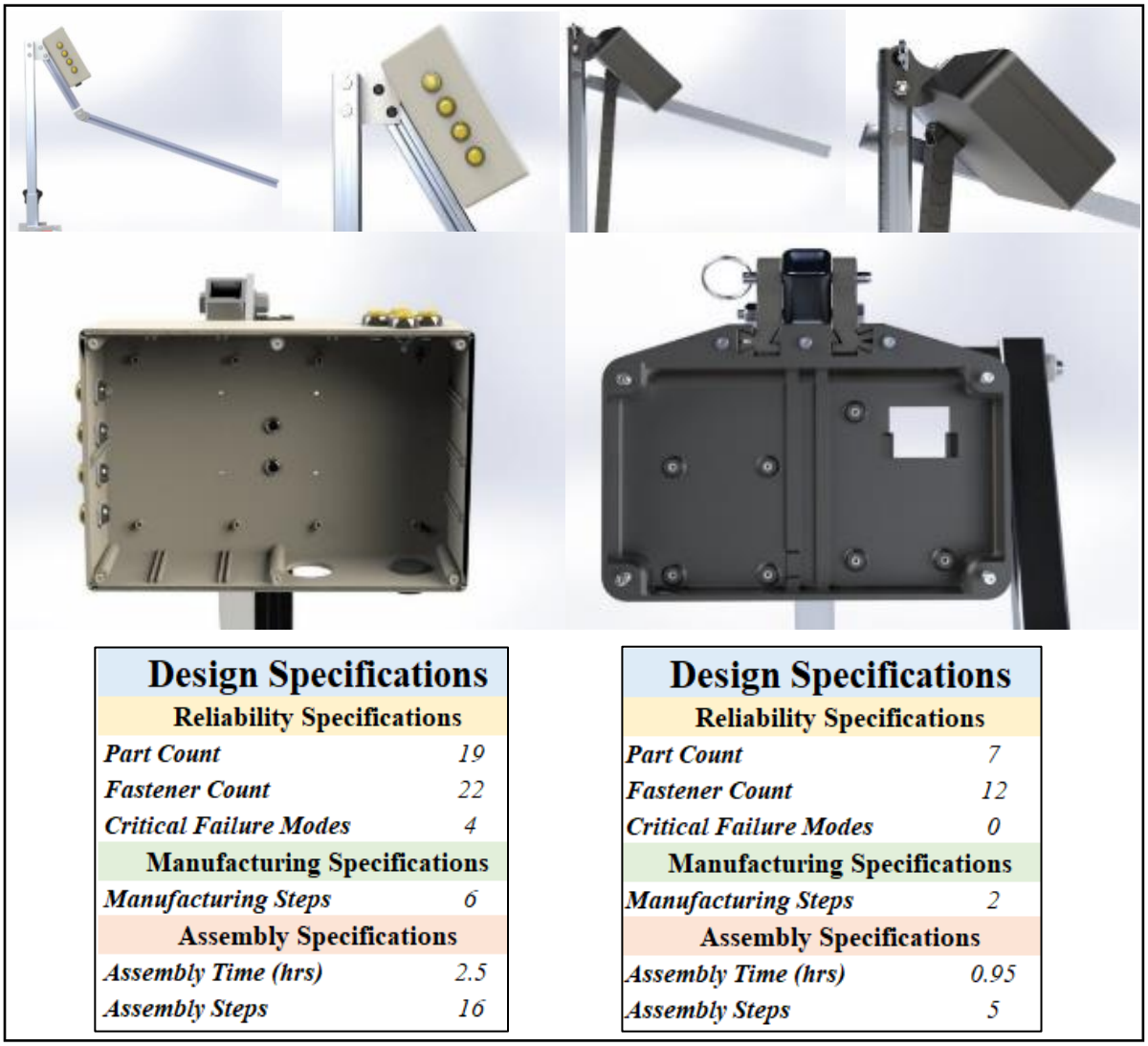

Design Specifications	
Reliability Specifications	
Part Count	19
Fastener Count	22
Critical Failure Modes	4
Manufacturing Specifications	
Manufacturing Steps	6
Assembly Specifications	
Assembly Time (hrs)	2.5
Assembly Steps	16

Design Specifications	
Reliability Specifications	
Part Count	7
Fastener Count	12
Critical Failure Modes	0
Manufacturing Specifications	
Manufacturing Steps	2
Assembly Specifications	
Assembly Time (hrs)	0.95
Assembly Steps	5

Figure 13: LEFT: Specifications of the original data management system design. RIGHT: Specifications of the revised data management system. Successive iteration produced a design with improved specification and significantly reduced failure modes. Through the scrutinizing of each component, most parts and fasteners were consolidated, replaced, or eliminated. This method, combined with other design practices resulted in an assembly of increased reliability and quality. Cost and lead time were also reduced, and the results are described at the end of this chapter.

2.4 Applied Force Measurement System

Applied force is utilized to calculate both bending stiffness and bending strength (see equations *(1)*and *(2)*). During each test, an s-beam load cell records the value of force continuously as it is applied to the specimen. Due to the design of the load cell, only forces along one axis can be accurately measured, thereby requiring the load cell to follow and remain normal to the stem as it rotates.

Additionally, the load must be applied at different heights depending on stem height to achieve optimal results. To fulfill these constraints, a bracket bolted to a sliding tube with adjustable height served as the mounting point for the load cell. Several reliability and manufacturing shortcomings of this design were addressed through application of the principles mentioned beforehand.

The original design of the applied force measurement system is rather straightforward. Two 3/8” hex bolts clamp an aluminum plate and L-bracket to a sliding aluminum tube (Figure 14-1). The inside dimensions of the sliding tube (Figure 14-2) are slightly larger than the outside dimensions of the upright frame beam, allowing the tube to freely slide for height adjustment. To lock the tube at the correct height during testing, a ¼”- hole for a threaded knob is drilled and tapped into the side of the sliding tube (Figure 14-3). When tightened, the threaded knob bites into the internal tube and secures the external tube. Despite its simplicity, there are several failure modes surrounding this design. First, the shallow hole in the aluminum sliding tube frequently strips and requires replacement of the sliding tube. The minimal available material and the clearance requirements to allow for sliding inhibited simple fixes. Second, the brackets securing the load cell often became misaligned if the device is dropped or the bolts loosen, which introduced error into load cell height measurement. Thirdly, the cable connecting the load cell to the data management system was not secured and often snagged on adjacent plants or the frame itself. This resulted in damage to the costly load cell, or damaged connections inside PCB of the data management system. To remedy these failure modes, several improvements were made and are addressed in the following sections. Table 5 describes the failure modes and their solutions in detail.

Table 5: Failure modes present in the original design and the method with which they were addressed in the final design. Red fill indicates that the failure mode is present in that iteration of the design. Yellow fill indicates that an unsuccessful or a partial attempt was made to address the failure mode and that the failure mode is still present in that it. No fill indicates that the failure mode was effectively addressed and is not present for that iterative design.

Critical Failure Modes Addressed	**Original Design**	**Final iteration**
Locking knob hole stripping		3D printed knob system implemented
Load cell bracket misalignment		Integral locknut and bolt system implemented
Cable snagging		Cable chain from bracket to data management system implemented.

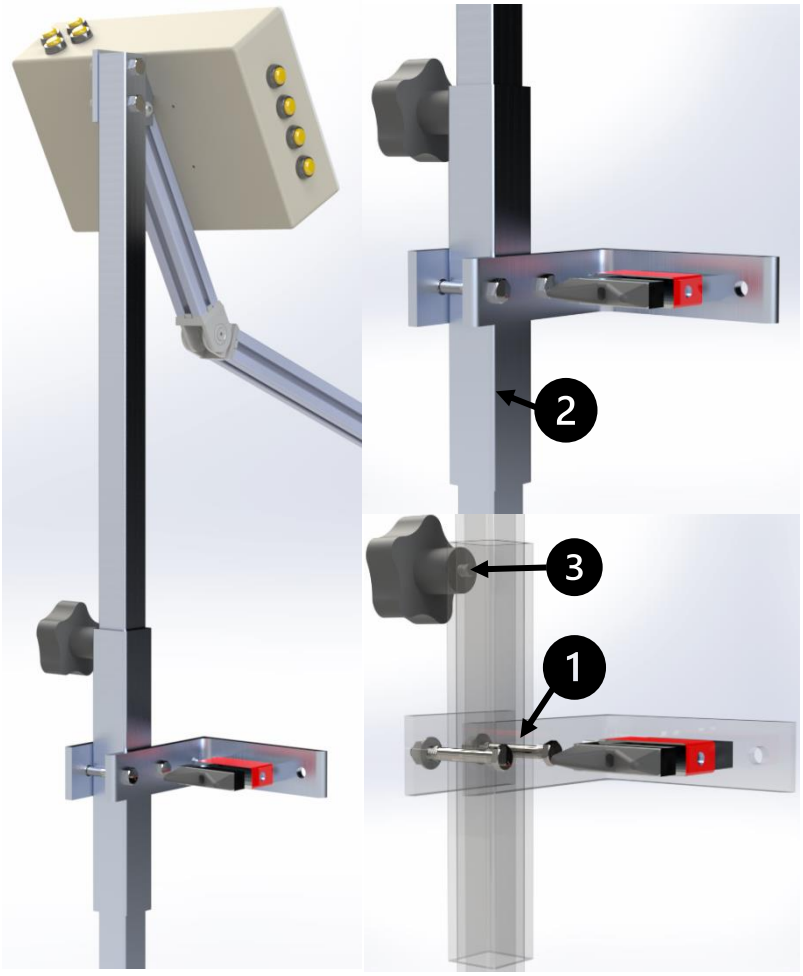

Design Specifications	
Reliability Specifications	
Part Count	*6*
Fastener Count	*2*
Critical Failure Modes	*2*
Manufacturing Specifications	
Manufacturing Steps	*2*
Assembly Specifications	
Assembly Time (hrs)	*0.5*
Assembly Steps	*4*

Figure 14: Original applied force measurement system and the three aspects of the design which introduced failure modes. Specifications for this design are shown in the table on the right.

2.4.1 Revised Applied Force Measurement System

All three failure modes were addressed in the improved applied force measurement system. A custom knob threading into an integrated steel hex nut improved the resilience of the tube securing system (Figure 15-1). Similar integrated lock nuts secured the load cell bracket to the sliding tube and eliminated opportunity for bracket misalignment (Figure 15-2). The integrated locknuts and hex nuts were fabricated by gluing the nuts into 3D printed inset pockets. Finally, a cable chain effectively guided the wiring for the height sensor and load cell into the data management system (Figure 15-3). The additional constraint of mounting the height sensor was met using a custom load cell bracket which allowed the height sensor to bolt directly to the assembly (Figure 15-4).

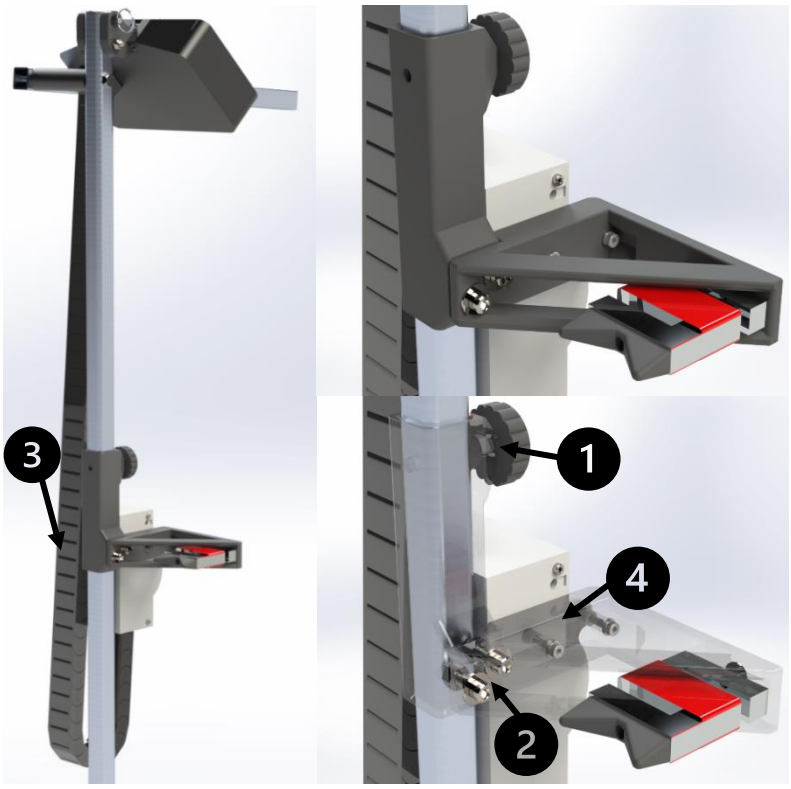

Design Specifications	
Reliability Specifications	
Part Count	*6*
Fastener Count	*5*
Critical Failure Modes	*0*
Manufacturing Specifications	
Manufacturing Steps	*1*
Assembly Specifications	
Assembly Time (hrs)	*0.25*
Assembly Steps	*3*

Figure 15: Improved applied force measurement system. Each failure mode mentioned in the original design description was addressed with this final iteration. Specifications related to other valuable criteria are described in the table above. Green fill in the specification table indicates a positive change, and red fill indicates a negative, or retrogressive change. No fill indicates no change.

2.4. Original and Revised Applied Force Measurement Systems

Figure 16 displays the original and improved design adjacent to each other. An increased number of fasteners was the most negative impact of the improved design. However, the improved design addressed the three critical failure modes of the original design and significantly improved the rest of the specifications related to reliability, manufacturability, and ease of assembly.

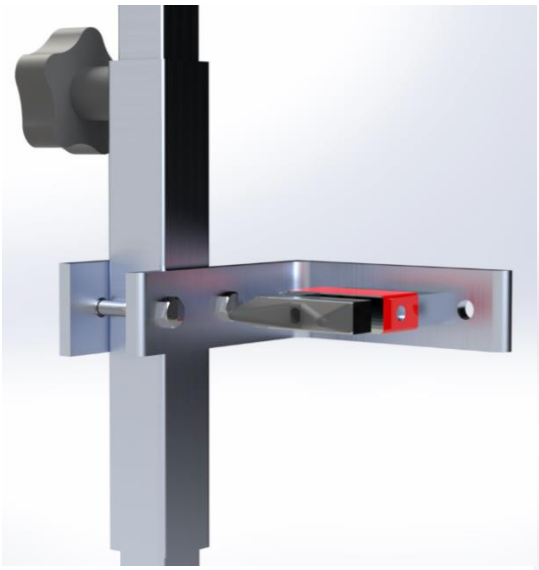

Design Specifications	
Reliability Specifications	
Part Count	*6*
Fastener Count	*2*
Critical Failure Modes	*2*
Manufacturing Specifications	
Manufacturing Steps	*2*
Assembly Specifications	
Assembly Time (hrs)	*0.5*
Assembly Steps	*4*

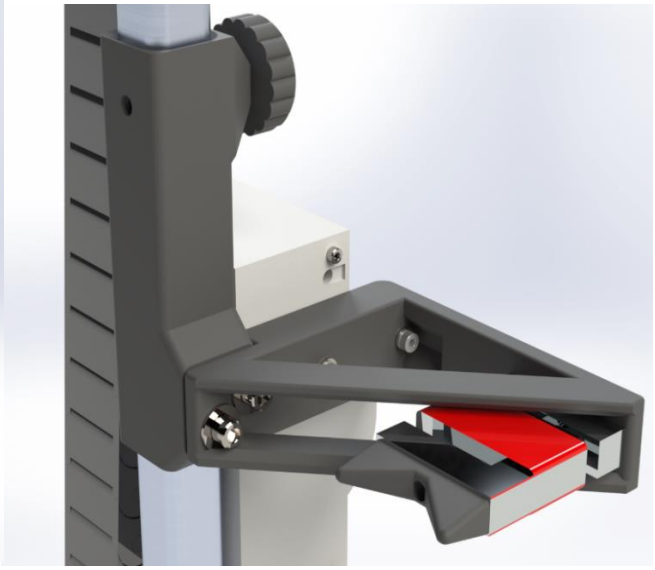

Design Specifications	
Reliability Specifications	
Part Count	*6*
Fastener Count	*5*
Critical Failure Modes	*0*
Manufacturing Specifications	
Manufacturing Steps	*1*
Assembly Specifications	
Assembly Time (hrs)	*0.25*
Assembly Steps	*3*

Figure 16: LEFT: The original design of the applied force measurement system and its specifications. RIGHT: The revised design with improved specifications.

2.5 Angular Deflection Measurement System

The angular deflection measurement subsystem records the angular position of the DARLING relative to the ground throughout each test. Differences in that vertical position throughout the test are used to calculate angular deflection (Figure 4: "θ"). In the original design, a rotary potentiometer measures angular displacement by mounting into several 3D-printed components which bolt to the frame and rotate via an 80-20 ® structural pivot (Figure 17). The potentiometer casing (Figure 17-2) secures the potentiometer body to the frame via two bolts and nylon locknuts. Those bolts also fix the structural pivot (Figure 20-3) and its flanges to the frame. To measure angular deflection, the potentiometer mount (Figure 17-4) fixes the potentiometer shaft relative to the footplate with a set screw and several t-nuts.

The system most often fails when the potentiometer is damaged, or the shaft is misaligned with the frame's axis of rotation. Either of these scenarios results in an incorrect angle measurement and often damages the sensor and casing. A frequent example of this failure mode is the progressive loosening of the pivot mounting bolt through normal use (Figure 17-5). Over time, the T-nut loosens and causes the pivot base and casing to rotate in the slotted rail. When the pivot rotates, the pivot axis and potentiometer shaft become misaligned relative to the potentiometer mount, resulting in damage to the sensor. In addition to this failure mode, the potentiometer can become damaged by the ingress of mud and dirt into the casing. These two specific failure modes and the metrics outlined in the design specification table provided the design focus for successive iteration. Several iterations produced a revised design with improved specifications and reduced failure modes (Table 6).

Critical Failure Modes Addressed	**Original Design**	**Final iteration**
Potentiometer Shaft Misalignment	Present	Base component integrating pivot axis and potentiometer shaft implemented
Dirt Ingress into Potentiometer	Present	Potentiometer casing cover implemented
Mechanical Pivot Loosening	Present	80-20 pivot replaced by shoulder bolt, sleeve bearing and lock nut pivot

Table 6: Critical failure modes present in the original angular deflection measurement system and the resultant solutions to eliminate failure modes. For concision, intermediate design iterations and their changes were excluded. Red fill indicates that the failure mode is present in that iteration of the design. Yellow fill indicates that an unsuccessful or a partial attempt was made to address the failure mode and that the failure mode is still present in that it. No fill indicates that the failure mode was effectively addressed and is not present for that iterative design.

Design Specifications	
Reliability Specifications	
Part Count	*6*
Fastener Count	*8*
Critical Failure Modes	*3*
Manufacturing Specifications	
Manufacturing Steps	*2*
Assembly Specifications	
Assembly Time (hrs)	*0.75*
Assembly Steps	*6*

Figure 17: Previous Angle Sensor Design. The location of assembly relative to the rest of the assembly (left) and the details of hardware placement (Right top/bottom).

2.5.1 Revised Angular Deflection Measurement System

The revised design utilizes a simplified assembly and a more reliable pivot joint. Four flanged bronze sleeve bearings (Figure 18-1) and a shoulder bolt with a nylon locknut (Figure 18-2) replace the structural pivot. One pair of bearings press fit into the aluminum frame, while the second pair glues into pockets of the mount (Figure 18-3). Alterations to the casing design include an alignment nub to replace one of the threaded fasteners and a clip-fit casing cover (Figure 18-4) to protect the potentiometer and strengthen the assembly. The revised angle sensor design eliminated three failure modes and offered improved specifications. In the new pivot design, the potentiometer shaft and the pivot shoulder bolt are located with a single component which prevents shaft and pivot axis misalignment. Additionally, the potentiometer casing is fully enclosed and protects the sensor from impacts and dirt ingress. Finally, the set of flanged sleeve bearings and a shoulder bolt provide a simple, reliable pivot assembly with minimal play and a prodigious cycle life. Figure 19 shows a side-by-side comparison of the original and improved designs.

Design Specifications	
Reliability Specifications	
Part Count	*4*
Fastener Count	*4*
Critical Failure Modes	*0*
Manufacturing Specifications	
Manufacturing Steps	*1*
Assembly Specifications	
Assembly Time (hrs)	*0.25*
Assembly Steps	*4*

Figure 18: Revised angle sensor assembly. Green fill in the specification table indicates a positive change, and red fill indicates a negative, or retrogressive change. No fill indicates no change.

2.5.2 Original and Revised Angular Deflection Measurement Systems

Design Specifications	
Reliability Specifications	
Part Count	6
Fastener Count	8
Critical Failure Modes	3
Manufacturing Specifications	
Manufacturing Steps	2
Assembly Specifications	
Assembly Time (hrs)	0.75
Assembly Steps	6

Design Specifications	
Reliability Specifications	
Part Count	4
Fastener Count	4
Critical Failure Modes	0
Manufacturing Specifications	
Manufacturing Steps	1
Assembly Specifications	
Assembly Time (hrs)	0.25
Assembly Steps	4

Figure 19: LEFT: The initial angular deflection measurement system and its specifications. RIGHT: The revised design and featuring improved specification. Through this revision, component counts, fastener counts, and assembly time were drastically reduced. Most importantly however, the revised design eliminated critical failure modes.

2.6 DARLING Design Improvement Summary

After extensive revision, the specifications of the DARLING changed significantly. Figure 20 displays the specifications of the original and revised DARLING designs. It is valuable to note that the addition of a height sensor significantly increased part count, fastener count, manufacturing time and assembly time. The system is worthwhile, but its introduction came at the cost of these specifications. Figure 21 reflect the significance of the height sensors hardware by excluding the system from critical calculations. Another apparent change is the increased lead and fabrication time in the revised design. These increased times are reflective of the quantity of 3D printed parts in the revised design. This choice of manufcturing method is appropriate for the phase of iterative design the DARLING is in now, but it results in a large amount of time required to fabricate a device from start to finish. Chapter 5 explains this tradeoff in more detail and addresses impending changes that will occur when the DARLING design becomes more permanent and production quantity increases. The cost calculations presented in each figure consider current fabrication and assembly labor costs.

Original DARLING design	Subassembly	Manufacturing Cost	Lead time (hrs)	Manufacturing Time (hrs)	Part Count	Fastener count	Critical Failure Modes	Manufacturing Steps	Assembly time (hrs)	Assembly steps
	Data Management System			2	19	22	4	6	2.5	16
	Applied Force Measurement System			4	6	2	2	2	0.5	4
	Angular Deflection Measurement System			12	6	8	3	2	0.75	6
	Frame			6	8	11	2	2	0.5	4
	SYSTEM TOTAL	$2,200.00	9	24	39	43	11	12	4.25	30

Revised DARLING Design	Subassembly	Manufacturing Cost	Lead time (hrs)	Manufacturing Time (hrs)	Part Count	Fastener count	Critical Failure Modes	Manufacturing Steps	Assembly time (hrs)	Assembly steps
	Data Management System	$692.99		19	7	12	0	2	0.95	5
	Applied Force Measurement System	$646.69		13.79	6	5	0	1	0.25	3
	Angular Deflection Measurement System	$137.26		9.825	4	4	0	1	0.25	4
	Load Cell Height Measurement System	$279.27		25	21	22	1	3	3	10
	Frame	$144.66		1	13	12	0	2	1.5	4
	SYSTEM TOTAL	$1,900.87	46.6	68.615	51	55	1	9	5.95	26

	Material Cost	Lead time (hrs)	Fabrication Time (hrs)	Part Count	Fastener count	Critical Failure Modes	Fabrication Steps	Assembly time (hrs)	Assembly steps
Revised Design Specifications Compared to Original Design Specifications	**-299$**	**+38**	**+45**	**+12**	**+12**	**-10**	**-3**	**+2**	**-4**
	-14%	**+418%**	**+186%**	**+31%**	**+28%**	**-91%**	**-25%**	**+40%**	**-13%**

*Figure 20: Design parameters of previous and revised DARLING subsystems **including** the height sensor subassembly. In the bottommost row positive progress is indicated with a negative number and negative progress with a positive number. It is important to note that the addition of the height sensor offset a significant amount of the work done to reduce component and fastener counts. Because the design of the height sensor is in the early stages of development, it has yet to be optimized. It is expected that with successive iterations significant improvement will be made in the areas used to quantify reliability, DFM and DFA progress.*

	Subassembly	Manufacturing Cost	Lead time (hrs)	Manufacturing Time (hrs)	Part Count	Fastener count	Critical Failure Modes	Manufacturing Steps	Assembly time (hrs)	Assembly steps
Original DARLING design	Data Management System			2	19	22	4	6	2.5	16
	Applied Force Measurement System			4	6	2	2	2	0.5	4
	Angular Deflection Measurement System			12	6	8	3	2	0.75	6
	Frame			6	8	11	2	2	0.5	4
	SYSTEM TOTAL	$2,200.00	9	24	39	43	11	12	4.25	30

	Subassembly	Manufacturing Cost	Lead time (hrs)	Manufacturing Time (hrs)	Part Count	Fastener count	Critical Failure Modes	Manufacturing Steps	Assembly time (hrs)	Assembly steps
Revised DARLING Design	Data Management System	$692.99		19	7	12	0	2	0.95	5
	Applied Force Measurement System	$646.69		13.79	6	5	0	1	0.25	3
	Angular Deflection Measurement System	$137.26		9.825	4	4	0	1	0.25	4
	Load Cell Height Measurement System									
	Frame	$144.66		1	13	12	0	2	1.5	4
	SYSTEM TOTAL	$1,621.60	46.6	43.615	30	33	0	6	2.95	16

	Unit Cost	Lead time (hrs)	Fabrication Time (hrs)	Part Count	Fastener count	Critical Failure Modes	Fabrication Steps	Assembly time (hrs)	Assembly steps
Revised Design Specifications Compared to Original Design Specifications	**-578$**	**+38**	**+20**	**-9**	**-10**	**-11**	**-6**	**-1**	**-14**
	-26%	**+418%**	**+82%**	**-23%**	**-23%**	**-100%**	**-50%**	**-31%**	**-47%**

Figure 21: Design parameters of previous and revised DARLING systems excluding the height sensor subassembly. In the bottommost row, positive progress is indicated with a negative number and negative progress with a positive number. This comparison serves to directly highlight the improves made to preexisting features without considering the additional complexity of new hardware which has yet to undergo optimization.

Chapter 3: DARLING Lite Development

3.1 Hardware Description of DARLING Lite

The DARLING accurately measures lodging correlative parameters with high resolution and throughput. However, such high resolution and accuracy are not required for all studies. Many research groups would prefer a more modular "Lite" version of the DARLING which could be made available at a lower price point. To accomplish this, we identified three separate modular, yet essential functions the DARLING must perform, namely: data management, bending strength measurement, and angular deflection measurement. These functions were combined into four different DARLING Lite configurations as shown in Figure 22. The paragraphs below describe each of these functional modules in more detail.

	Data Management Module		Bending Strength Module	Angular Deflection Module
	Option 1: *Wood Writing Desk*	**Option 2:** *Aluminum Clipboard*		
Configuration 1	✓	✗	✓	✓
Configuration 2	✗	✓	✓	✓
Configuration 3	✓	✗	✓	✗
Configuration 4	✗	✓	✓	✗

Figure 22: Configurations 1-4 and their module combinations.

3.1.1 Data Management Module

In the improved DARLING design, the data management system collects and stores specimen data. A custom PCB and Raspberry Pi process data, while a touch LCD screen allows the user to interact with the system. This design provides a seamless UI and rapid collection of a large amount of high-quality data. These features are ideal for studies with a large amount of data collection requiring high throughput. However, in the case of smaller-scale research projects, these features are unnecessary. A cheaper, independently functioning data collection module is significantly more justifiable in price and function. Switching to a manual data collection method facilitated these changes effectively. With this manual operation, the design of the hardware changed significantly.

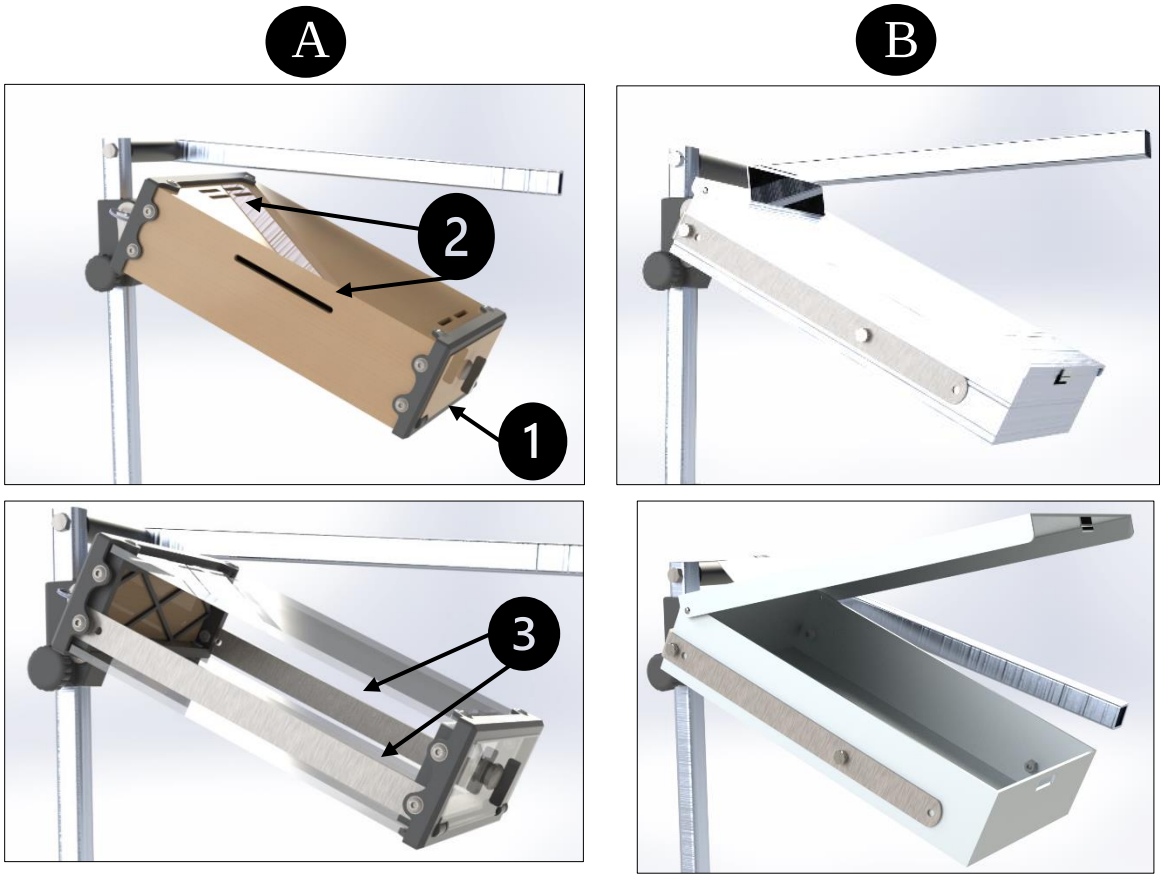

Design Specifications	
Reliability Specifications	
Component Count	15
Fastener Count	18
Critical Failure Mod	1
Low Reliability Faste	0
Manufacturing Specifications	
Manufacturing Steps	4
Manufacuturing Cos.	$154.35
Assembly Specifications	
Assembly Time (hrs)	1
Assembly Steps	8

Design Specifications	
Reliability Specifications	
Component Count	6
Fastener Count	6
Critical Failure Modes	2
Low Reliability Fasteners	0
Manufacturing Specifications	
Manufacturing Steps	4
Manufacuturing Costs	$92.86
Assembly Specifications	
Assembly Time (hrs)	0.3
Assembly Steps	4

Figure 23: LEFT: Data management module hardware options A. RIGHT: Hardware option B and its respective specifications. The unit cost measurements include all material, fabrication, and assembly related costs.

Manual data collection requires a robust flat writing surface with adequate area and storage. These requirements resulted in two options. The first option is a customizable writing desk composed of wood panels and 3D-printed components (Figure 23: Panel A). This option provides the user with extra storage and slots on the side and upper panels to mount sunshades, tablet stands, and other accessories (Figure 23: 1-2). Two stainless steel brackets tie the assembly together and mount to the

sliding tube system (Figure 23-3). Distinct features of this option are easily customizable dimensions, durability, serviceability, and reliability. The second option for the data collection module is an aluminum clipboard. (Figure 23: Panel B). As an alternative, the clipboard option is cheaper and straightforward to replace at the expense of durability and customization.

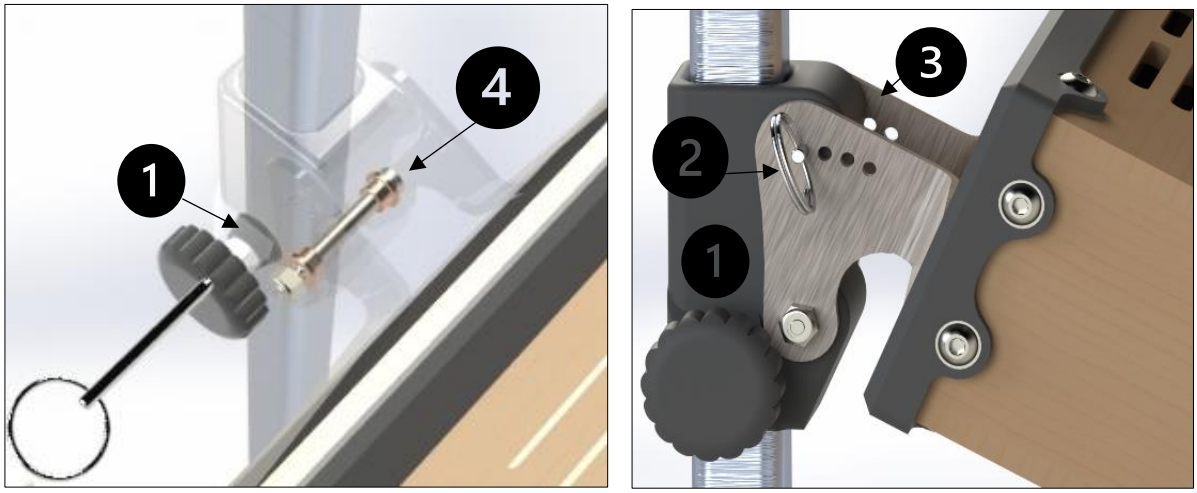

Figure 24: Detailed view of the data management module and adjustment hardware.

It is valuable to note that both these options have customization of height and writing surface angle to serve a variety of user statures. The vertical height of the writing surface adjusts via the 3D-printed sliding tube and knob system and the horizontal angle of the surface can be adjusted via the position of a quick-release pin in the sheet metal connecting bracket (Figure 24:1-3). The writing surface and bracket assembly pivot on the sliding tube using a sleeve bearing and shoulder bolt system like the angle sensor pivot (Figure 24-4).

In this case, the most impactful design decision was the change to manual data recording and collection. While a single operator can perform manual collection, many smaller studies can increase throughput by temporarily employing two operators per device. In most cases, however, the performance achieved with a single operator is sufficient for the demands of smaller-scale studies. In addition to simplifying the design by altering the data collection method, the redesigned system functions as a standalone module. Implementing modularity and simplification resulted in an independently functioning data management system at 13.4% of the cost of the DARLING's original system. This revised system also offered appropriate performance, and increased durability and serviceability.

3.1.2 Bending Strength Measurement Module

The DARLING Lite's second essential function is measuring bending strength. Bending strength calculation requires applied normal force and load cell height measurement. An S-beam load cell measures force applied by the DARLING, and the absolute height sensor measures load cell height. This combination of hardware offers accurate, detailed data with high throughput, but it is not required by all research groups. The DARLING lite requires a modular, simpler version of this system.

The DARLING Lite's bending strength measurement system utilizes a readily available force gauge bolted to a low-profile 3D printed plate (Figure 26:1-2). This plate notches into the grooved channel of the gauge bracket and is secured by a compliant tab (Figure 26-3). The gauge bracket bolts to a sliding tube and knob assembly secured with a notched mechanical joint (Figure 26-4). Before each test, a ruler engraved into the frame provides load cell height measurement with a design identical to the original DARLING load cell height measurement system. Although this design may allow for user error, it was the best available option as the DARLING Lite's data collection module can't support a system like the height sensor introduced in chapter 2. This requirement of user input agrees with the DARLING Lite's design intent however, as other aspects of the design require increased attention to detail during operation.

Figure 25: Force gauge options. LEFT: Low accuracy gauge of +/- 1% on the RIGHT: A high accuracy gauge of +/- 0.2% .

The simplified design consolidates applied force measurement and the UI into one independent piece of hardware with two accuracy levels. The readily available force gauge replaces the load cell

and measures, temporarily stores, and displays the max measured force after each test (Figure 25). The low and high accuracy gauges measure force with an accuracy of +/-1% and +/-0.2% respectively, both feature a 500N measurement range and a resolution of 0.1N [37],[38]. While the original S-beam load cell had much higher accuracy and resolution [39], specifications of this lower level are appropriate for most studies, and two accuracy levels allow groups to select an appropriate sensor for the chosen study. The less sensitive sensor is also more resistant to calibration drift and noise, and it removes the need for supportive electronics and system interdependence.

Developing a Lite version required that performance would be impacted. Reduced accuracy, and lower throughput results from the manual recording of the values between tests. Additionally, the force gauge requires increased attention to detail as it has no significant device memory and only temporarily stores the values. If a technician fails to correctly record the peak force values following each test, then the data is lost and the sample no longer testable. The drastically reduced cost and complexity of the system outweighed these tradeoffs for this application.

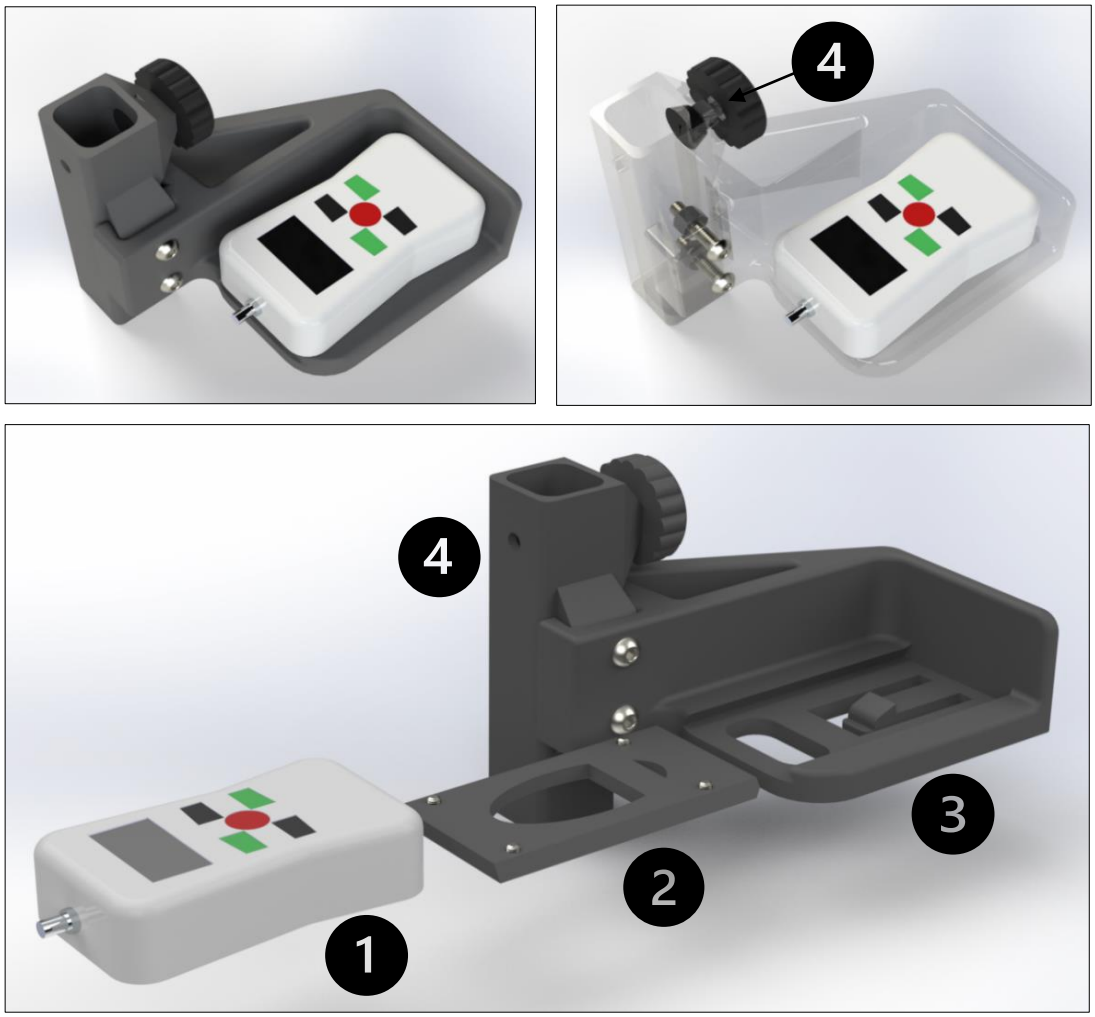

Low Accuracy Force Gauge Specifications	
Reliability Specifications	
Component Count	6
Fastener Count	7
Critical Failure Modes	1
Low Reliability Fasteners	0
Manufacturing Specifications	
Manufacturing Steps	1
Manufacuturing Costs	$167.51
Assembly Specifications	
Assembly Time (hrs)	0.25
Assembly Steps	4

High Accuracy Force Gauge Specifications	
Reliability Specifications	
Component Count	6
Fastener Count	7
Critical Failure Mode	1
Low Reliability Faster	0
Manufacturing Specifications	
Manufacturing Steps	1
Manufacuturing Cost:	$235.01
Assembly Specifications	
Assembly Time (hrs)	0.25
Assembly Steps	4

Figure 26: Force gauge subassembly used for applied force measurement. The unit cost measurements include all material, fabrication, and assembly related costs.

3.1.3 Angular Deflection Measurement Module

The quantity of bending stiffness shares two measured inputs with bending strength but requires the additional measurement of horizontal deflection. In the DARLING, a rotary potentiometer and the supportive electronic hardware provided measurement of angular deflection, which is used in

combination with load cell height to calculate horizontal deflection in equation *(3)*. The DARLING Lite bending strength module records applied force and load cell height, and the angular deflection measurement module records the additional measurement of angular deflection. The DARLING lite measures angular deflection using a needle and marked housing assembly akin to a protractor (Figure 27). In this assembly, a set of steel rods (Figure 27-6) guide a marked fin (Figure 27-2) into two sleeve bearings (Figure 27-7) which are glued into the base component (Figure 27-1). In addition to ensuring the system is aligned, the guide rods stiffen the assembly. An integral knob (Figure 27-5) clasps the system together by threading into a captive nut glued into the base (Figure 27-9). A shoulder bolt and sleeve bearing system allows the assembly to pivot while a needle (Figure 27-3) rotates co-axially to the assembly on an independent ball bearing (Figure 27-8). At the start of each test, the device rotates forward and a small, flanged plate (Figure 27-4) pushes the needle forward, stranding it at the maximum angular rotation value when the frame rotates backwards after the test is complete. Numbered angular increments provide measurement of the max angular deflection value after each test. Once the test is recorded, a protruding, foot operated flange allows the operator to reset the system prior to the next test.

The revised hardware is quite distant from the original high-level design. Horizontal deflection is still measured through angular deflection, but the angular deflection measurement is manually recorded. For some studies, however, bending stiffness and therefore, angular deflection, are not required measurements. Even if angular deflection is not needed, the footplate and mechanical pivot are still required for the DARLING Lite to function correctly. To accommodate this, a “pivot only” version of the angular deflection measurement module without the marked fin or needle is offered in combination with the other modules (Figure 28). In its complete form, the angular deflection measurement module features tradeoff similar to the other two DARLING Lite modules. Implementing modularity provided a much simpler independent measurement tool with increased reliability and durability at reduced cost. Those factors came at the cost of resolution, measurement range, ease of use and throughput.

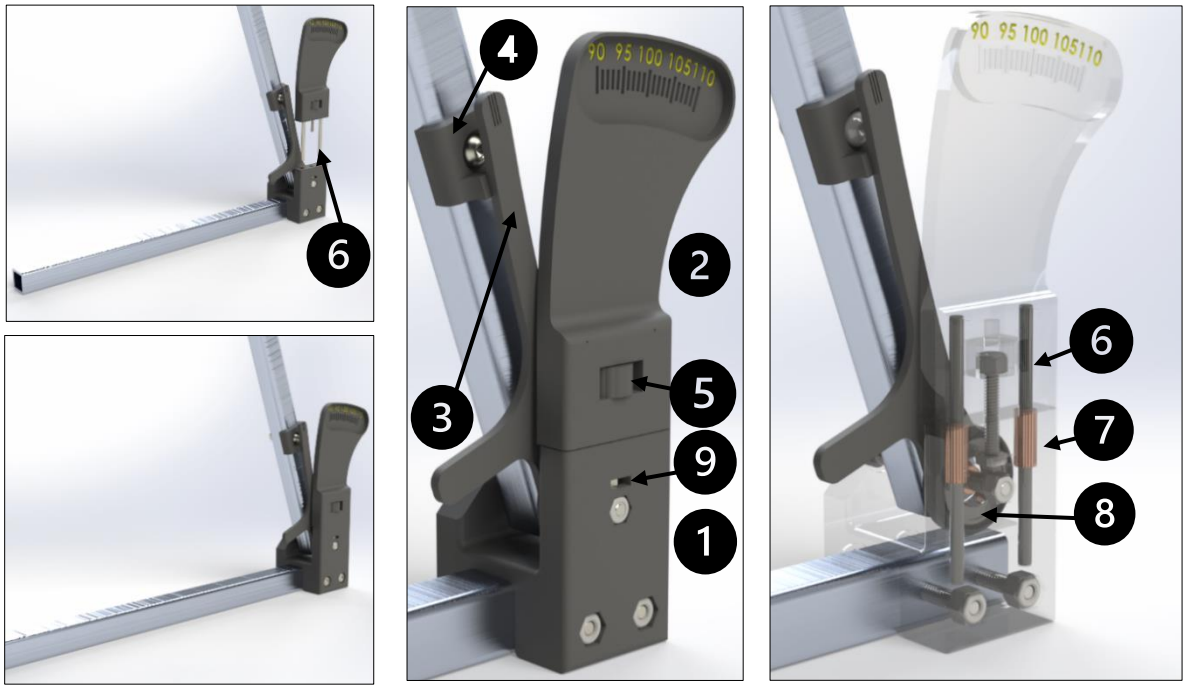

Deflection Gauge Specifications	
Reliability Specifications	
Component Count	13
Fastener Count	5
Critical Failure Modes	1
Low Reliability Fasteners	1
Manufacturing Specifications	
Manufacturing Steps	2
Manufacuturing Costs	$45.00
Assembly Specifications	
Assembly Time (hrs)	0.5
Assembly Steps	7

Deflection Gauge Specifications Pivot Only	
Reliability Specifications	
Component Count	8
Fastener Count	3
Critical Failure Modes	1
Low Reliability Fastener.	0
Manufacturing Specifications	
Manufacturing Steps	2
Manufacuturing Costs	$25.00
Assembly Specifications	
Assembly Time (hrs)	0.25
Assembly Steps	3

Figure 27: Angular deflection measurement system with specifications for both complete and pivot only configurations. The unit cost measurements include all material, fabrication, and assembly related costs.

3.2 Resultant Configurations of the DARLING Lite

After extensive redesign, the design of the DARLING Lite provided a cheaper, modular design with increased reliability and simplicity. Based on the requirements of the study, the modules combine to produce different options (Figure 28). A fully fabricated version of the configuration 1, the most extensive configuration, is shown in Figure 29.

Configuration 1 specifications	
Reliability Specifications	
Component Count	37
Fastener Count	33
Critical Failure Modes	3
Low Reliability Fasteners	1
Manufacturing Specifications	
Manufacturing Steps	7
Manufacuturing Costs	$434.36
Assembly Specifications	
Assembly Time (hrs)	1.75
Assembly Steps	19

Configuration 2 specifications	
Reliability Specifications	
Component Count	28
Fastener Count	21
Critical Failure Modes	3
Low Reliability Fasteners	1
Manufacturing Specifications	
Manufacturing Steps	7
Manufacturing Costs	$372.87
Assembly Specifications	
Assembly Time (hrs)	1.05
Assembly Steps	15

Configuration 3 specifications	
Reliability Specifications	
Component Count	32
Fastener Count	31
Critical Failure Modes	3
Low Reliability Fasteners	0
Manufacturing Specifications	
Manufacturing Steps	7
Manufacuturing Costs	$414.36
Assembly Specifications	
Assembly Time (hrs)	1.5
Assembly Steps	14

Configuration 4 specifications	
Reliability Specifications	
Component Count	23
Fastener Count	19
Critical Failure Modes	3
Low Reliability Fasteners	0
Manufacturing Specifications	
Manufacturing Steps	7
Manufacuturing Costs	$352.97
Assembly Specifications	
Assembly Time (hrs)	0.8
Assembly Steps	10

Figure 28: Configuration options for DARLING Lite. Each configuration offers a unique combination of measurement and data storage features. The unit cost information for each configuration considers the cost of the high accuracy force gauge. In addition to raw material and component costs, labor costs for manufacturing and assembly are also considered in the unit price calculations.

Figure 29: DARLING Lite configuration 1. Being the highest level of the configuration line, this combination provides a custom writing desk supported by bending strength measurement, and angular deflection measurement gauges.

3.3 Throughput evaluation and validation

Table 7 highlights the results of a process analysis for individual stalk measurement. the DARLING Lite had a throughput of 1 min 25s/ stalk compared to the high-end DARLING's throughput of 50s/stalk. This amounts to 41% lower throughput speed for the DARLING Lite.

Table 8: Throughput analysis results of the DARLING and DARLING Lite.

Operation Steps	**DARLING operation time (secs)**	**DARLING Lite operation time (secs)**
1) Device placement	20	20
2) Load cell height adjustment	5	5
3) Pre-test data entry	5	20
4) Stiffness Measurement	5	10
5) Bending Strength Measurement	5	10
6) Post-test data entry	10	20
Total Time:	**50 secs**	**1 min 25 secs**

3.4 Ergonomics Evaluation of DARLING Lite

During especially intense workdays, users will measure 250-350 stalks with the DARLING Lite. Several aspects of the DARLING Lite's design minimize strain on the user to reduce fatigue which can lead to incorrect operation. To reduce strain during operation and transportation, lightweight materials were implemented where possible and the modules are oriented so that they offer balanced movement during operation and a comfortable carrying position during transportation. Adjustability and customization also affect ergonomics. To reduce strain on the user, the height and angle of the writing desk adjust to fit a 1.53m height female (10% height percentile) and a 1.98m height male (90% height percentile)[40]. The height and angle adjustment hardware are described prior in Figure 24. The device can also accommodate right and left-handed users by switching the handle and exchanging the bending strength module. The final consideration for ergonomics was the placement of sensors and the kinetic operation movements. The orientation of the force gauge in the bending strength module allows the user to record measurements while standing upright. While the stiffness gauge in the bending stiffness module requires the user to crouch slightly beside the indicator and record the reading, a foot-operated reset tab prevents the user from bending over after each test.

3.5 Measurement Uncertainty Analysis

3.5.1 Uncertainty calculation method

To investigate the reliability of the data recorded by the DARLING Lite a measurement uncertainty analysis was conducted. To quantify lodging resistance, the DARLING and DARLING Lite measure two correlative quantities; Bending stiffness defined by equation *(1)* and bending strength defined by equation *(2)*. Because both quantities are a function of several inputs, uncertainty in these measured inputs propagates into resultant error as dictated in equation (4). Equation (4) combines partial derivates and measurement input errors utilizing the Root Sum Squares method to calculate resultant error [41].

$$R = f(x, y, z) \; and \;\; u_R = f(u_x, u_y, u_z) = \sqrt{\left[\left(\frac{\partial R}{\partial x} u_x\right)^2 + \left(\frac{\partial R}{\partial y} u_y\right)^2 + \left(\frac{\partial R}{\partial z} u_z\right)^2\right]} \qquad (4)$$

Design stage uncertainty was used to predict the uncertainty of the DARLING Lite measurements [41]. Although design stage uncertainty doesn't consider all sources of error it is an effective method to estimate the accuracy of the DARLING Lite's instruments (i.e., angle and force sensors). Design stage uncertainty is a function of both the zero-order uncertainty u_0 and the instrument uncertainty u_c [41]. Zero order uncertainty is calculated from instrument resolution, while instrument uncertainty is either given as a single value or as individual sources of error which require calculation [41]. Combining these two uncertainty values with the root sums squares method produces a unique design stage uncertainty value for each sensor as shown in equations (5)-(7). These sensor specific uncertainty values combine with partial derivatives of the equations [in this case, equations *(1)* and *(2)*] to produce a relative design stage uncertainty for the measurement using equation (4).

$$u_d = \sqrt{u_0^2 + u_c^2} \qquad (5)$$

$$u_0 = \frac{1}{2} \cdot (Sensor\ Resolution) \qquad (6)$$

$$u_c = \sqrt{u_1^2 + u_2^2 + u_3^2 + \cdots u_n^2} \qquad (7)$$

3.5.2 Uncertainty calculation for measured inputs

The measured inputs of applied force, load cell height (i.e., the applied moment arm), and angular deflection each possess unique uncertainties. In the bending strength module, uncertainties using both a low and a high accuracy force gauge were calculated. Each gauge provided the same measurement

resolution of 0.1 N. However, the low accuracy gauge possesses an instrument uncertainty of $\pm 1\%$ of measured value, and the high accuracy gauge possesses an instrument uncertainty $\pm 0.2\%$ of measured value. The respective design stage uncertainties of the low and high accuracy force gauges are shown in equations (8) and (9).

$$u_{FLac} = \sqrt{u_0^2 + u_c^2} = \sqrt{0.05^2 + (F * .01)^2} \tag{8}$$

$$u_{FHac} = \sqrt{u_0^2 + u_c^2} = \sqrt{0.05^2 + (F * .002)^2} \tag{9}$$

The design stage uncertainty in load cell height (u_L) is a product of the engraved ruler's resolution and fabrication process. Across its measurement range, the engraved ruler provides a resolution of 10 mm. Possible inaccuracies in the fabrication process produced an instrument uncertainty $\pm 2.5\ mm$. The resultant uncertainty in load cell height is shown in equation (10).

$$u_L = \sqrt{u_0^2 + u_c^2} = \sqrt{5^2 + 2.5^2} = \pm 5.6\ mm \tag{10}$$

The final measured input considered is the angular displacement used to calculate horizontal deflection. Marks at .5-degree increments provided a reasonably high resolution, and a fabrication accuracy estimation of +/- .05 deg generously accommodated error in the 3D printing process. These two values resulted in a design stage uncertainty defined by equation (11).

$$u_\theta = \sqrt{u_0^2 + u_c^2} = \sqrt{0.25^2 + 0.05^2} = \pm 0.26\ deg \tag{11}$$

The design stage uncertainties of the three input measurements propagate their error to the quantities of bending stiffness and bending strength. Considering the form of equations *(1)* and *(2)*, equation (4) results in equations (12) and (13) for uncertainty in stiffness and strength respectively. Once the derivatives of equation (4) are applied, the final uncertainty functions for a combination of measured inputs are produced (equations (15) and (16)).

$$U_{EI} = \sqrt{\left(\frac{\partial EI}{\partial \theta} u_\theta\right)^2 + \left(\frac{\partial EI}{\partial F} u_F\right)^2 + \left(\frac{\partial EI}{\partial L} u_L\right)^2} \tag{12}$$

$$U_s = \sqrt{\left(\frac{\partial S}{\partial F}u_F\right)^2 + \left(\frac{\partial S}{\partial L}u_L\right)^2} \tag{13}$$

Where

$$EI = \frac{FL^2}{3\sin(\theta)} \quad \text{and} \quad S = FL \tag{14}$$

Partial differential yields:

$$U_{EI} = \sqrt{\left(-\frac{FL^2\cos(\theta)}{3\sin^2(\theta)}u_\theta\right)^2 + \left(\frac{L^2}{3\sin(\theta)}u_F\right)^2 + \left(\frac{2FL}{3\sin(\theta)}u_L\right)^2} \tag{15}$$

And:

$$U_s = \sqrt{\left(Lu_f\right)^2 + (Fu_L)^2} \tag{16}$$

Equations (15) and (16) output the absolute design stage uncertainty for any given combination of input measurements. Relative uncertainty defined by equation (17) provides a less abstract, more general quantification and is found as a percentage of the original function [41].

$$U_{relative} = \frac{U_{Abs}}{F(x,y,z)} \tag{17}$$

Uncertainty for Input Combinations Across Measurement Range.

With the respective input uncertainties and the resultant uncertainty equations defined, it was necessary to identify which input uncertainties have the most significant impact on resultant uncertainty. Corn stalk bending stiffness and bending strength measurements typically encounter values of applied force, load cell height, and angular deflection within a certain range. The bounds of this measurement range defined the combinations of simulated values used to evaluate the impact input measurement uncertainty on resultant uncertainty. Within a given data set, applied force has limits of 1 to 100N. Values from .01N to 100N were evaluated to also consider minute outliers. Within that same set, angular deflection measurements range from 0.1 to 20 degrees. To also consider outliers in angular deflection, values from 0 rads to .35 rads (~20 degrees) were assessed. The remaining measurement, load cell height, ranges from 0.2m to 1.2m, these exact bounds were assessed. The uncertainty produced by combining these three measurements within the defined bounds was calculated for both bending

strength and bending stiffness. The resultant distribution of that uncertainty is shown in Figure 30-Figure 33.

Uncertainty in Bending Strength

Figure 30 and Figure 31 show the relative design stage uncertainties in bending strength as a function of a representative range of input measurements. These figures show the resultant uncertainty in bending strength for both the high and low accuracy force gauges, respectively. Two details become apparent from these plots. Firstly, exceptionally weak stalks experience the highest levels of design stage uncertainty reaching values of 5.5% for force gauges of both accuracies. Interestingly, the differences in accuracies were not significant enough to noticeably alter the uncertainty values. Considering this, the low resolution of 0.1N common to both force gauges likely has a bigger impact on uncertainty than force gauge accuracy. The second detail described by the plots is the less significant impact of load cell height measurement. Uncertainty in load cell height measurement plays a smaller role in error contribution as the uncertainty value relative to the magnitude of measured values is exceptionally small.

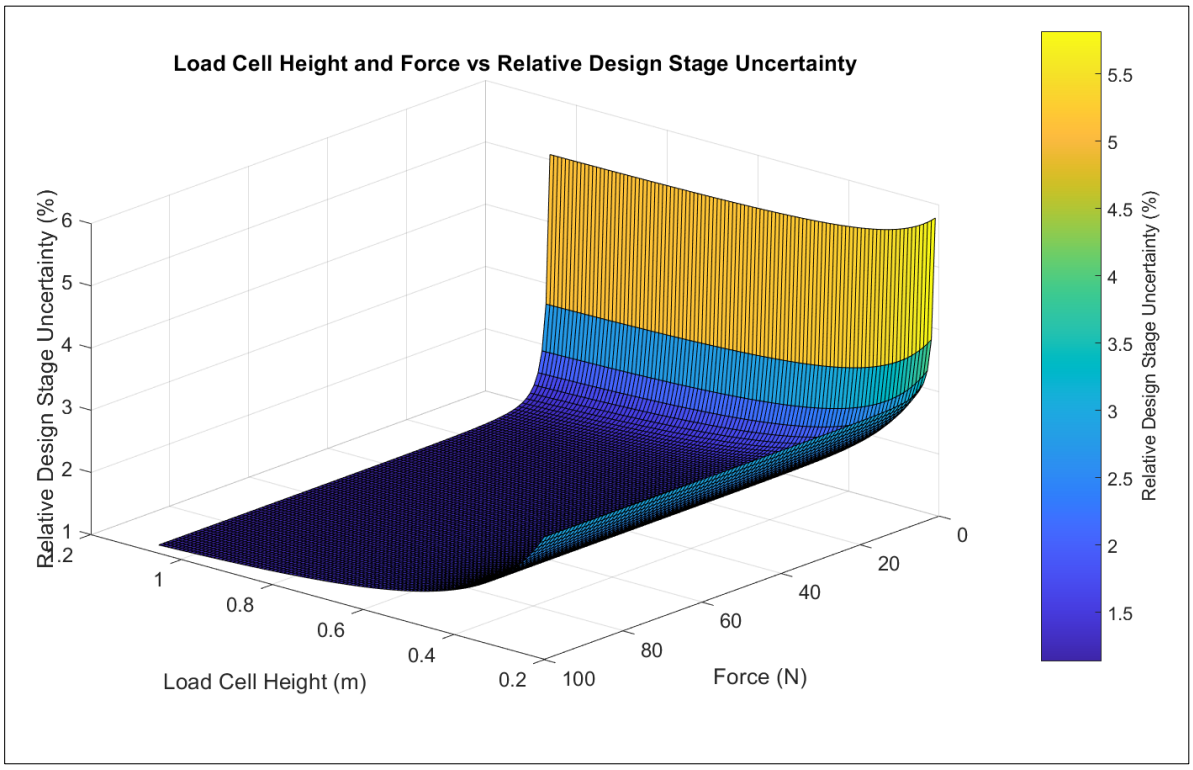

Figure 30: Design Stage Uncertainty in Strength for a high accuracy force gauge. Peak values in uncertainty arise for extremely small values of force and moment arm. The highest uncertainty values produced within the measurement range were 5.5%

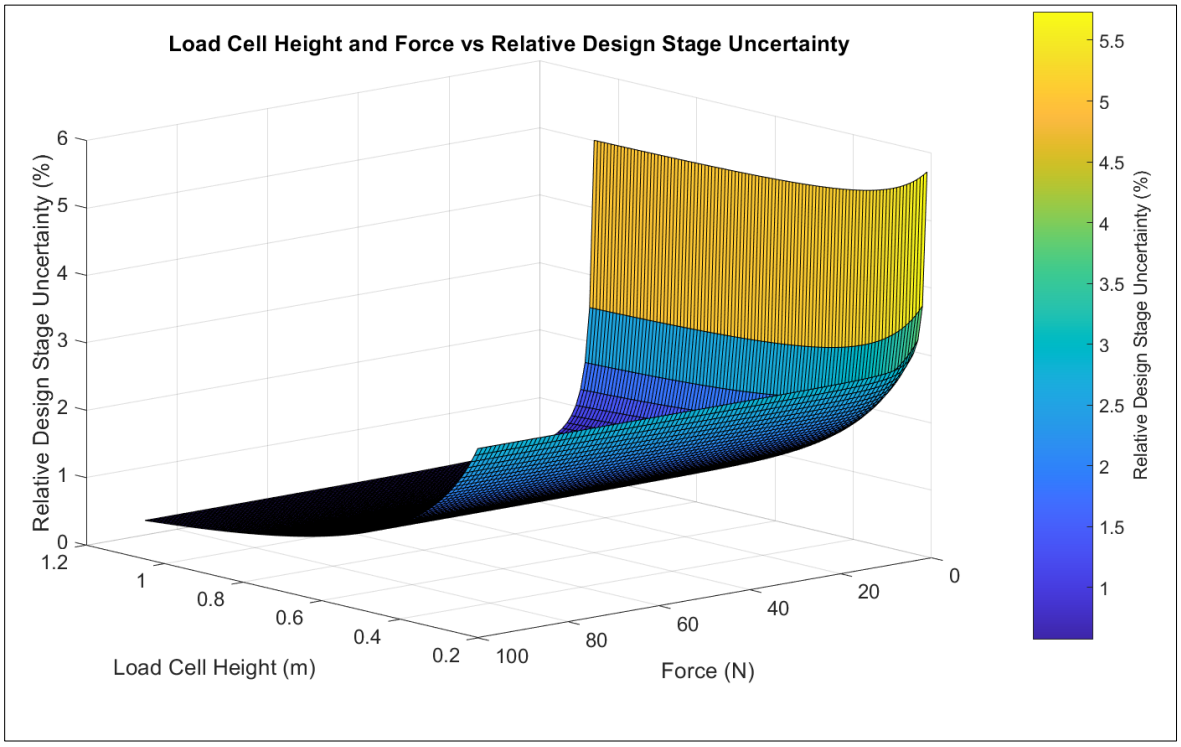

Figure 31: Design stage uncertainty in bending strength for a lower accuracy force gauge. Peak values in uncertainty arise for extremely small values of force and moment arm. The highest uncertainty values produced within the measurement range were 5.5% at minute values of force.

Uncertainty in Bending Stiffness

Uncertainty in Bending stiffness is a function of three measurements which independently affect uncertainty: applied force, load cell height, and angular deflection. The calculation weight of each of these inputs uncertainties shows a similar pattern to bending strength, with uncertainty in a single input primarily driving overall uncertainty. However, in the case of stiffness, angular deflection is the primary determinant of uncertainty. For meager values of angular deflection, uncertainty in stiffness reached $\pm 25\%$. For most measurements, however, uncertainty will be significantly lower. Figure 32 and Figure 33 show the uncertainty using a low and high accuracy force gauge respectively.

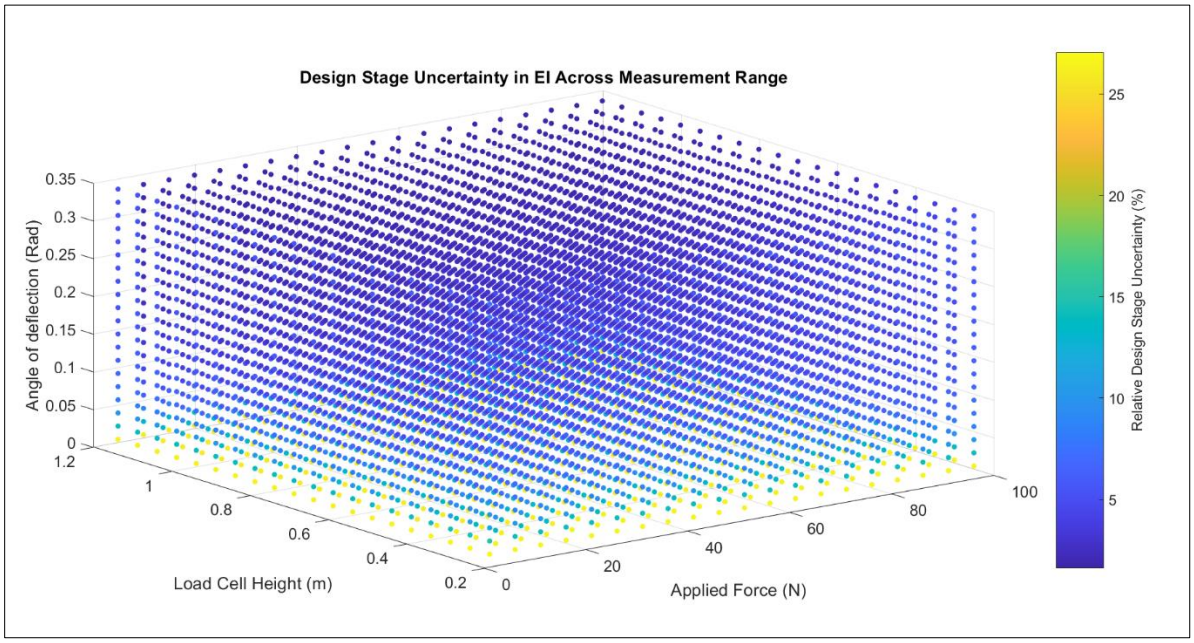

*Figure 32: Maximum design stage uncertainty in EI at various values of theta. Sensor specific uncertainty values are calculated based off resolution and accuracy of the **low accuracy force gauge**. The color bar on the right-hand side of the plat displays the relative design stage uncertainty (%) of each respective theoretical value.*

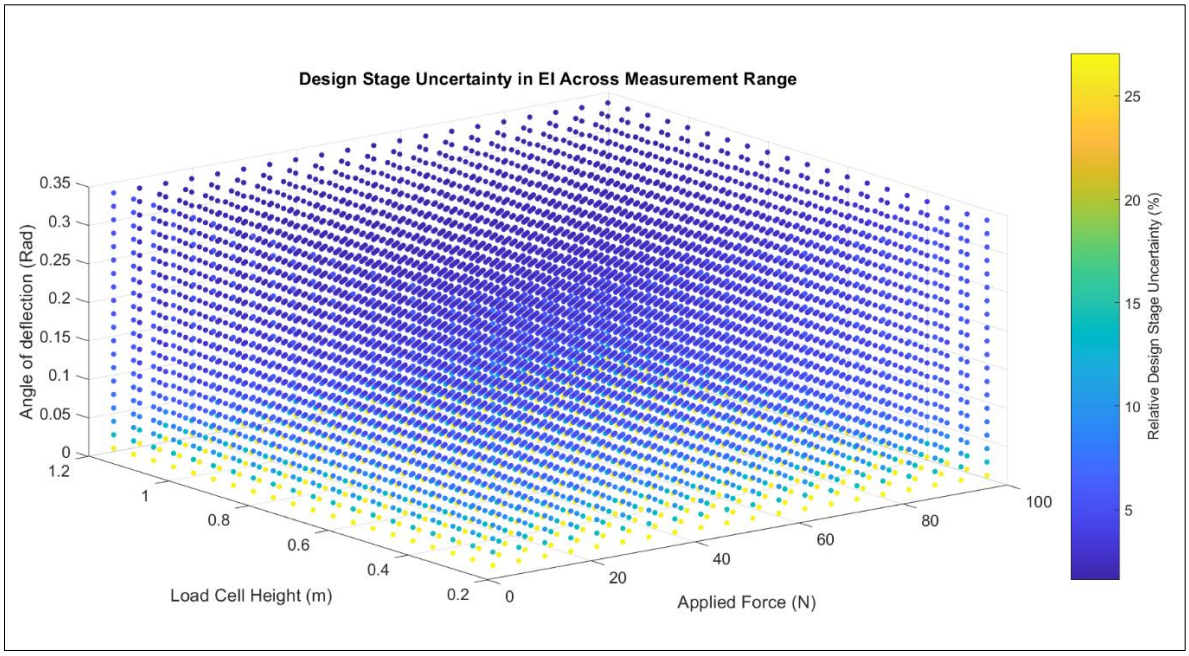

*Figure 33: Maximum design stage uncertainty in EI at various values of theta. Sensor specific uncertainty values are calculated based off resolution and accuracy of the **high accuracy force gauge.** The color bar on the right-hand side of the plot displays the relative design stage uncertainty (%) of each respective theoretical value.*

Example Data Set Analysis

In previous studies, the DARLING collected bending stiffness and bending strength data sets for thousands of individual stalks. Analyzing these existing data sets provides a realistic distribution of measurement uncertainty for the DARLING Lite. Computing individual relative design stage uncertainties involved the identification of data used for previous stiffness and strength calculation and applying the respective measurement uncertainties to produce theoretical uncertainty values for each sample. These theoretical values simulate the measurement uncertainty to be expected if the DARLING Lite replaces the DARLING.

Two separate data sets provided individual measurements for uncertainty distribution analysis: 608 hybrid stalks grown at Clemson University in 2021, and 5184 inbred stalks grown at the University of Kentucky in 2020. Inbred stalks are not grown for commercial use but exhibit large variation in phenotypes between varieties and provide a diverse test pool for evaluating realistic uncertainty distribution. On the other hand, hybrid stalks tend to be taller than inbred stalks with more consistent phenotypes and are frequently used in commercial agriculture. Uncertainty in the inbred data set quantifies uncertainty for phenotypic relationship studies, while uncertainty distribution of the hybrid stalks quantifies error for studies aimed at improving those commercial varieties. For uncertainty calculation in both data sets, uncertainty using the low accuracy force gauge was used. Figures 34-38 display the uncertainty distributions for the two data sets in both bending stiffness and bending strength.

Simulated Uncertainty in Bending Strength: Inbred Data Set.

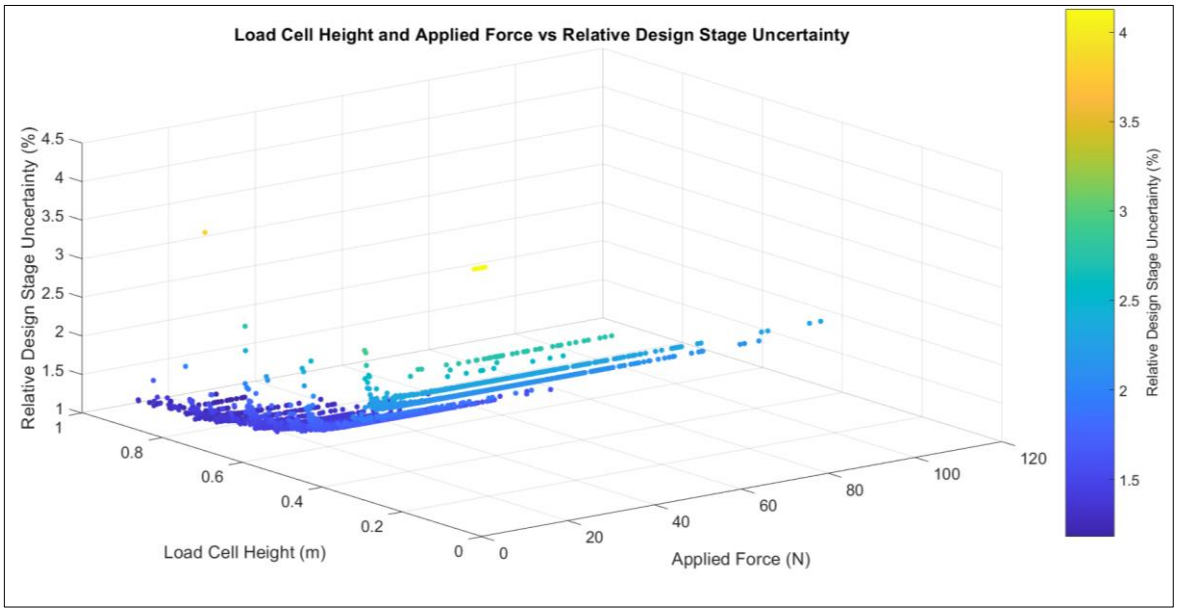

*Figure 34: Relative design stage uncertainties in bending strength for a set of 5184 inbred stalks. An uncertainty value for a **low accuracy** force gauge was used.*

Simulated Uncertainty in Bending Stiffness: Inbred Data Set

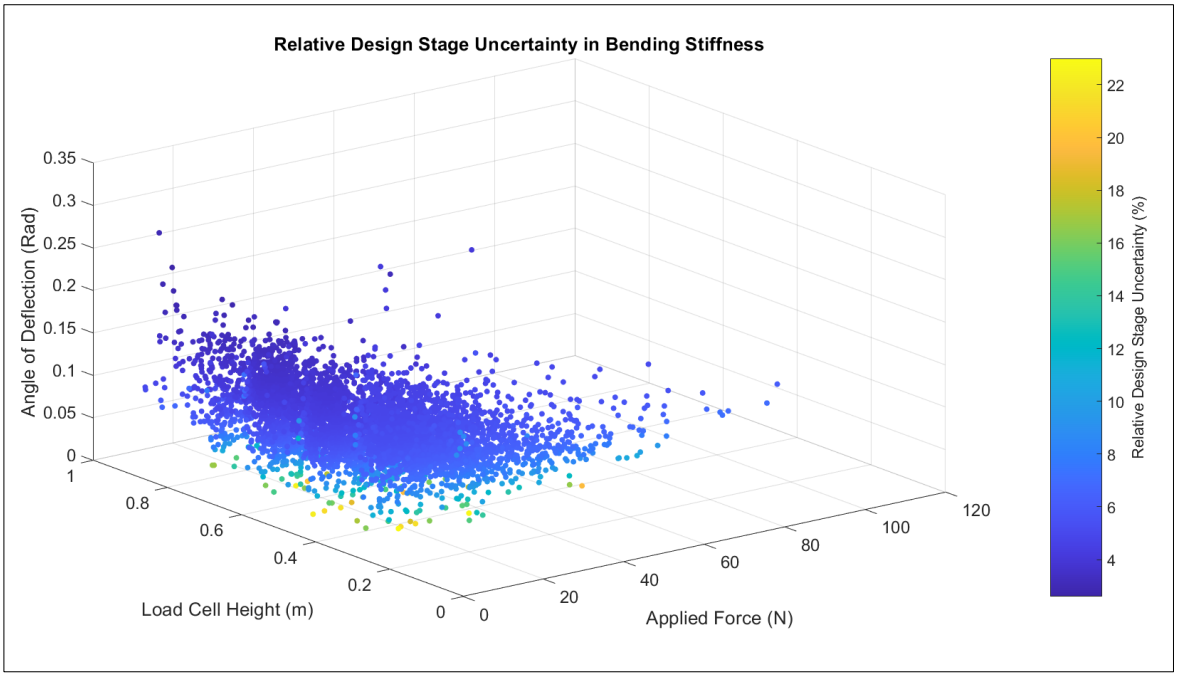

*Figure 35: Relative design stage uncertainty in flexural stiffness. This data set included 5184 samples. Uncertainty in this case was calculated with the **low accuracy** force gauge. The color bar on the right-hand side of the plat displays the relative design stage uncertainty (%) of each respective theoretical value.*

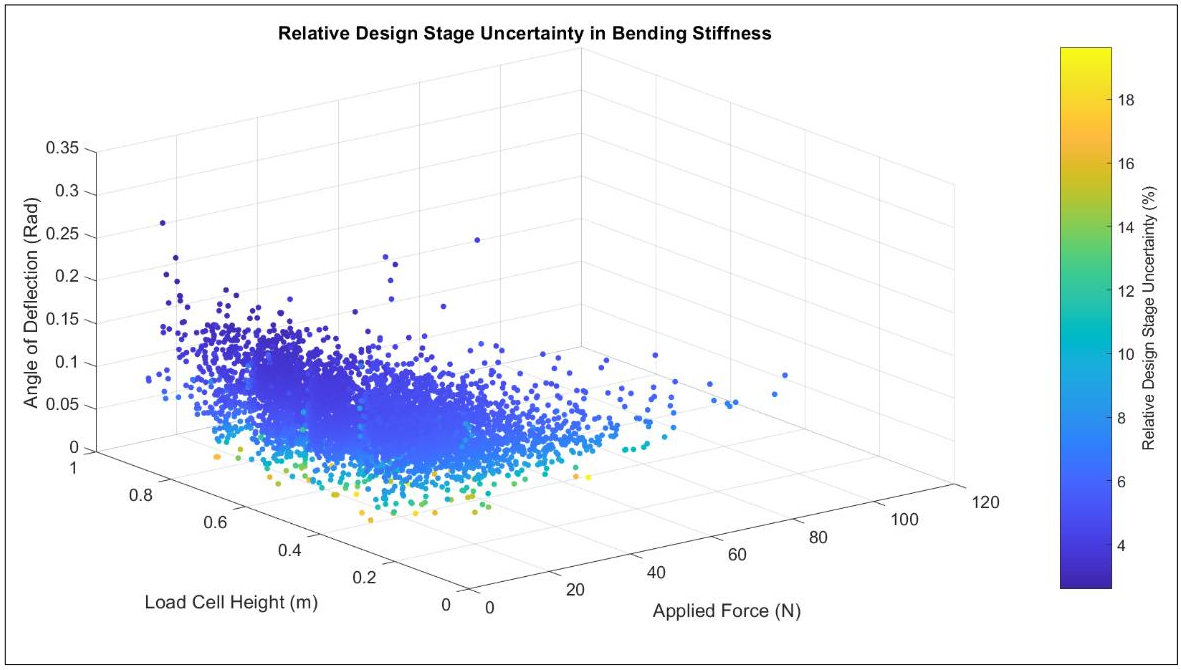

*Figure 36: Relative design stage uncertainty in flexural stiffness measurements. Samples with uncertainty values higher than 20% were removed to improve resolution. This data set included 5173 of 5184 evaluable samples. Uncertainty values for the **low accuracy** force gauge were used. The color bar on the right-hand side of the plat displays the relative design stage uncertainty (%) of each respective theoretical value.*

Simulated Uncertainty in Bending Stiffness: Hybrid Data Set.

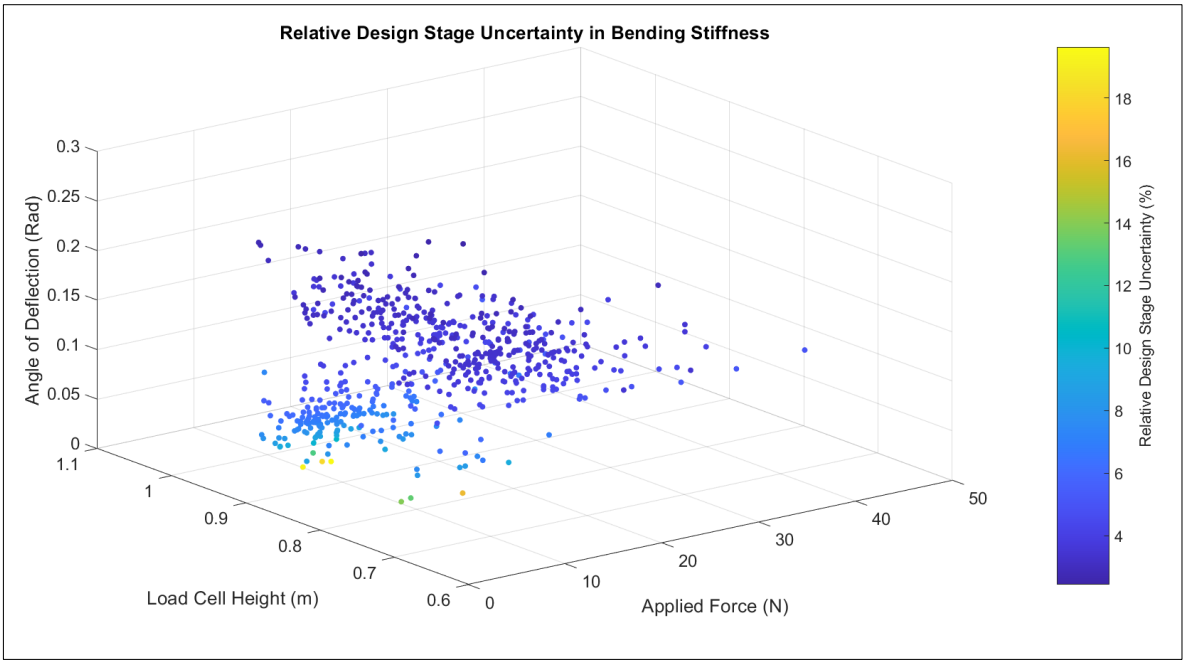

*Figure 37: Relative design stage uncertainty in flexural stiffness for a hybrid data set of 608 stalks. Design stage uncertainty for the **low accuracy** force gauge was used. The color bar on the right-hand side of the plat displays the relative design stage uncertainty (%) of each respective theoretical value.*

Simulated Uncertainty in Bending Strength: Hybrid Data Set.

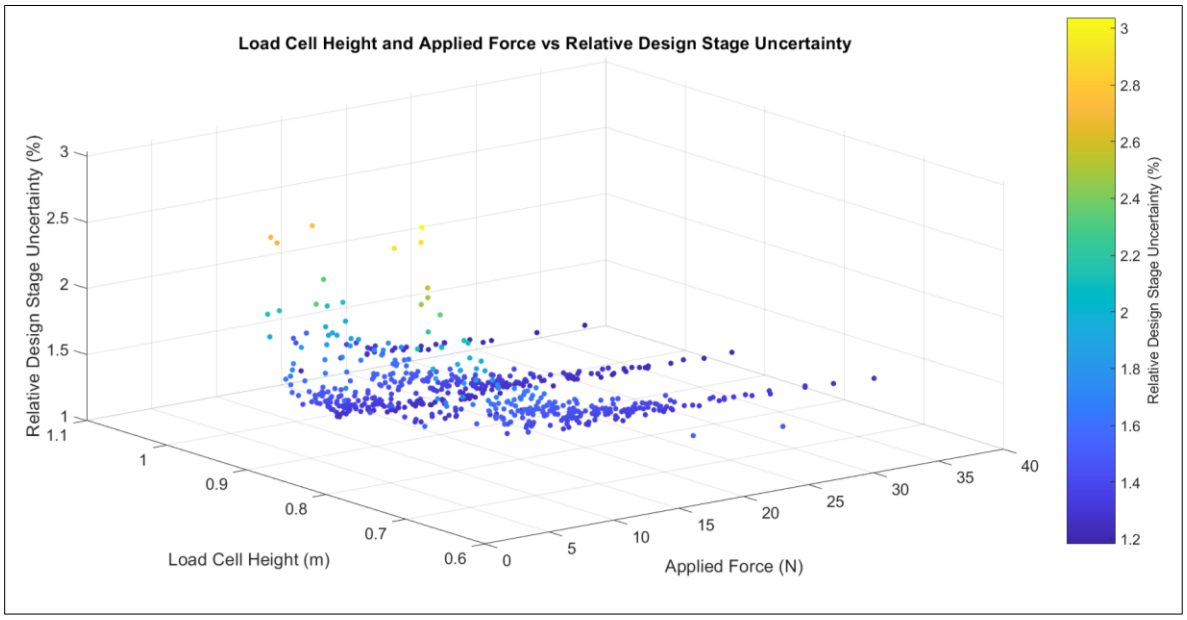

*Figure 38: Relative design stage uncertainty in bending strength for a set of 603, of 608 hybrid stalks. Five outlying measurements from that data set were excluded compared to the previous data set. The design stage uncertainty utilized error propagation techniques and the uncertainty value of the **low accuracy** force gauge.*

Uncertainty summary.

High degrees of measurement uncertainty can confound correlations and require larger sample sizes. Two comprehensive data sets produced simulated uncertainty values for the DARLING Lite's in-field measurements. Figure 39 shows uncertainty distribution for each data set. Mean values of relative design stage uncertainty for the inbred data set were $\sim \pm 5\%$ & $\sim \pm 2\%$ for bending stiffness and bending strength, respectively. A hybrid data set produced relative design stage uncertainty means of $\sim \pm 3\%$ & $\sim \pm 2\%$ for bending stiffness and bending strength, respectively. Outliers reached uncertainty values no higher than 25%.

The most significant contributor to design stage uncertainty in bending strength is inaccuracy in load cell height measurement. Uncertainty in applied force affects overall uncertainty to a lesser degree regardless of force gauge accuracy. For Bending stiffness, the primary contributor to uncertainty is the angular deflection measurement. Applied force and load cell height values played little role in error propagation comparatively. Improvement in load cell height measurement hardware, and angular deflection measurement hardware would further reduce uncertainty in bending strength and bending stiffness respectively.

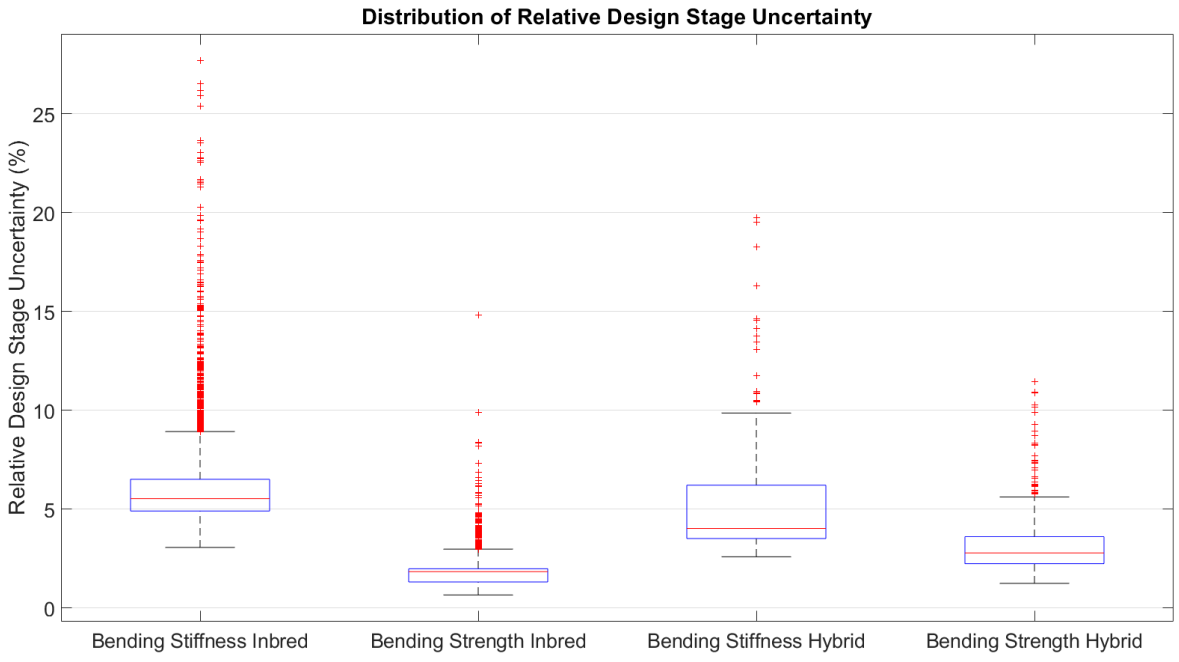

Figure 39: Distribution of relative design stage uncertainty in flexural stiffness (EI) and bending strength (s) for both hybrid and inbred data sets. Values of uncertainty greater than 30% were excluded in this figure. This exclusion reduced the inbred data set from 5184 to 5183 samples, and the inbred data set from 608 to 603 samples.

3.6 Conclusions

After optimizing the design of the DARLING to be better suited for large scale high accuracy phenotyping studies, its performance level and price point overreached smaller research group's needs. To accommodate these groups and provide a product to a larger consumer base, the DARLING was simplified, and modularity was implemented. The redesign process also reduced costs and improved the system in several critical categories. Ergonomics and throughput evaluation clarified how comfortably and quickly the device can collect data, while measurement uncertainty analysis evaluated the accuracy and effectiveness of the hardware. Relative design stage uncertainty quantification identified the weight of each hardware's accuracy in uncertainty contributions and provided hardware specification ranges to further improve the DARLING Lite's relevance as a measurement tool.

Chapter 4: DARLING - Experimental Error Analysis

"***Field Based Phenotyping for Stalk Lodging Resistance: Experimental Error Analysis"***

Joseph DeKold[1], Daniel Robertson[1*]

[1] Department of Mechanical Engineering, University of Idaho, 875 Perimeter Drive, MS 0902, Moscow, Idaho 83844-0902 USA

* Corresponding author: danieljr@uidaho.edu

Submitted to the journal *Plant Methods.*

4.1 Abstract

4.1.1 Background:

Meeting the global demand for grain is becoming increasingly difficult due to numerous factors including climate variability, urbanization, increasingly frequent extreme weather events and drought. Stalk lodging destroys between 5%-25% of grain crops annually. Developing crop varieties with improved lodging resistance will reduce the frequency and impact of stalk lodging and consequently reduce the yield gap. Field-phenotyping equipment is critical to develop lodging resistant crop varieties, but the effectiveness of current equipment is hindered by measurement error. Relatively little research has been done to identify and rectify sources of measurement error in biomechanical phenotyping platforms. This study specifically investigated sources of error in bending stiffness and bending strength measurements which are often acquired using field-phenotyping devices. Three specific sources of error in bending stiffness and bending strength measurements were evaluated: horizontal device placement, vertical device placement and incorrect recordings of load cell height.

4.1.2 Results:

Incorrect load cell heights introduced errors as large as 130% in bending stiffness and 50% in bending strength. Results indicated that errors on the order of 15%-25% in bending stiffness and 1% to 10% in bending strength are common in field-based measurements. Improving operating procedures and protocols can mitigate this error. Such improvements include emphasizing attention to detail while conducting tests and improving the design of phenotyping equipment.

4.1.3 Conclusion:

Reducing measurement error in field-phenotyping equipment is crucial for advancing the development of improved, lodging-resistant crop varieties. The study found that incorrect load cell height entry and

incorrect device placement both significantly contributed to measurement error in bending stiffness and bending strength measurements. These findings have important implications for reducing the yield gap in staple crops and meeting the global demand for grain.

4.2 Background

It is estimated that grain crops account for over 50% of the average person's caloric consumption [1], [42]. The global demand for grain continues to grow each year as the global population increases. For example, the global corn export market grew by 7.2% annually between 2012 and 2021 [43]. In the United States, maize (Zea mays) exports totaled $9.2 billion in 2021, which was a 20% increase ($1.6 billion) from 2020 [44] . Meeting the global demand for grain is becoming increasingly difficult due to numerous factors including: climate variability, urbanization, increasingly frequent extreme weather events and drought [5]. Reducing the yield gap and improving agronomic efficiencies will be necessary to continue meeting the global food, fuel and fiber demand of the future [4].

The problem of stalk lodging significantly reduces the annual yield of vital grain crops like maize, rice (*Oryza sativa)* and wheat (*Triticum)*. For example, lodging is estimated to reduce cereal crop yields by up to 20%, resulting in billions of dollars of lost grain annually [43], [7]. Lodging occurs when plant stems break during windstorms, often preventing the grain from being harvested and increasing the presence of pests and disease in the field. Reducing yield losses by 1% would provide an additional 6.9 million metric tons of corn commodity in the United States alone [43].

Selective breeding has reduced lodging rates and increased yield/hectare [8], [15], [45]. However, despite such advances, stalk lodging is still a major unsolved agronomic problem. For over a century, groups have been developing devices and techniques to quantify the lodging resistance of crops to aid in selective breeding efforts (e.g., [46], [47], [30], [34], [48]–[57]). These devices have been used in numerous studies to investigate the biomechanical response of plant stems [33], [58]–[68]. However, best practices and clear methodological details for many of these devices are lacking in scientific literature. The purpose of this study is to conduct an experimental error analysis of commonly used, electromechanical, field-deploying devices which acquire measurements of stalk bending strength and stalk bending stiffness.

Field deploying devices which measure bending strength and bending stiffness often utilize similar form factors and methods to acquire these measurements. These devices typically approximate the stalk as a cantilever beam and apply a force at a specified height. To ensure the force is applied at the intended height most devices consist of a rigid, rotating, vertical bar supporting a load cell. The

load cell can typically be adjusted vertically to accommodate plants of varying heights. In most cases, the vertical bar pivots about a foot plate or a fixed point on the ground. One such field-based device is the Device for Accessing Resistance to Lodging In Grains (aka DARLING) (Figure 40: Left panel) [48], [69]. During operation, the vertical bar of the DARLING rotates at the stalk's base while the force sensor applies a measured load to the specimen (Figure 40: Middle panel). An electronic sensor suite continuously records applied force and angle during the test and allows the user to record the height at which the load was applied. An example plot of data collected by the DARLING is shown in the right panel of Figure 1. This type of plot is common to many devices, and the data is used to calculate bending strength and bending stiffness. Bending strength and bending stiffness are two of the most commonly measured quantities as they have been shown to strongly correlate with lodging resistance [25]. Bending stiffness (aka, flexural rigidity) and bending strength are defined in equations 1 and 2 respectively, where F is applied force, Φ is the slope of the linear portion of the force/deflection curve (Figure 40: Right) and h is load cell height (moment arm) [48]. The deflection is calculated using equation (20) where θ is the angular displacement measured by the DARLING.

$$EI = \frac{\phi \cdot h^3}{3} \tag{18}$$

$$S = F_{max} \cdot h \tag{19}$$

$$Deflection = h \cdot \sin(\theta) \tag{20}$$

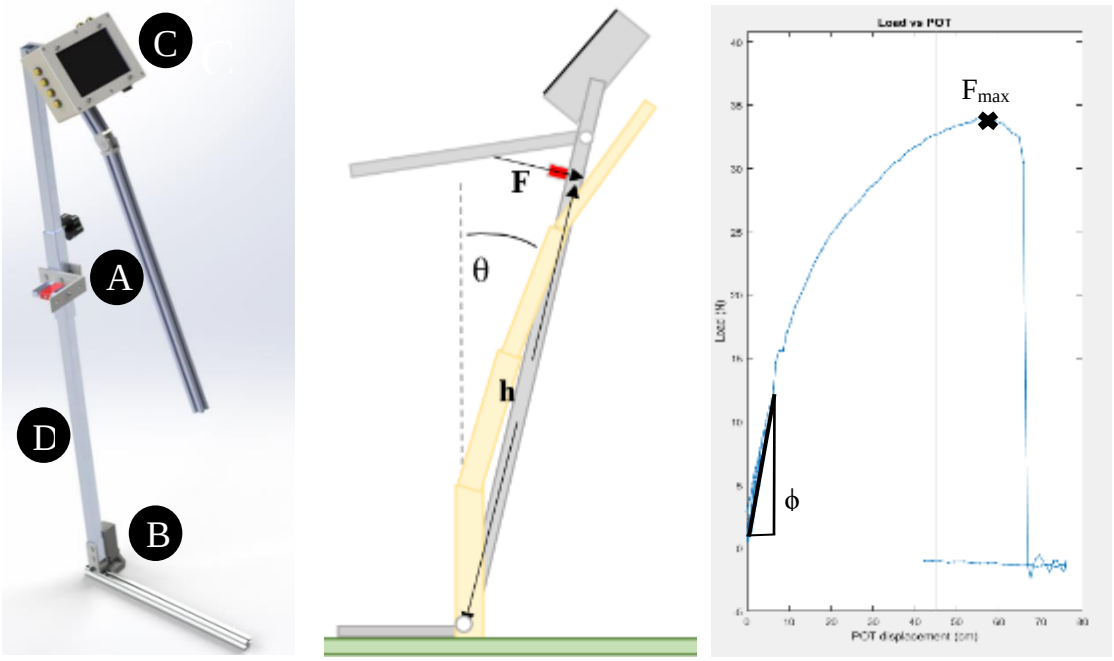

Figure 40: ***(LEFT)*** *Like many field-based devices, the DARLING uses force sensors (A) and angular rotation sensors (B) to measure applied force and angular displacement. A user interface (C) enables editing of recorded data and appending of metadata to each test sample. The sensors and user interface are mounted to a supportive skeleton (D).* ***(MIDDLE)*** *Schematic illustrating load cell height, applied force and angular displacement. (****RIGHT****) A typical force vs displacement curve generated while deforming a maize stalk. Bending stiffness is calculate based on the slope of the initial, linear portion of the data curve (Φ), and bending strength is calculated based on the maximum value of force supported (F_max).*

Several sources of experimental error can reduce the accuracy of data used to calculate bending strength and bending stiffness. The most obvious source of error is in the recorded load cell height (h). Perhaps less obvious is the error due to placement of the device relative to the base of the stalk. Irregularities in the surface of a field, the presence of brace roots, and user fatigue can often lead to the device pivoting either in front of the stalk or behind the stalk. In addition, when stalks undergo large deflection before breaking several other sources of error are introduced. These are explained in more detail below.

Plant stalks behave comparably to classical cantilever beams and engineering beam theory is frequently used to calculate mechanical properties of stalks during in-field phenotyping tests. For example, equation 1 comes directly from Euler Bernoulli beam theory. When a cantilever beam subjected to a follower load undergoes large deflections (>10 degrees) the deflected path of the end of the beam is approximately circular. However, the center of curvature of this path is centered at some point along the length of the beam and not at its base [70]. This phenomena is well known and the center of the curvature (often referred to as the characteristic pivot) generally resides at 15% of the

length of the beam, measured from the fixed end [70], [71] (Figure 41). However, field-based phenotyping devices often pivot at ground level (i.e., base of the stalk). Discrepancies between the location of the device's pivot point and the plant's characteristic pivot cause the load cell to slide along the length of the stalk as the plant is deflected (see Figure 42). When this occurs, the load cell axis will not remain perpendicular to the stalk. This is problematic as the type of load cells used in these devices are designed to measure normal loads only. When the load cell is no longer perpendicular to the stalk non normal loads are introduced, creating error in force measurements. Discrepancies between the location of the device's pivot point and the plant's characteristic pivot also introduce error into angular deflection measurements. The effect of these errors on calculations of bending stiffness and bending strength have yet to be quantified.

To quantify the amount of error introduced by, 1) inaccurate placement of the device pivot relative to the base of the stalk, 2) the characteristic pivot phenomena and 3) inaccurate load cell heights, an artificial maize stalk was created and submitted to a barrage of experimental tests using a DARLING device. The systematic error and random error present in each test were calculated.

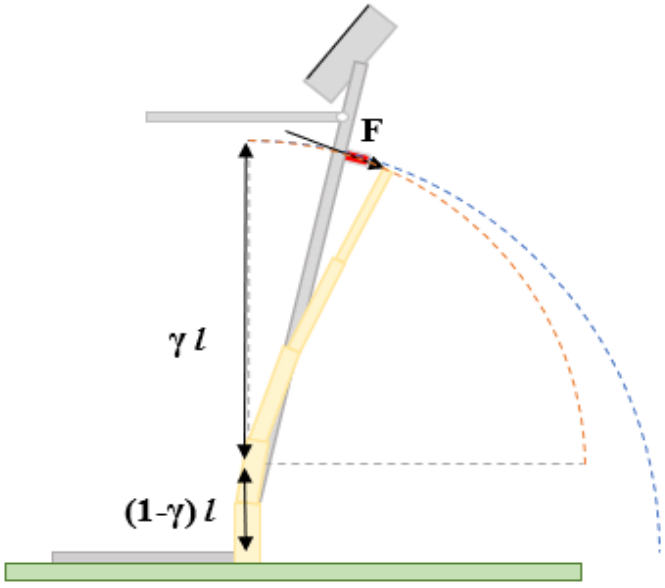

Figure 41: The deflected path of a plant stem is approximately circular (shown in orange), but the center of the curvature of the path is centered at some point along the stem's length. The location of the center of curvature of the deflected path is often denoted using (γ) where γ ~ 0.15. The path of the DARLING is also circular (shown in blue) but the center of curvature of the DARLING's path is centered at the pivot point of the darling. This difference in path center points results in path divergence as angular deflection increases.

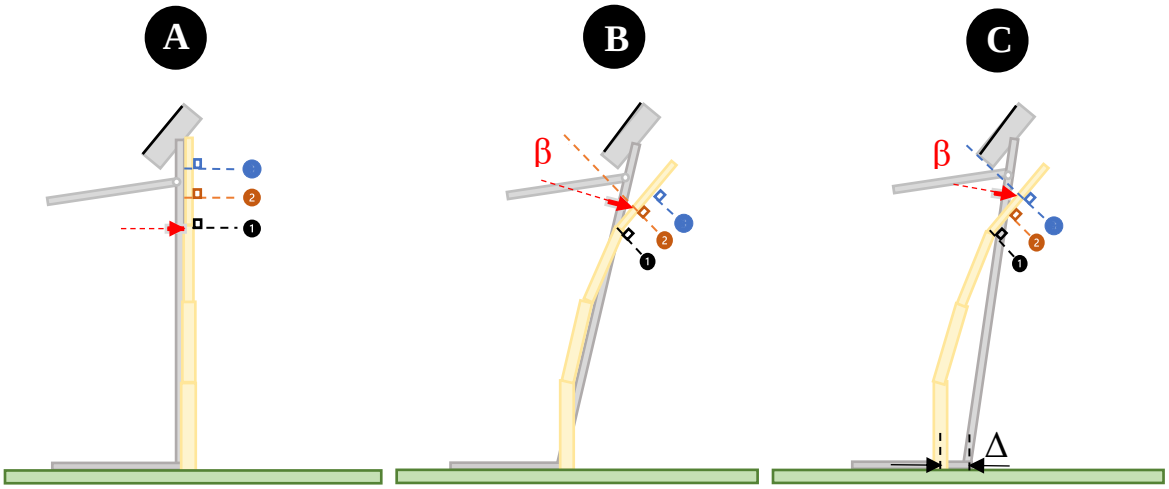

Figure 42: Illustration of load cell sliding along the length of a stalk during testing. Panel A shows the undeflected stalk. Panel B shows a deflected stalk in which the DARLING was properly aligned at the base of the stalk. Note that even when properly aligned with the base of the stalk the load cell will still slide along the length of the stalk and will not remain perpendicular to the deflected stalk. Panel C illustrated a deflected stalk in which the DARLING was not properly aligned with the base of the stalk. In this case the load cell starts non-normal to the stalk. As the stalk deflects the load cell will slide up the stalk to point 2 or point 3 as illustrated in panels B and C. If the device is positioned behind the stalk (+Δ), the load cell will slide less but it will be oriented at a more obtuse angle (β).

4.3 Methods

When subjected to external loading, plant stems often exhibit viscoelastic behaviors that can change with moisture content and time of day [72]. Therefore, in this study we created an artificial stalk specimen that could be repeatedly tested and reliably provide the same mechanical response over time. To create this artificial stalk, we analyzed a data set of 200 inbred maize stalks. The internode lengths, and the moment of inertia of the stalks were used to inform the construction of a protruded carbon fiber rod. In particular, the relative reduction in moment of inertia along the length of the rod was proportional to the reduction in moment of inertia along the length of an average inbred maize stalk. This ensured the rod would deflect in a similar manner to an average inbred maize stalk from our dataset. The exact dimensions of the rod are shown in Figure 43.

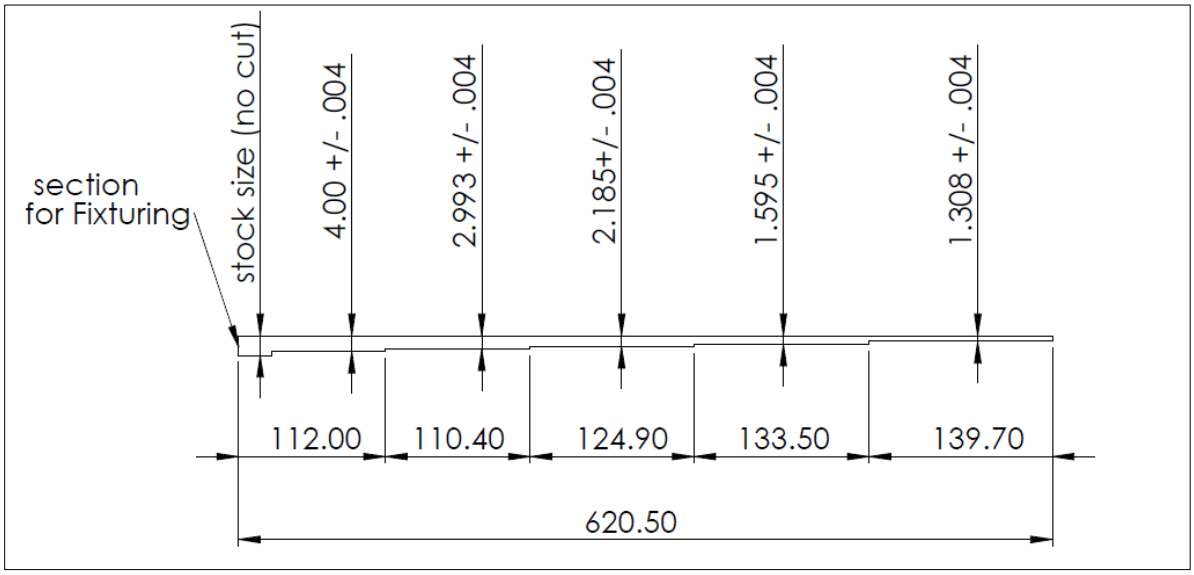

Figure 43: An artificial inbred maize stalk was constructed from a protruded carbon fiber rod. The dimensions of the beam shown above were determined based on the average stalk geometric ratios of 200 stalks from an inbred data set. Units are in mm and the drawing is not shown to scale to increase definition and clarity.

An aluminum test fixture, shown in Figure 44: Left panel, enabled the DARLING to be positioned relative to the base of the protruded rod in both the vertical and horizontal directions. Tests were performed at five horizontal positions (±6.4%, ±12.8%, 0% of load cell height) and three vertical positions (0%, 7.5%, 15% of load cell height) as shown in the right-hand panel of Figure 5. At each position, 10 tests were performed. This resulted in a total of 150 tests (five horizontal positions x three vertical positions x 10 tests at each position = 150 tests). During each test a proximity sensor alerted the user when the stalk was deflected to 10 degrees. At this point, the user returned the DARLING to the upright position and then deflected the stalk again to 25 degrees at which point another sensor alerted the user. The DARLING was then returned to the upright position and the test was stopped. Note that the test fixture sensors were used to detect stalk deflection (and not DARLING deflection). In other words, even though the horizontal and vertical positions of the DARLING were changed throughout the study, the stalk was deflected to the same two points in every test. The portion of the test in which the stalk was deflected to 10 degrees was used to determine the bending stiffness of the rod. This is standard practice as the load deflection curve was linear below 10 degrees of deflection. The load at 25 degrees of stalk deflection was used as a surrogate bending strength measurement. A custom MATLAB program was used to determine flexural stiffness and bending strength of the protruded rod in each test as described in [48] using equations 1-3.

After computing bending strength and flexural stiffness measurements the systematic error in each measurement was calculated. The systematic error was defined as:

$$\%\ error\ S = \frac{S_{measured} - S_{actual}}{S_{actual}} \cdot 100 \tag{21}$$

$$\%\ error\ EI = \frac{EI_{measured} - EI_{actual}}{EI_{actual}} \cdot 100 \tag{22}$$

Where S_{actual} and EI_{actual} were the average measured values of S and EI from ten tests performed at zero horizontal offset and 15% vertical offset. At this position the DARLING pivot is closely aligned with the characteristic pivot of the protruded carbon fiber rod and the load cell does not slide along the length of the stalk during the test. The relative standard deviation at each testing position was calculated to determine the presence of random error, where:

$$RSD = \frac{\sigma}{\bar{m}} \cdot 100 \tag{23}$$

With σ representing standard deviation and $\bar{m}$ representing the mean of the ten tests performed at each test location. To determine the effects of erroneous load cell height on calculations of bending stiffness and bending strength these quantifies were recalculated for the data set described above using incorrect load cell heights. All 150 tests were performed at a load cell height of 47 cm. The data from these tests were then reanalyzed using stand-in erroneous load cell heights of 32cm, 46cm, 48cm and 62cm.

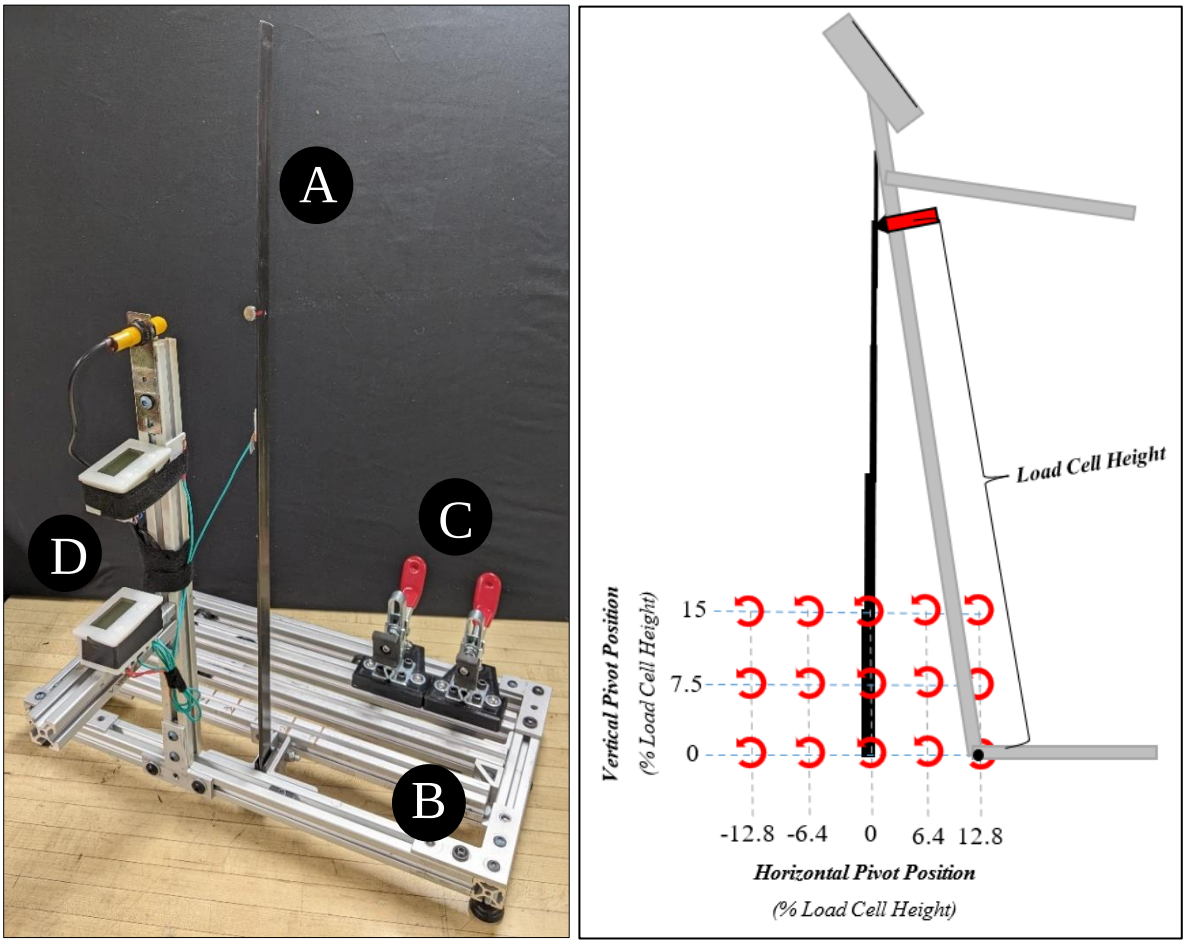

*Figure 44: **(Left)** Carbon fiber stalk (A) fixtured into test frame. The frame consists of an aluminum skeleton (B), toggle clamps used to secure the foot of the DARLING in place and (C) a deflection sensor system (D). **(Right)** Position of the DARLING pivot relative to the carbon fiber rod for each of 15 locations. Ten tests were performed at each testing location, resulting in 150 total tests. Note that visual spacing between axis tick lines is exaggerated to increase definition.*

4.4 Results

Of the 150 tests performed, 2 were excluded due to excessive noise. Results from the remaining 148 tests demonstrated that horizontal placement of the DARLING significantly affected both bending strength and bending stiffness measurements. Vertical placement of the DARLING significantly affected bending stiffness measurements but had a minimal effect on bending strength measurements. The systematic error in stiffness measurements was highest at +12.8% horizontal offset and 0% vertical offset. Relative standard deviation was used to determine the amount of random error present at each testing position. The random error in bending strength measurements was typically below 1%. For both bending stiffness and bending strength, pivoting at positions less than 15% of the load cell height tended to increase random error. Figure 45 displays the mean bending strength and bending stiffness obtained

at each testing position. Table 9 displays the percentage error (systematic error) and relative standard deviation (random error) of bending strength and bending stiffness measurements at each testing position.

Error due to incorrect load cell height was investigated by recalculating bending stiffness and bending strength for all 148 tests using incorrect load cell heights of 32cm, 46cm, 48cm and 62cm. The actual load cell height during the experiments was 47 cm. The systematic error in bending strength measurements was directly proportional to error in load cell height when the horizontal offset was 0%. This was expected considering the linear dependency of bending strength on load cell height (see equation (19)). However, at other horizontal and vertical offsets the resultant error was less predictable. In general, erroneous load cell height values had a more drastic impact on bending stiffness measurements than on bending strength measurements. This was expected as bending strength is proportional to load cell height whereas bending stiffness is proportional to load cell height raised to the third power (see equations (18) and (19)). Table 10 shows the resultant systematic error in bending strength and bending stiffness measurement as a function of erroneous load cell heights. Figure 46 displays the erroneous load cell height stiffness and strength values compared to the true stiffness and strength values.

	Horizontal Δ (% Height)	Vertical Δ (% Height)	S Error (%)	EI Error (%)	S RSD (%)	EI RSD (%)
Testing Position	-12.8	0	11.15%	-5.04%	0.25%	1.13%
	-6.4	0	5.57%	-8.99%	0.29%	1.12%
	0	0	1.11%	-15.83%	0.52%	2.05%
	6.4	0	-2.71%	-25.18%	0.65%	1.41%
	12.8	0	-9.24%	-31.65%	0.93%	2.43%
	-12.8	7.5	9.24%	4.68%	0.42%	1.25%
	-6.4	7.5	4.46%	-1.08%	0.32%	1.07%
	0	7.5	-0.48%	-11.87%	0.32%	2.06%
	6.4	7.5	-5.10%	-17.63%	0.41%	1.13%
	12.8	7.5	-12.26%	-26.62%	0.81%	3.69%
	-12.8	15	10.83%	15.83%	0.45%	0.43%
	-6.4	15	4.78%	10.07%	0.40%	1.00%
	0	15	0.00%	0.00%	0.33%	2.55%
	6.4	15	-7.01%	-6.12%	1.22%	1.93%
	12.8	15	-13.85%	-17.99%	0.60%	2.29%

Table 9: Percentage (systematic) error and relative standard deviation (random error) in bending strength (S) and bending stiffness (EI) at 15 testing positions for a 47cm load cell height.

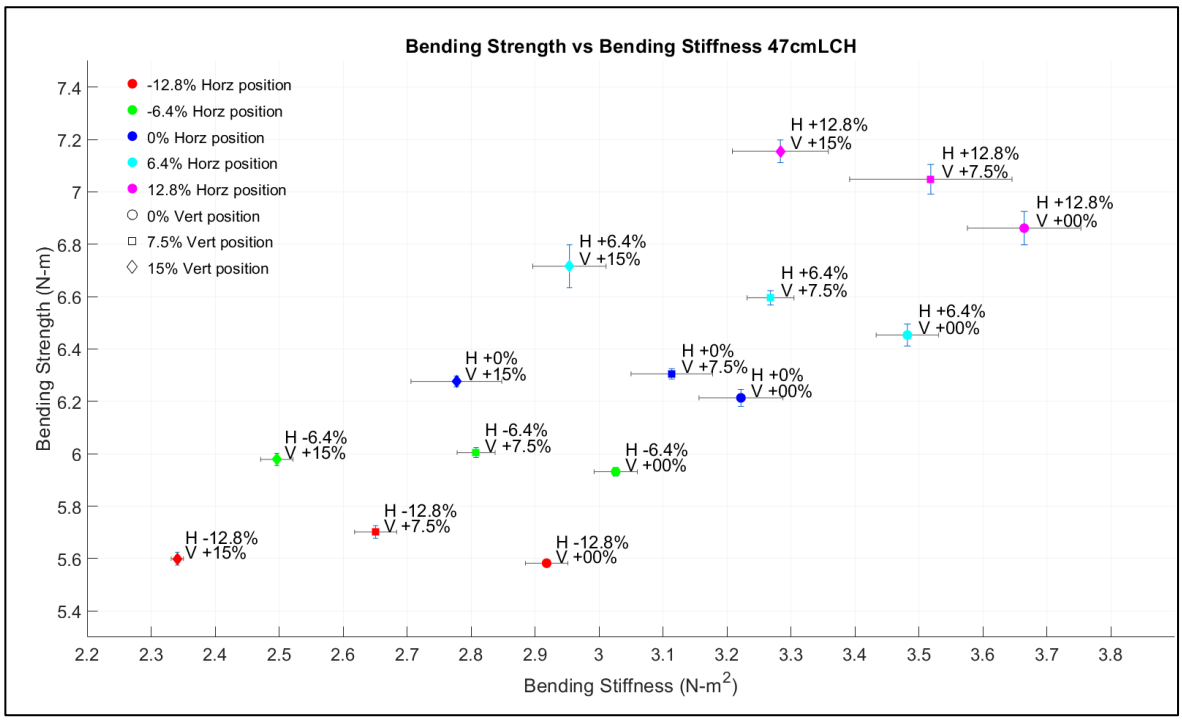

Figure 45: The average bending stiffness and bending strength obtained at each testing position. Error bars are 1 standard deviation in length in both the EI and S axes. Marker color indicates horizontal position, while marker shape indicates vertical position.

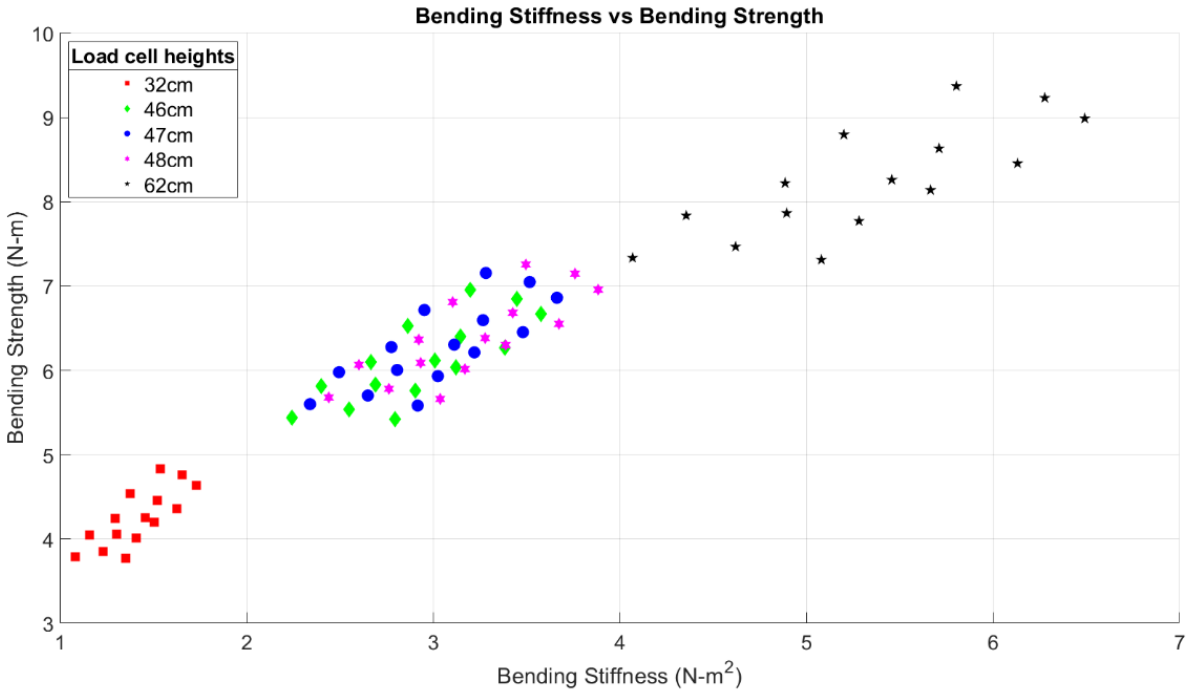

Figure 46: Spread of bending stiffness and bending strength measurements for erroneous load cell heights. Each colored data set consists of average bending stiffness and bending strength values at each of the 15 testing positions mentioned previously.

Table 10: Percentage error for bending strength (S) and bending stiffness (EI) at 15 testing positions for erroneous load cell heights of 32cm, 46cm, 48cm and 62cm.

	Horizontal Δ (cm)	Vertical Δ (% 47cm LCH)	S Error (%)					EI Error (%)				
			32cm LCH	46cm LCH	47cm LCH	48cm LCH	62cm LCH	32cm LCH	46cm LCH	47cm LCH	48cm LCH	62cm LCH
Testing Position	-6	0	-39.87	-13.56	-11.06	-9.80	16.50	-51.25	0.76	5.08	9.42	82.98
	-3	0	-36.10	-8.17	-5.49	-4.15	23.81	-49.18	4.67	8.96	14.18	90.26
	0	0	-33.07	-3.79	-1.00	0.39	29.67	-45.76	12.43	16.01	22.05	104.06
	3	0	-30.52	-0.13	2.82	4.39	34.71	-41.44	21.86	25.38	32.35	120.85
	6	0	-26.10	6.24	9.32	10.86	43.19	-37.68	28.89	31.95	39.91	133.83
	-6	7.5	-38.59	-11.72	-9.16	-7.89	18.97	-55.63	-8.19	-4.55	-0.47	66.42
	-3	7.5	-35.32	-7.03	-4.33	-2.99	25.31	-53.06	-3.10	1.11	5.64	76.29
	0	7.5	-32.20	-2.54	0.46	1.70	31.60	-47.57	8.35	12.12	18.09	96.58
	3	7.5	-29.01	2.05	5.08	6.47	37.53	-45.17	13.26	17.68	23.42	105.70
	6	7.5	-24.09	9.13	12.29	13.87	47.08	-40.37	24.22	26.69	35.43	126.11
	-6	15	-39.69	-13.30	-10.78	-9.53	16.86	-60.95	-19.16	-15.70	-12.09	46.55
	-3	15	-35.56	-7.37	-4.74	-3.35	24.85	-58.28	-13.59	-10.11	-6.27	56.90
	0	15	-32.40	-2.82	0.00	1.40	30.98	-53.28	-3.94	0.00	5.28	75.99
	3	15	-27.66	3.99	7.00	8.51	40.15	-50.41	3.14	6.36	11.83	87.32
	6	15	-22.94	10.78	14.00	15.60	49.31	-44.63	15.20	18.23	25.95	109.05

4.5 Discussion

Bending strength is determined by two measured inputs: load cell height and applied force. Bending stiffness is determined by three measured inputs: load cell height, applied force, and displacement. Error in each of these measured inputs can create resultant error in bending strength and bending stiffness calculations. For example, when the pivot of the DARLING is not aligned with the characteristic pivot of the stalk, then discrepancies between DARLING deflection and stalk deflection are introduced. This measurement input error (i.e., error in deflection) directly creates resultant

systematic error in calculations of bending stiffness but does not affect calculations of bending strength. The discrepancy between DARLING deflection and stalk deflection is evidenced by the load cell sliding along the length of the stalk during the test. As the load cell slides along the stalk, frictional forces between the load cell and stalk generate noise in the force measured by the DARLING. This creates random error that further reduces the accuracy of bending stiffness calculations and affects bending strength calculations as well. In addition, when the DARLING's pivot and the characteristic pivot of the stalk are not aligned then the load cell becomes non-normal to the stalk, creating forces misaligned with the measurement axis of the load cell. This introduces discrepancies between the actual force applied to the stalk and the force measured by the DARLING. Lastly, when the DARLING is not horizontally aligned with the characteristic pivot of the stalk then there is a discrepancy between the load cell height of the DARLING and the height at which loads are being applied to the stalk. This likewise produces systematic errors in both bending stiffness and bending strength. Finally, errors in load cell height can be introduced when the user incorrectly measures or records the load cell height. This can occur when the user forgets to record the height value after raising or lowering the load cell to test plants of a different height. Table 11 summarizes the effects of the DARLING pivot being misaligned with the characteristic pivot of the stalk.

Table 11: Sources of error and their observed effects on each measured input.

Measured Inputs	***Vertical discrepancy between the DARLING pivot and the characteristic pivot of the stalk***	***Horizontal discrepancy between the DARLING pivot and the characteristic pivot of the stalk***
Applied force (F)	Non-normal forces and frictional forces are introduced from the load cell sliding	Non-normal forces and frictional forces are introduced from the load cell sliding
Load cell height (h)	N/A	The load cell height is not equal to the height at which forces are applied to stalk
Angular deflection (θ)	N/A	Angular deflection of DARLING differs from stalk deflection

Bending strength and bending stiffness are primary determinants of stalk lodging resistance [18], [28], [73]. Unfortunately, significant amounts of human labor are required to attain measurements of bending strength and bending stiffness. The cost of attaining these measurements is often prohibitive and phenotyping for these traits has become a bottleneck limiting genetic improvement of stalk lodging resistance [74], [75]. The significant amounts of systematic and random error present in field-based measurements of bending stiffness and bending strength further exacerbates this issue. Based on the results of this study, and the authors' prior experience using phenotyping devices like the DARLING, we suspect that most field studies regularly incur errors between 15% to 25% in bending stiffness and 1% to 10% in bending strength. One way to partially mitigate systematic and random error is to increase the number of sampled plants in a study and to calculate average or median values for each variety

included in the study. Unfortunately, increasing sample size requires additional human labor inputs. In this study we sought to identify principal sources of error present in field-based measurements of stalk bending strength and bending stiffness so that they may eventually be rectified. This is the first error analysis of any field based biomechanical phenotyping methodology of which the authors are aware.

Results from this study as well as prior experience using the DARLING device over several years suggest that improvements can be made to operating procedures and phenotyping devices to mitigate systematic errors in bending strength and bending stiffness measurements. When spending long hours in the field collecting phenotyping data it is common to make mistakes when recording load cell height. In particular, we have found that users sometimes forget to record a new load cell height in the DARLING software after physically changing the height of the load cell. This can produce very large systematic error (>100%) in bending strength and bending stiffness measurements. This type of error is difficult to detect when postprocessing the data. Training and standardizing operating protocols cannot fully eliminate this source of error. Including a load cell height sensor on the device that automatically records load cell height, or that notifies the user when the load cell has been changed is a promising approach to mitigate this source of systematic error. The amount of systematic error introduced by incorrect horizontal placement of the phenotyping device pivot can be partially mitigated by using the highest reasonable load cell height. The amount of systematic error produced by horizontal offsets is a function of the horizontal offset expressed as a percentage of load cell height. Thus a 3 cm horizontal offset will produce less systematic error when the load cell height is 75 cm than when the load cell is 45cm. This source of systematic error can also be mitigated by simply explaining the effects of horizontal placement on measurement error to device users. Additionally, this source of systematic error could be mitigated by adding an extra feature to phenotyping devices to help the user ensure the phenotyping device pivot is correctly aligned with the stalk. However, the constantly varying conditions found within agricultural plots (e.g., uneven ground, brace roots, adjacent plants etc.) make this a nontrivial design challenge. Other more complex modifications to testing equipment could minimize systematic error due to vertical discrepancies between the device pivot and the characteristic pivot of the plant being tested. Ideally the device would pivot at the characteristic pivot height of each plant. However, the characteristic pivot height is a function of the height at which the load is being applied to the stalk. Thus, the pivot height would have to change every time the load cell height was changed. Requiring users to manually change the pivot height would significantly reduce throughput. Alternatively, a mechanical linkage could be designed that would change the pivot height whenever the load cell height was changed. This linkage would increase device cost, and weight which would in turn

increase user fatigue. Alternatively, one could attempt to account for and correct systematic errors due to vertically misaligned pivot points during data postprocessing. This is a promising approach but requires additional research into the large deflection response of stepped cantilever beams. Finding other ways to reduce systematic error are warranted as they will enable future researchers to utilize reduced sample sizes (and human labor inputs) in phenotyping trials.

Results indicated that random error was also a function of testing position. Random error was quantified by calculating the relative standard deviation (aka coefficient of variation) at each test location. Both random error and systematic error increase the sample size required to attain reliable average bending strength and bending stiffness values of plant varieties of interest. While the magnitude of random error was less than that of systematic error it was still significant and warrants discussion. Results demonstrated that testing at positive horizontal pivot positions

resulted in the largest values of relative standard deviation for both bending stiffness and bending strength. Testing at negative horizontal positions minimized the random error but should be avoided as it introduces significant systematic error. Like systematic error, the random error was minimized when the device pivot and characteristic pivot of the stalk were vertically aligned. However, as described previously the technical challenges associated with vertical aligning the pivots for every tested sample may outweigh its benefit.

Systematic and random error was calculated at 15 different test positions in the current study. These test positions were selected based on the authors' prior experience utilizing phenotyping devices. We estimate that it is common for users to horizontally misalign the pivot of a phenotyping device by ± 3cm which corresponds to a 6.4% offset if the load cell height is 47 cm. A 47 cm load cell height is typical when testing inbred maize stalks. We estimate that horizontally misaligning the device pivot by ± 6 cm (i.e., 12.8% of a 47 cm load cell height) is quite noticeable to most users. However, this is also somewhat common due to user fatigue and variations present in the field environment (e.g., uneven ground and other plants obstructing the phenotyping device). Horizontal placement errors greater than ± 6 cm are uncommon as beyond this range the ergonomics of the device become uncomfortable and unwieldy. We choose to select three positions for vertical offsets. A 0% vertical offset is the norm for most phenotyping devices. A 15% vertical offset was chosen as it is the approximate location of the characteristic pivot of a prismatic cantilever beam. A 7.5% vertical offset was chosen simply because it evenly separated the 0% and 15% offsets. The exact position of the characteristic pivot has not been precisely determined for stepped cantilevered beams though it is assumed to be slightly greater than 15%. Further research into the exact position of the characteristic pivot position of stepped cantilevered

beams is required to calculate systematic error more accurately. The magnitudes of systematic error presented in this study should therefore be viewed as the minimum possible value. The values of load cell height utilized were also chosen based on the author's experience. The DARLING device has a ruler engraved on it that is separated into 15 cm increments. We have observed that users typically align the load cell precisely with these markings. However, an exceptionally careless user may place the load cell 1 cm above or below a mark. A far more common type of error is for a diligent but tired user to move the load cell up or down by a 15 cm increment and forget to input the new load cell height into the DARLING. These observations led us to choose four erroneous load cell height measurements: 46cm and 48cm (error of ± 1cm), as well as 37cm and 62cm (error of ± 15cm).

Several other sources of error are present in field based biomechanical measurements of plants stems that were not investigated in this study. For example, if plants are rapidly deflected inertial effects can introduce additional forces that are detected by the load cell. The measured force can also be significantly altered if the stalk being tested contacts adjacent plants or the ground during the test. In addition, if the top section of the stalk is not removed prior to testing it can oscillate during the test which introduces error in the measured force. To prevent the tested stalk from contacting adjacent plants the leaves and the top portion of the stalk are often removed immediately prior to testing [76]. When doing so care should be taken to either leave the leaf sheath completely intact or to remove it completely. Several studies have shown that the leaf sheath contributes significantly to bending strength and bending stiffness [77], [78]. The types of devices investigated in this study often assume the stalk is rigidly anchored in the soil. However, if the soil is loose or wet the stalk and root structure may rotate in the soil. This does not alter bending strength measurements, but it can drastically alter bending stiffness measurements. Lastly, any electronic or analog sensor has inherent limits, resolution, and accuracy. Low-cost sensors are appealing but they are often unreliable. For example, low-cost load cells are widely available, but their readings can be significantly affected by temperature, relative humidity, and electronic noise. Simultaneously accounting for and mitigating all these sources of error can be especially challenging. Ideally researchers with agricultural, genetic, or biological backgrounds should collaborate with individuals who possess expertise in metrology, or engineering when conducting biomechanical phenotyping studies. Doing so will improve the accuracy and reliability of measured quantities (e.g., [79], [80]). Metrology and engineering expertise can also be leveraged to establish regular and standardized calibration routines for biomechanical phenotyping devices.

4.6 Conclusion

To the best of the authors' knowledge, this is the first formal study which attempted to quantify systematic and random error present in field-based phenotyping methodologies used to quantify

bending strength and bending stiffness of plant stems. We conclude that significant amounts of error can easily be introduced when conducting field based biomechanical measurements of plant stems. We estimate that errors on the order of 15% - 25% in bending stiffness and 1-10% in bending strength measurements are common. This error can be mitigated by following best practices and strict operating protocols to ensure that the pivot of the phenotyping device is aligned with the characteristic pivot the stalk being measured. Several design improvements can also be made to current phenotyping devices that would reduce both systematic and random error in biomechanical measurements. Future research in this area is warranted and could lead to further genetic improvements in stalk lodging resistance.

Chapter 5: Conclusion and Future Work

5.1 Conclusion:

The DARLING is a valuable tool in the struggle to improve lodging resistance of critical crops. Improving lodging resistance requires a developed understanding of the problem's complexity, which can be attained by analyzing tens of thousands of individual stalk samples and developing correlations between their phenotypes and lodging resistance. Accessible, accurate, reliable high-quality measurement tools significantly improve the field measurement process. After the application of well-established design principles, the revised DARLING offers higher reliability, manufacturability, and ease of assembly at lower cost than the previous version. Additionally, the introduction of new equipment promises reduced error for future studies. All these features increase the feasibility of using the DARLING on a large scale, in an effective manner, to make crops more reliable for those who grow and consume them.

Although the design may seem retrogressive in performance, the newly developed DARLING Lite effectively fills a unique niche. Research-minded individuals with differing needs and wallet sizes are now offered a simplified version of a relevant measurement tool. Simplicity is king, and complexity confounding. At some cost to throughput, ease of use, and data quality, the DARLING Lite measures the same quantities of stiffness and strength with sensible accuracy and justifiable cost. This unembellished testing tool enables more hands to aid in uncovering the phenomenon of lodging and increasing food supply globally.

High amounts of measurement error require larger sample sizes, more labor, and more time to collect reliable data. When multiple sources of error interact, often the resultant error can be hard to predict and characterize. To quantify the impact and significance of three sources of error, a representative carbon fiber rod was subjected to repeated measurements and the results analyzed for patterns and trends. Through this analysis, it was determined that certain sources of error contribute more significantly to overall measurement error, and that their impacts vary with the type of quantity measured. This insight informs future decisions regarding the design and methods of field measurement devices, in order to reduce measurement error, sample size, labor, and time required. This effect in turn, will accelerate the process of developing lodging resistant breeds.

5.2 Future Manufacturing Methods

Currently, both the DARLING and DARLING Lite are constantly undergoing change, as both designs are relatively new and require frequent alterations to improve. Because their designs are in this

phase, most of the plastic components are 3D printed. 3D printing is a valuable tool for the rapid prototyping and development process as changes can easily be implemented to a design file that can be 3D printed in as quickly as a few hours. Compared to other subtractive (milling/cutting) or molding/casting operations, iterations can be completed in a fraction of the time and time to market can be significantly reduced. 3D printing is not without its shortcomings however as it is ideal for producing single prototypes at a time. It is not suited well to produce batches of end-use parts.

As the designs of the DARLING and DARLING Lite become more permanent and production increases, other manufacturing methods should be utilized. Injection molding is better suited for producing a large amount of components in a short amount of time at reduced cost. Injection molding requires more time up front to fabricate tooling, but the initial cost is outweighed by the dramatically reduced unit cost of components. Considering this, current and future part designs for the DARLNG and DARLING Lite should be injection moldable with minimal design alteration. Although 3D printing is still an applicable method and will be used for the near future, the long-term objective to manufacture using injection molding must not be neglected. It is expected that extensive filed testing must be performed to solidify design features before a shift to batch manufacturing methods should be undertaken.

5.3 Reduction of Measurement Error

In chapter 4, analysis of several sources of error was performed. Two of these error sources (Incorrect placement and incorrect load cell height entry) were user errors. The significance in error from both these sources warrants design changes. The height sensor, (2.2 Load Cell Height Measurement System.), is a good example of how a design change can reduce user error. Incorporating this sensor removed the need for user input, as the sensor automatically measures load cell height after initial calibration. A similar sensor or system to reduce incorrect placement would be similarly valuable. The form of that system could vary, but it could reduce incorrect placement by mechanically inhibiting it, or by alerting the user when the device is placed incorrectly. Taking that idea one step further could reduce error resulting from the characteristic pivot phenomenon. Error from the characteristic pivot is least significant when the device pivots at the same height as the characteristic pivot. Implementing an adjustable pivot height system into the DARLING would enable it to rotate at the characteristic pivot of each individual stalk it tests. These systems, like the height sensor, would significantly reduce the DARLING's measurement error but would extensive development to deliver reliable, robust performance.

Implementing systems like this must be done with caution however, as complexity and reliability often have an inverse relationship. Although error reduction is critical, added complexity could cause more problems in the future. A simple, straightforward mechanical solution is ideal in this case, and although it may not completely solve the problem, a balance must be struck between perfect performance and reasonable reliability. Alternatively, methods of recognizing and mitigating error utilizing software require zero mechanical design change. By further analyzing the trends of error resulting from the three sources, the DARLING data collection and post-processing software could be modified to automatically recognize and rectify error in the data. This method would be less likely to hamper reliability and maintains simplicity in the mechanical design of the DARLING.

5.4 Artificial Test Plot

One of the challenges in validating design changes is the logistics surrounding field testing. Currently, the only corn test plots associated with the project are in the southeastern United States. This location means that many design changes are incorporated without intermediate field validation. Field validation is extremely valuable, as it uses the intended environment to representationally analyze the impact of design changes. A test plot closer to the University of Idaho would allow for this kind of validation without requiring excessive travel. However, corn does not grow well in the northern Idaho climate, and the frequency at which the natural test plot could be used would be limited by the number of growth cycles provided. Alternatively, a plot of artificial stalk specimens could be used. This plot, which could consist of carbon fiber rods like those used in chapter 4, would provide a year-round, repeatable, and consistent test plot. The plot would be relatively small (8’ by 8’) and would be designed to fit indoors.

Bridging the gap between DARLING’s development and in-use locations would allow for much more effective, relevant, and confident design changes to be made. An artificial plot would also open the door for even more representative measurement error analysis and performance evaluation. Finally, a plot like this like this would provide an excellent show/demonstration piece for stakeholders and project newcomers alike. A model render of this plot is shown in Figure 118.

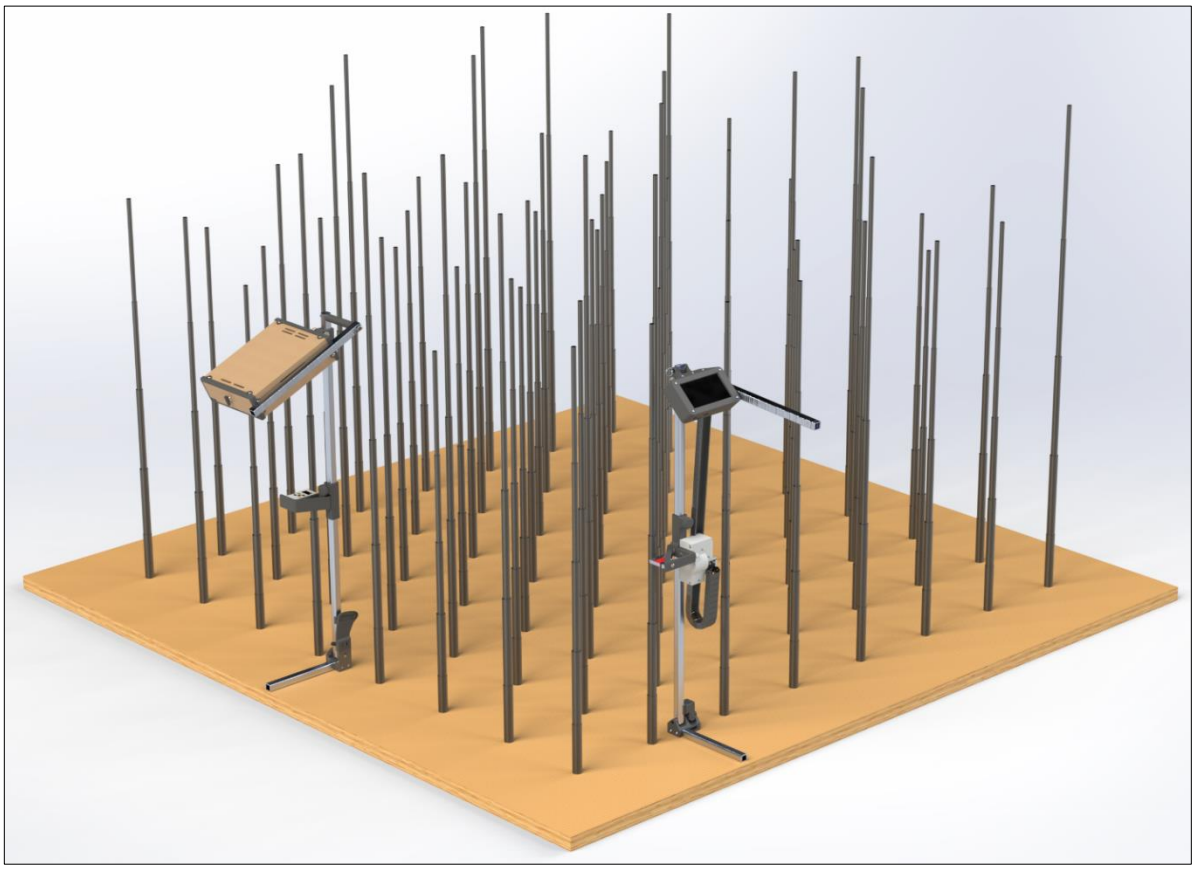

Figure 118: Artificial test plot with DARLINGs to scale. The test plot would consist of ~64 carbon fiber rods machined with similar dimensions to an inbred data set. Several different configurations of stalks would be fabricated to offer variety.

Bibliography

[1] "FAOSTAT." https://www.fao.org/faostat/en/#data/FBS (accessed Jan. 13, 2023).

[2] "What Are the World's Most Important Staple Foods?," *WorldAtlas*, Jun. 07, 2019. https://www.worldatlas.com/articles/most-important-staple-foods-in-the-world.html (accessed Sep. 06, 2022).

[3] H. Sarwar, "The importance of cereals (Poaceae: Gramineae) nutrition in human health: A review," *J. Cereals Oilseeds*, vol. 4, no. 3, pp. 32–35, Jun. 2013, doi: 10.5897/JCO12.023.

[4] H. Valin *et al.*, "The future of food demand: understanding differences in global economic models," *Agric. Econ.*, vol. 45, no. 1, pp. 51–67, 2014, doi: 10.1111/agec.12089.

[5] J. Rattray and S. C. Brokaw, "The Implications of the Increasing Global Demand for Corn," 2012. Accessed: Jan. 13, 2023. [Online]. Available: https://www.semanticscholar.org/paper/The-Implications-of-the-Increasing-Global-Demand-Rattray-Brokaw/94e733c3de0bc2485c3fa4f7e3a26e740d01f36a

[6] D. B. Lobell, K. G. Cassman, and C. B. Field, "Crop Yield Gaps: Their Importance, Magnitudes, and Causes," *Annu. Rev. Environ. Resour.*, vol. 34, no. 1, pp. 179–204, 2009, doi: 10.1146/annurev.environ.041008.093740.

[7] S. A. Flint-Garcia, C. Jampatong, L. L. Darrah, and M. D. McMullen, "Quantitative trait locus analysis of stalk strength in four maize populations," *Crop Sci.*, vol. 43, pp. 13–22, Feb. 2003, doi: DOI 10.2135/cropsci2003.0013.

[8] D. N. Duvick, "The Contribution of Breeding to Yield Advances in maize (Zea mays L.)," *Adv. Agron.*, vol. 86, pp. 83–145, 2005, doi: 10.1016/S0065-2113(05)86002-X.

[9] P. M. Berry and J. Spink, "Predicting yield losses caused by lodging in wheat," *Field Crops Res.*, vol. 137, pp. 19–26, Oct. 2012, doi: 10.1016/j.fcr.2012.07.019.

[10] T. Kashiwagi, E. Togawa, N. Hirotsu, and K. Ishimaru, "Improvement of lodging resistance with QTLs for stem diameter in rice (Oryza sativa L.)," *Theor. Appl. Genet.*, vol. 117, no. 5, pp. 749–757, 2008.

[11] "Green Revolution - an overview | ScienceDirect Topics." https://www.sciencedirect.com/topics/earth-and-planetary-sciences/green-revolution (accessed Sep. 29, 2022).

[12] "green revolution | Definition, Advantages, Importance, & Facts | Britannica." https://www.britannica.com/event/green-revolution (accessed Sep. 29, 2022).

[13] "chapter 1 - rice in the world." https://www.fao.org/3/W8439E/w8439e08.htm (accessed Jan. 13, 2023).

[14] D. K. Ray, N. Ramankutty, N. D. Mueller, P. C. West, and J. A. Foley, "Recent patterns of crop yield growth and stagnation," *Nat. Commun.*, vol. 3, no. 1, Art. no. 1, Dec. 2012, doi: 10.1038/ncomms2296.

[15] P. M. Berry and S. T. Berry, "Understanding the genetic control of lodging-associated plant characters in winter wheat (Triticum aestivum L.)," *Euphytica*, vol. 205, no. 3, pp. 671–689, Oct. 2015, doi: 10.1007/s10681-015-1387-2.

[16] J. Zhang *et al.*, "Lodging resistance characteristics of high-yielding rice populations," *Field Crops Res.*, vol. 161, pp. 64–74, May 2014, doi: 10.1016/j.fcr.2014.01.012.

[17] P. M. Berry, "Lodging Resistancecereallodgingresistancein Cerealscereal," in *Sustainable Food Production*, P. Christou, R. Savin, B. A. Costa-Pierce, I. Misztal, and C. B. A. Whitelaw, Eds. New York, NY: Springer, 2013, pp. 1096–1110. doi: 10.1007/978-1-4614-5797-8_228.

[18] D. J. Robertson, M. Julias, B. W. Gardunia, T. Barten, and D. D. Cook, "Corn Stalk Lodging: A Forensic Engineering Approach Provides Insights into Failure Patterns and Mechanisms," *Crop Sci.*, vol. 55, no. 6, pp. 2833–2841, 2015, doi: 10.2135/cropsci2015.01.0010.

[19] H. X. Hu, Y. J. Meng, H. W. Wang, H. Liu, and S. J. Chen, "Identifying quantitative trait loci and determining closely related stalk traits for rind penetrometer resistance in a high-oil maize

population," *Theor. Appl. Genet.*, vol. 124, pp. 1439–1447, May 2012, doi: 10.1007/s00122-012-1799-5.

[20] S. Twumasi-Afriyie and R. B. Hunter, "Evaluation of quantitative methods for determining stalk quality in short-season corn genotypes," *Can. J. Plant Sci.*, vol. 62, no. 1, pp. 55–60, Jan. 1982, doi: 10.4141/cjps82-008.

[21] N. S. Inc, "Pinch and Push Test in Corn." https://www.n2seed.com/n2-seed-blog/pinch-and-push-test-in-corn (accessed Feb. 04, 2021).

[22] "Comparative Strength of Corn Stalk Internodes1 - Thompson - 1964 - Crop Science - Wiley Online Library." https://acsess.onlinelibrary.wiley.com/doi/abs/10.2135/cropsci1964.0011183X000400040015x (accessed Oct. 15, 2022).

[23] H. Hu *et al.*, "QTL mapping of stalk bending strength in a recombinant inbred line maize population," *Theor. Appl. Genet.*, vol. 126, no. 9, pp. 2257–2266, 2013.

[24] P. M. Berry *et al.*, "Controlling plant form through husbandry to minimise lodging in wheat," *Field Crops Res.*, vol. 67, no. 1, pp. 59–81, Jul. 2000, doi: 10.1016/S0378-4290(00)00084-8.

[25] D. J. Robertson, S. Y. Lee, M. Julias, and D. D. Cook, "Maize Stalk Lodging: Flexural Stiffness Predicts Strength," *Crop Sci.*, vol. 56, no. 4, p. 1711, 2016, doi: 10.2135/cropsci2015.11.0665.

[26] D. D. Cook, W. de la Chapelle, T.-C. Lin, S. Y. Lee, W. Sun, and D. J. Robertson, "DARLING: a device for assessing resistance to lodging in grain crops," *Plant Methods*, vol. 15, p. 102, 2019, doi: 10.1186/s13007-019-0488-7.

[27] J. D. Holmes, *Wind loading of structures*. CRC press, 2015.

[28] R. S. Sekhon, C. N. Joyner, A. J. Ackerman, C. S. McMahan, D. D. Cook, and D. J. Robertson, "Stalk Bending Strength is Strongly Associated with Maize Stalk Lodging Incidence Across Multiple Environments," *Field Crops Res.*, vol. 249, p. 107737, Apr. 2020, doi: 10.1016/j.fcr.2020.107737.

[29] L. Gou, M. Zhao, J.-J. Huang, B. Zhang, T. Li, and R. Sun, "Bending mechanical properties of stalk and lodging resistance of maize," *Acta Agron. Sin.*, vol. 34, no. 4, pp. 653–661, 2008.

[30] Q. Guo *et al.*, "A Non-Destructive and Direction-Insensitive Method Using a Strain Sensor and Two Single Axis Angle Sensors for Evaluating Corn Stalk Lodging Resistance," *Sensors*, vol. 18, no. 6, p. 1852, 2018.

[31] Q. Guo *et al.*, "Classification of Corn Stalk Lodging Resistance Using Equivalent Forces Combined with SVD Algorithm," *Appl. Sci.*, vol. 9, no. 4, p. 640, 2019.

[32] "DuPont Unveils Innovative Mobile Wind Machines to Help Improve Corn Yield," *PRWeb*. https://www.prweb.com/releases/2009/02/prweb2121264.htm (accessed Feb. 07, 2023).

[33] P. M. Berry, J. Spink, M. Sterling, and A. A. Pickett, "Methods for Rapidly Measuring the Lodging Resistance of Wheat Cultivars," *J. Agron. Crop Sci.*, vol. 189, pp. 390–401, 2003.

[34] D. Jo Heuschele, J. Wiersma, L. Reynolds, A. Mangin, Y. Lawley, and P. Marchetto, "The Stalker: An open source force meter for rapid stalk strength phenotyping," *HardwareX*, vol. 6, p. e00067, Oct. 2019, doi: 10.1016/j.ohx.2019.e00067.

[35] Austin Bebee, "A Model and Device for High Throughput Measurements of Stem Flexural Stiffness in Grains," University of Idaho, 2020.

[36] "Instron Homepage." http://www.instron.com/en/ (accessed Aug. 22, 2022).

[37] "Amazon.com: BAOSHISHAN ZP-500N Digital Force Gauge Push Pull Gauge with Output Function, Carrying Caase, LCD Backlit Display, Metal Enclosures for Tension and Compression Load Plug Force Destructive Tests : Industrial & Scientific." https://www.amazon.com/BAOSHISHAN-Interface-Measuring-Instruments-Destructive/dp/B07VSDF1CX/ref=sr_1_7_sspa?crid=1TF63DPHIW7P7&keywords=Force%2Bgauge%2Bhigh%2Baccuracy%2B300N%2Bpeak%2Bload&qid=1665681011&sprefix=force%2Bgauge%2Bhigh%2Baccuracy%2B300n%2Bpeak%2Bload%2Caps%2C122&sr=8-7-spons&spLa=ZW5jcnlwdGVkUXVhbGlmaWVyPUFJU05MU0dZOThQSFAmZW5jcnlwdGV

kSWQ9QTA4NjQwNDIyQTUyS1daQ0FQQktUJmVuY3J5cHRlZEFkSWQ9QTA0OTc0MzhKQVpaS0lEV0kxWk4md2lkZ2V0TmFtZT1zcF9tdGYmYWN0aW9uPWNsaWNrUmVkaXJlY3QmZG9Ob3RMb2dDbGljaz10cnVl&th=1 (accessed Dec. 22, 2022).

[38] "Amazon.com: Mxmoonfree 500N Digital Force Gauge Push Pull Gauge Portable Force Meter with Units N/ LB/ Kg/ Oz, Storage Case, Auto Backlit LCD, Auto Power-Off (ZMF-500N) : Industrial & Scientific." https://www.amazon.com/Mxmoonfree-Digital-Portable-Power-off-ZMF-500N/dp/B08YJNGVKM/ref=sr_1_1_sspa?crid=HJ6BHWTWNE0Z&keywords=mxmoonfree%2B300N%2Bdigital%2Bforce%2Bgauge&qid=1671726951&sprefix=mxmoonfree%2B300n%2Bdigital%2Bforce%2Bgauge%2Caps%2C202&sr=8-1-spons&ufe=app_do%3Aamzn1.fos.006c50ae-5d4c-4777-9bc0-4513d670b6bc&spLa=ZW5jcnlwdGVkUXVhbGlmaWVyPUEyTUg0MzQ4UzIxOEhCJmVuY3J5cHRlZElkPUEwNTc3OTk3MjNTT05FV0U1U1pUWCZlbmNyeXB0ZWRBZElkPUEwMTk0MzIwMlFEUVlOTTQyREtCNSZ3aWRnZXROYW1lPXNwX2F0ZiZhY3Rpb249Y2xpY2tSZWRpcmVjdCZkb05vdExvZ0NsaWNrPXRydWU&th=1 (accessed Dec. 22, 2022).

[39] "S-Beam Tension and Compression Load Cell LSB302 : FSH04205." https://www.futek.com/store/load-cells/s-beam-load-cells/s-beam-LSB302/FSH04205 (accessed Dec. 22, 2022).

[40] PK, "Height Percentile Calculator by Gender (United States)," *DQYDJ – Don't Quit Your Day Job...*, Feb. 25, 2019. https://dqydj.com/height-percentile-calculator-for-men-and-women/ (accessed Oct. 14, 2022).

[41] "Theory and Design for Mechanical Measurements, 7th Edition | Wiley," *Wiley.com*. https://www.wiley.com/en-us/Theory+and+Design+for+Mechanical+Measurements%2C+7th+Edition-p-9781119475651 (accessed Oct. 21, 2022).

[42] ChartsBin, "Daily Calorie Intake Per Capita," *ChartsBin*. http://chartsbin.com/view/1150 (accessed Sep. 06, 2022).

[43] "Corn," *USDA Foreign Agricultural Service*. https://www.fas.usda.gov/commodities/corn (accessed Sep. 27, 2022).

[44] "World Agricultural Production," *USDA Foreign Agricultural Service*. https://www.fas.usda.gov/data/world-agricultural-production (accessed Aug. 22, 2021).

[45] L. Shah *et al.*, "Improving Lodging Resistance: Using Wheat and Rice as Classical Examples," *Int. J. Mol. Sci.*, vol. 20, no. 17, p. 4211, Aug. 2019, doi: 10.3390/ijms20174211.

[46] L. Erndwein, D. D. Cook, D. J. Robertson, and E. E. Sparks, "Field-based mechanical phenotyping of cereal crops to assess lodging resistance," *Appl. Plant Sci.*, vol. 8, no. 8, p. e11382, 2020.

[47] A. M. Stucker, E. Morris, C. J. Stubbs, and D. J. Robertson, "The Crop Clamp – A non-destructive electromechanical pinch test to evaluate stalk lodging resistance," *HardwareX*, vol. 10, p. e00226, Oct. 2021, doi: 10.1016/j.ohx.2021.e00226.

[48] D. D. Cook, W. de la Chapelle, T.-C. Lin, S. Y. Lee, W. Sun, and D. J. Robertson, "DARLING: a device for assessing resistance to lodging in grain crops," *Plant Methods*, vol. 15, no. 1, p. 102, 2019.

[49] K. L. Khanna, "An improved instrument for testing rind hardness in sugarcane," *Agr Live Stock India*, vol. 5, pp. 156–8, 1935.

[50] C. J. Stubbs, C. McMahan, W. Seegmiller, D. D. Cook, and D. J. Robertson, "Integrated Puncture Score: force–displacement weighted rind penetration tests improve stalk lodging resistance estimations in maize," *Plant Methods*, vol. 16, no. 1, pp. 1–12, 2020.

[51] D. J. Robertson, D. D. Cook, K. Meehan, and L. Asatiani, "The Effect of Probe Geometry on Rind Puncture Resistance Testing of Maize Stalks," 2020.

[52] D. L. Thompson, “Stalk Strength of Corn as Measured by Crushing Strength and Rind Thickness,” *Crop Sci.*, vol. 3, no. 4, pp. 323–329, 1963, doi: 10.2135/cropsci1963.0011183X000300040013x.
[53] L. Al-Zube, W. Sun, D. Robertson, and D. Cook, “The elastic modulus for maize stems,” *Plant Methods*, vol. 14, no. 1, p. 11, Feb. 2018, doi: 10.1186/s13007-018-0279-6.
[54] L. Al-Zube, D. J. Robertson, J. N. Edwards, W. Sun, and D. D. Cook, “Measuring the compressive modulus of elasticity of pith-filled plant stems,” *Plant Methods*, vol. 13, Nov. 2017, doi: ARTN 99 10.1186/s13007-017-0250-y.
[55] C. J. Stubbs, W. Sun, and D. D. Cook, “Measuring the transverse Young’s modulus of maize rind and pith tissues,” *J. Biomech.*, vol. 84, pp. 113–120, Feb. 2019, doi: 10.1016/j.jbiomech.2018.12.028.
[56] C. J. Stubbs, Y. A. Oduntan, T. R. Keep, S. D. Noble, and D. J. Robertson, “The effect of plant weight on estimations of stalk lodging resistance,” *Plant Methods*, vol. 16, no. 1, pp. 128–128, 2020, doi: 10.1186/s13007-020-00670-w.
[57] W. H. Seegmiller, J. Graves, and D. J. Robertson, “A novel rind puncture technique to measure rind thickness and diameter in plant stalks,” *Plant Methods*, vol. 16, no. 1, p. 44, Apr. 2020, doi: 10.1186/s13007-020-00587-4.
[58] A. Ching, J. A. Rafalski, S. Luck, and M. G. Butruille, “Genetic loci associated with mechanical stalk strength in maize,” Jul. 14, 2009
[59] A. Butron, R. A. Malvar, P. Revilla, P. Soengas, and A. Ordas, “Rind puncture resistance in maize: inheritance and relationship with resistance to pink stem borer attack,” *Plant Breed.*, vol. 121, pp. 378–382, Oct. 2002, doi: DOI 10.1046/j.1439-0523.2002.716313.x.
[60] R. Kumar *et al.*, “Genetic Architecture of Maize Rind Strength Revealed by the Analysis of Divergently Selected Populations,” *Plant Cell Physiol.*, no. pcab059, Jun. 2021, doi: 10.1093/pcp/pcab059.
[61] D. J. Robertson, Z. W. Brenton, S. Kresovich, and D. D. Cook, “Maize lodging resistance: Stalk architecture is a stronger predictor of stalk bending strength than chemical composition,” *Biosyst. Eng.*, vol. 219, pp. 124–134, Jul. 2022, doi: 10.1016/j.biosystemseng.2022.04.010.
[62] C. J. Stubbs, K. Seegmiller, C. McMahan, R. S. Sekhon, and D. J. Robertson, “Diverse maize hybrids are structurally inefficient at resisting wind induced bending forces that cause stalk lodging,” *Plant Methods*, vol. 16, pp. 1–15, 2020.
[63] B. Anderson and D. G. White, “Evaluation of Methods for Identification of Corn Genotypes with Stalk Rot and Lodging Resistance,” *Plant Dis.*, vol. 78, pp. 590–593, Jun. 1994.
[64] C. J. Baker *et al.*, “A Method for the Assessment of the Risk of Wheat Lodging,” *J. Theor. Biol.*, vol. 194, no. 4, pp. 587–603, 1998, doi: DOI: 10.1006/jtbi.1998.0778.
[65] L. L. Bashford, J. W. Maranville, S. A. Weeks, and R. Campbell, “Mechanical-Properties Affecting Lodging of Sorghum,” *Trans. Asae*, vol. 19, pp. 962–966, 1976.
[66] S. M. Davis and P. L. Crane, “Recurrent Selection for Rind Thickness in Maize and Its Relationship with Yield, Lodging, and Other Plant Characteristics,” *Crop Sci.*, vol. 16, pp. 53–55, 1976.
[67] G. V. Forell, D. Robertson, S. Y. Lee, and D. D. Cook, “Preventing lodging in bioenergy crops: a biomechanical analysis of maize stalks suggests a new approach,” *J. Exp. Bot.*, vol. 66, no. 14, pp. 4367–4371, Jan. 2015, doi: 10.1093/jxb/erv108.
[68] A. Sayad *et al.*, “The semi-automated development of plant cell wall finite element models,” *Plant Methods*, vol. 19, no. 1, p. 3, Jan. 2023, doi: 10.1186/s13007-023-00979-2.
[69] D. D. Cook, D. Robertson, M. Julias, and S. Y. Lee, “Apparatus and method for assessing plant stem strength,” WO2016205244A1, Dec. 22, 2016 Accessed: May 31, 2021. [Online]. Available: https://patents.google.com/patent/WO2016205244A1/en
[70] L. L. Howell, “Compliant Mechanisms. John Wiley & Sons, New York.,” 2001.

[71] A. Bebee, C. J. Stubbs, and D. J. Robertson, “Large Deflection Model for Multiple, Inline, Interacting Cantilever Beams,” *J. Appl. Mech.*, vol. 88, no. 4, p. 041005, Apr. 2021, doi: 10.1115/1.4049072.

[72] R. Song and A. Muliana, “Modeling mechanical behaviors of plant stems undergoing microstructural changes,” *Mech. Mater.*, vol. 139, p. 103175, Dec. 2019, doi: 10.1016/j.mechmat.2019.103175.

[73] D. J. Robertson, M. Julias, S. Y. Lee, and D. D. Cook, “Maize Stalk Lodging: Morphological Determinants of Stalk Strength,” *Crop Sci.*, vol. 57, no. 2, pp. 926–934, 2017, doi: 10.2135/cropsci2016.07.0569.

[74] P. Song, J. Wang, X. Guo, W. Yang, and C. Zhao, “High-throughput phenotyping: Breaking through the bottleneck in future crop breeding,” *Crop J.*, vol. 9, no. 3, pp. 633–645, Jun. 2021, doi: 10.1016/j.cj.2021.03.015.

[75] H. Feng *et al.*, “An integrated hyperspectral imaging and genome-wide association analysis platform provides spectral and genetic insights into the natural variation in rice,” *Sci. Rep.*, vol. 7, no. 1, p. 4401, Jun. 2017, doi: 10.1038/s41598-017-04668-8.

[76] C. J. Stubbs, C. McMahan, K. Tabaracci, B. Kunduru, R. S. Sekhon, and D. J. Robertson, “Cross-Sectional Geometry Predicts Failure Location in Maize Stalks,” *Plant Methods*, vol. 18, no. 1, pp. 1–9, 2022.

[77] D. Robertson, J. Cornwall, C. Stubbs, and McMahan Christopher, “The Overlooked Biomechanical Role of the Clasping Leaf Sheath in Wheat Stalk Lodging,” *Front. Plant Sci.*, p. 1774, 2021, doi: doi: 10.3389/fpls.2021.617880.

[78] A. Kempe, M. Sommer, and C. Neinhuis, “A Comparative Analysis of the Mechanical Role of Leaf Sheaths of Poaceae, Juncaceae, and Cyperaceae,” *J. Bot.*, vol. 2013, p. 6, 2013, doi: 10.1155/2013/690549.

[79] D. Robertson, S. Smith, B. Gardunia, and D. Cook, “An Improved Method for Accurate Phenotyping of Corn Stalk Strength,” *Crop Sci.*, vol. 54, no. 5, p. 2038, 2014, doi: 10.2135/cropsci2013.11.0794.

[80] D. J. Robertson, S. L. Smith, and D. D. Cook, “On measuring the bending strength of septate grass stems,” *Am. J. Bot.*, vol. 102, no. 1, pp. 5–11, 2015, doi: 10.3732/ajb.1400183.